Illumination Optimized Transmit Signals for Space-Time Multi-Aperture Radar

by

Vishal Sinha

B.E. (With Distinction), Electronics and Telecommunications Engineering

Army Institute of Technology

University of Pune, India 2002

Submitted to the Department of Electrical Engineering and Computer Science and the faculty of the Graduate School of the University of Kansas in partial fulfillment of the requirements for the degree of Master of Science

Thesis Committee

Chairperson: Dr. James M. Stiles

Dr. Chris Allen

Dr. Glenn Prescott

Date of Thesis Defense: January 23rd, 2006

i

The Thesis Committee for Vishal Sinha certifies
That this is the approved version of the following thesis:

Illumination Optimized Transmit Signals

for Space-Time Multi-Aperture Radar

Thesis Committee

_____

Chairperson: Dr. James M. Stiles

_____

Dr. Chris Allen

_____

Dr. Glenn Prescott

Date Approved: January 23rd, 2006

*To my Bhagwan**, Shri Sathya Sai Baba**,*

Who have taught me all that what matters, and because of

Whom, I am what I am today

ACKNOWLEDGEMENTS

To say that I express my sincere gratitude to Prof. Stiles, my research and graduate advisor, would be an understatement. Words cannot describe how fortunate I feel to have got this opportunity to work under him. No matter how many times I pestered him with my silly or irrelevant questions, he was always available and so patient in answering them. I have learnt so much from him over the past two and half years; and that pertains not only to my research or coursework, but also to all that which applies to being a good engineer. I wish and pray that in the life ahead, I can follow whatever he has taught me, and I am able to come up to his expectations of being a true Electrical Engineer. Working with him was so easy and so much fun; in fact it was one of the best parts of my stay in Lawrence. Prof. Stiles, thank you for everything.

I would also like to thank Dr. Allen and Dr. Prescott for being on my committee, and taking out time to review this document. I have been in classes under both of them, and have had a wonderful experience in each of the courses.

My most sincere thanks my father, Lt. Col. KC Sinha and mother, Mrs. Neelu Sinha, who brought me up so well and from whom I learnt the importance of values in life. They were always there when I needed them, and without their support, I would have never have reached where I am today. Thank you Papa, Thank you Ma!

My very very special thanks goes to my brother Sourabh (Dada), who envisioned my future for me. Without his planning and foresight I would not be graduating from this distinguished university. Dada, thank you so much!

My thanks to all the good people and friends whom I met and came across during my stay here in the Lawrence, and who in their own way have been responsible in contributing to my successes. In particular I would like to mention my friend Visweswaran Srinivasamurthy (Vishu), who was a constant companion in both good and bad times, and because of whom life has been so much fun at the Radar and Remote Sensing Lab and ITTC. Vishu, I have learnt a lot from you and earnestly thank you for your friendship.

Last but most importantly, my deepest gratitude to God, Who took care of me and showed me the way whenever I needed Him, and for Whom, any number of words would be insufficient to express my gratefulness.

TABLE OF CONTENTS

LIST OF FIGURES

LIST OF TABLES

ABSTRACT

Space-time coding and diversity techniques have been an active research area for wireless communication since long, and have been seen to significantly improve performances of communication systems. Although similar approaches for radars have not been attempted yet, it is rational to expect comparable performance gains for the multi-aperture radar provided we can come up with the optimal transmit solutions for these space-time systems. To make the most of a multi-aperture transmitter, it needs to be considered and utilized as a non-separable sensor in space and time, i.e. each aperture propagates a coherent but uncorrelated signal in time and frequency.

A methodology to create such non-separable space-time signals for various illumination optimization criteria is developed, and the performance validated through various tests and simulations. By expanding the space-time signal in terms of a set of orthonormal basis functions, the problem is reduced to that of finding the optimal set of weights for these functions, i.e. a vector. In combination with the vector-matrix models developed, the structure enables the use of linear algebraic techniques like eigen analysis for determining the optimal solutions.

Out of the many optimization criteria developed, the most applicable one is found to be the mini-max or maxi-min. However solutions to this criterion are not easy to find; an iterative procedure having a sound algebraic basis is presented as a solution. The efficacy of the method has been demonstrated with relevant results, and its dependence studied on a number of parameters. Particularly interesting is the form

of the resulting signal, which is examined both at the transmitter and also at the targets; some very important conclusions are drawn based on the observations.

Chapter 1

Introduction

1.1 Space-Time Multi-Aperture Radar

Let us begin with a brief description of a *space-time multi-aperture radar* as it forms the premise for this thesis. One way to visualize the multi-aperture sensor is to think about it as a single large radar which has been divided into a number of smaller apertures. Such a distributed sensor enables the radar to collect exclusive information across a third dimension of space, in addition to the two conventional dimensions of time and frequency – i.e. *operation in both space and time*.

The additional angle of arrival information collected (with respect to the targets) can greatly enhance radar functionality, and now a single space-time sensor can conceivably provide operation in multiple radar modes. For e.g. a single multi-aperture transmit array can be used to do a wide area SAR (synthetic aperture radar) that needs large timewidth and/or bandwidth, or even a GMTI (ground moving target indicator) or AMTI (airborne moving target indicator) which require large spatial arrays for fine angular resolution. The other obvious advantages that come along with the multi-aperture concept are also there. Like a more robust structure wherein the failure of one microsat just slightly degrades the performance of the overall system; in a comparable monolithic system, such an event will result in total system failure. The power requirements for the individual units are much more manageable vis-à-vis a single large radar. Also the radar performance can be enhanced if required at a later

stage by the addition of more units in the future. But in spite of the accompanying benefits, from our perspective, the biggest advantage or motivation for the distributed sensor concept still remains the potential for *true space-time operation* – i.e. utilizing both the transmitter and the receiver as a non-separable function of space and time.

Although the use of the multi-aperture sensor is not limited to a particular platform – ground based, airborne or even spaceborne distributed sensors can be developed, some of the more interesting designs have still been formulated keeping the spaced- based radar in mind - like the Interferometric Cartwheel [6] and the TechSat 21 [7]. For any multi-aperture radar the individual units can act only as receivers like in the Interferometric Cartwheel, or as both transmitters and receivers as in the TechSat 21 concept. However in either case all the transmitters and receivers on the individual units are perfectly coherent, i.e. all the systems work together in tandem and the shared data along with the spatial sampling of the configuration provides single big virtual radar. Figure 1:1 on the next page shows how a multi-aperture radar array may look like in space.
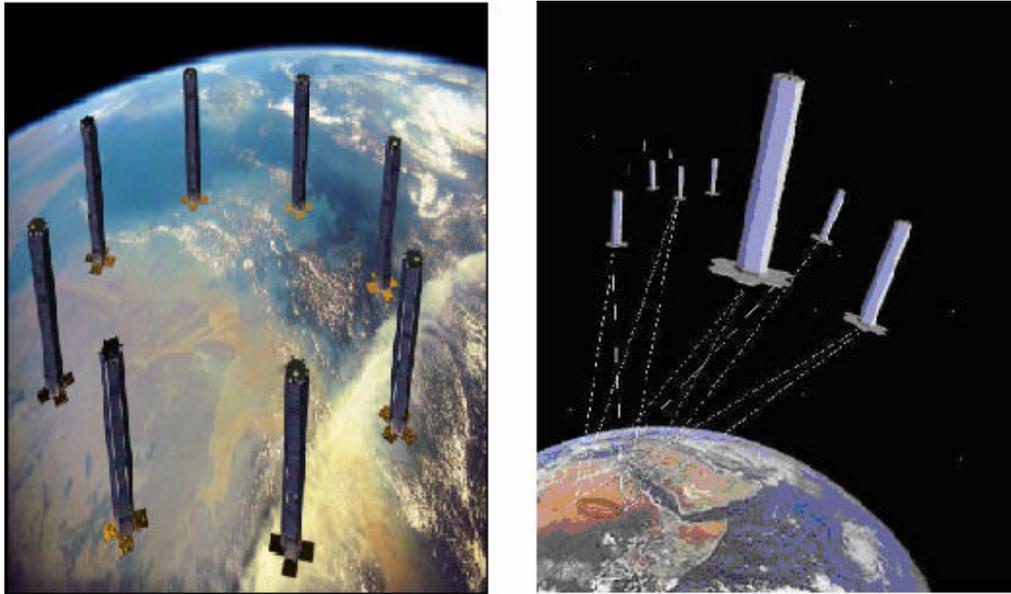
Figure 1:1 Example of a Multi-Aperture Array - spaceborne platform[7]

The antenna array for a multi-aperture system is made up of a number of elements which may be positioned contiguously, or might be spread across a wide space to form a three dimensional non-uniformly spaced sparse array (a design more suited for the spaced based platforms). For such sparsely populated random arrays the location of the nearest grating lobes can be pushed out by minimizing the distance between any two antenna elements. Similarly a fine angular or spatial resolution can be achieved by increasing the spatial extent of the physical array. But due to its sparse nature the array pattern will still have lot of sidelobes within the illuminated area which cannot be eliminated [4]. Therefore, care has to be taken to ensure that on the transmit side these sidelobes do not fall on the regions which we do not wish to illuminate (example would be stationary objects or ground clutter for MTI), and on the receive side, on targets whose returns are perfectly ambiguous in range or doppler with our target of interest [1]. Even for the contiguous array, means for controlling

the illumination pattern becomes an important radar problem; depending upon our definitions of the regions which we classify as desirable, or not desirable – i.e. *targets and clutter*.

The radar design therefore has to be altered to adapt to the different scenarios. This can be done through a number of ways like – enhancing the radar hardware, modifying the antenna array structure, adding more transmitters or receivers and/or changing the radar transmit signal. Out of the above, the most economical or convenient method to control radar performance, or the array illumination pattern is naturally to control the transmit signal feeding the array. This radar transmit waveform is a critical entity, and therefore becomes a very important '*tunable*' design parameter for the whole system (it can be modified depending upon the requirements). Consequently, coming up with the optimal transmit signal for the various optimization criteria becomes a very important radar problem. The perfect radar transmit signal will have two important characteristics –

- It will distribute the energy equally over our region of interest (the targets), and at the same time not illuminate the regions which we are not interested in (clutter).
- It will make the responses from all targets mutually orthogonal to each other.

Such a perfect transmit signal exists for only the most simple of radar problems, but it does provide us with two possible directions towards transmit signal optimization.

We call the first approach "*illumination optimization*", wherein we try to maximize the signal to clutter ratio (SCR) by putting most of the illuminated energy

on our regions of interest (targets), as compared to the regions from where we do not want unwanted signal returns (clutter). This idea of space-time illumination optimization forms the core of this thesis. We call it as space-time as both the spatial and temporal characteristics of the multi-aperture transmit array are utilized. The second approach is called the "*ambiguity optimization*", in which we try to minimize the correlation between responses from any two targets that have been illuminated. The idea is minimize the ambiguity between responses in order to get better detection/estimation ability. This study does not form a part of this thesis, but forms an interesting problem of its own. Some work has already been done in this area of making the responses from different targets as orthogonal as possible; the readers are referred to [8] for the complete details.

Before we describe our approach and methods towards the space-time illumination optimization problem mentioned above, let's first review the kind of work that has already been done in the area of optimal radar transmit signal design, and space-time antenna pattern synthesis.

1.2 Related Work

1.2.1 Space-Time Beamforming – Receive Side

Most of the work in the area of space-time beam forming or antenna pattern synthesis has been done on the receive side. It involves coming up with an optimal weight vector **"w"** for the received measurement samples, given the radar, target set and estimation goals. This approach focuses the space-time beam on the receive side

for each individual target, so as to discriminate against clutter, noise and ambiguities. Examples of such work can be found in [9, 10] and also in [4, 5]. Therefore, even though we have multiple antennas, the power of the spatial array is realized only at the receiver for space-time beamforming and clutter cancellation. To exploit the full potential of the antenna array, i.e. also on the transmit side, we wish to have an equivalent scheme wherein we come up with an optimal **space-time** transmit code **"s",** for a similar set of conditions.

At this point, let's digress a little and explain an important distinction. Note what we call space-time here, is a completely different concept from what has until now been considered as "space-time". Typically for multi aperture arrays, we just have a single time-frequency signal weighted by a complex weight at each of the spatial elements – essentially a *"phased array"*. And the transmit signal is a separable function of space and time; the transmitted waveform being a direct product of the temporal signal and the spatial weighting on the array elements. This is very different from the *true space-time transmitter* idea proposed in this thesis. The contention is that if each transmit element propagates an independent signal of time and frequency, radar performance can be significantly improved and much better results obtained. This is indeed found to be true, and the capabilities of the two techniques have been compared in later chapters through various simulations.
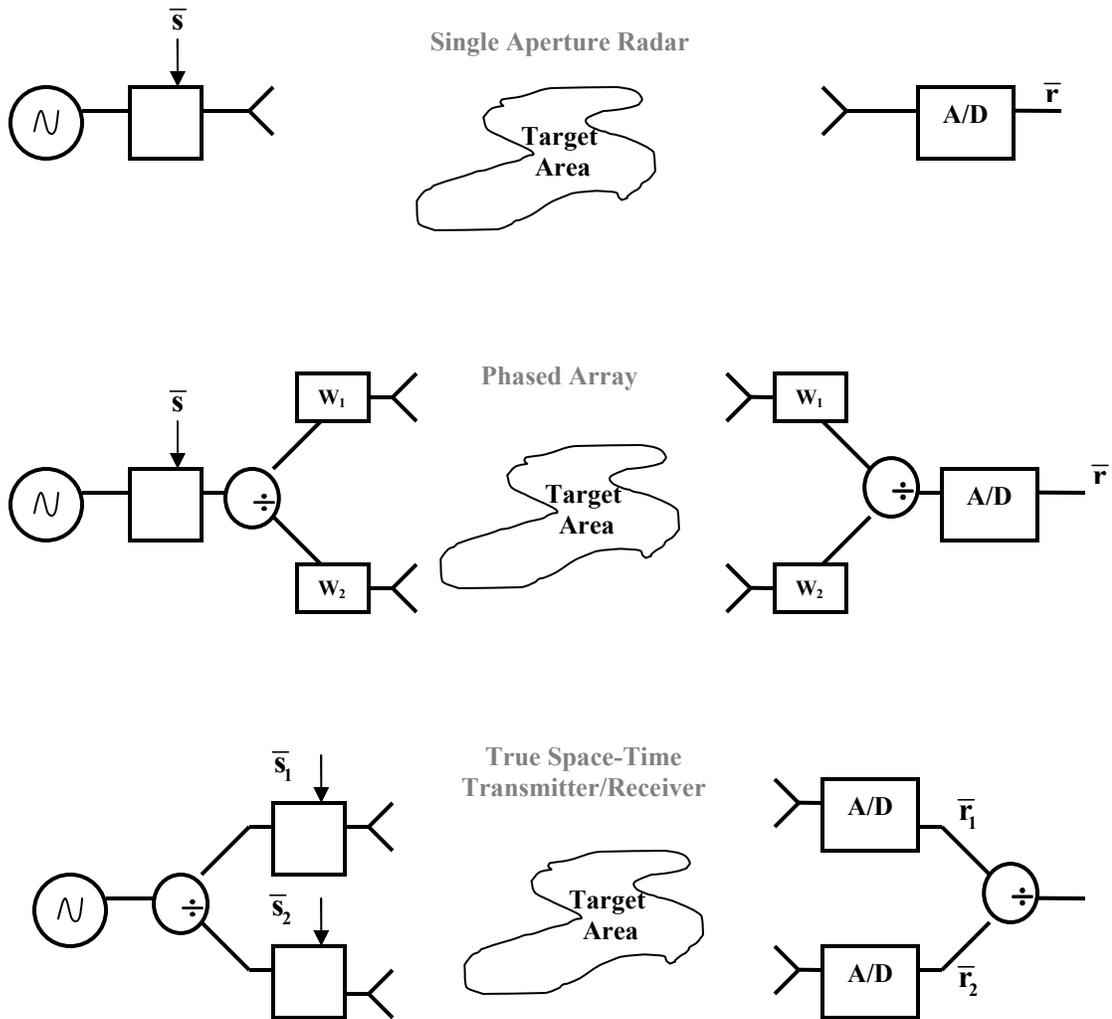
Figure 1:2 Difference between a single aperture, phased array and true space-time transmitter

The concepts for a single aperture radar, phased array and true space-time transmitter have been illustrated in Figure 1.3. For the first two cases we have a single temporal signal $\overline{\mathbf{s}}$, where as for the true space-time transmitter independent signals $\overline{\mathbf{s}}_1, \overline{\mathbf{s}}_2, \ldots \overline{\mathbf{s}}_n$ propagate on the different transmit elements. As an example say that for the first case (single aperture radar) 1000 time-frequency samples define our transmit signal $\overline{\mathbf{s}}$. Then for a phased array with 5 elements we will need to determine 1005 space-time samples (1000 for $\overline{\mathbf{s}}$, and 5 for the spatial weights – $\mathbf{w}_1 \mathbf{w}_2 \ldots \mathbf{w}_5$), and 5000

for the true space-time transmitter (1000 different time-frequency samples for each transmit antenna - $\overline{\mathbf{s}}_1, \overline{\mathbf{s}}_2, \ldots \overline{\mathbf{s}}_5$). It is evident that this is a more intricate and laborious problem than the phased array, but is also seen to give tremendous payoffs in terms of performance. Also note that all the individual signals in case of the true space-time transmitter are coherent, i.e. they modulate the same local oscillator.

1.2.2 Transmit Signal Design – Ambiguity Optimization

Note that although ambiguity optimization is not within the purview of this study, some related work in this area has been covered just to demonstrate the space-time efficacy. Early work in this field involved pushing out the delay-doppler ambiguities with the help of pushing codes like Costas and Lee-zero sequences. The idea was to get ambiguity functions with a clear area around the center, or an area containing no sidelobes in a connected region around the main lobe. This approach is consistent with the ambiguity optimization idea described before. Chang and Bell [13] have designed a way for constructing frequency coded waveforms for enhanced delay-doppler resolution. With the help of Lee-zero sequences which are derived from the Costas sequences themselves [11, 12], the delay-doppler ambiguities are pushed out of the illuminated area where no targets can exist. Thus locally optimal ambiguity functions are realized. Techniques for achieving arbitrary size clear areas have also been proposed. However this method relies only on the coding in the temporal dimension, i.e. controlling the frequency of each transmitted pulse to come up with the optimal ambiguity function. Such time-frequency codes can just push the

delay-doppler ambiguities farther away, but cannot knock them out completely. The total energy in the delay-doppler ambiguity function remains invariant, and to achieve a truly ideal ambiguity function with an infinitely large clear area around the main lobe, infinite number of frequencies will be required.

This constraint is not present for a space-time transmitter/receiver, as now the total ambiguity function is approximately the product of the spatial and temporal ambiguity functions and thus the energy in it is no longer invariant [4, 9]. Therefore it's even possible (theoretically) to get an ambiguity function with the total integrated sidelobe energy of zero – the ideal case. However once the spatial pattern is superimposed over the time-frequency, the total ambiguity function would no longer stay invariant with target location and the transmit code will need to be optimized for all targets simultaneously (instead of a single target). This turns out to be a much more difficult problem and requires more rigorous techniques [8].

The potential of space-time coding/processing for the application of ambiguity optimization can be intuited from Figure 1:3. Note that this is an example of space-time processing (or beamforming) on the receive side, but the same concept can also be extended to the transmit side with space-time coding.
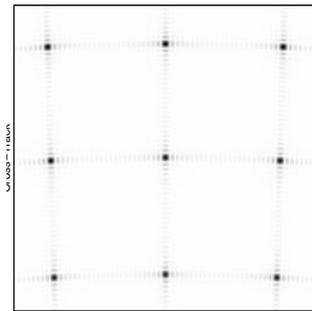
Delay-Doppler (Temporal) Ambiguity Function - with ambiguities
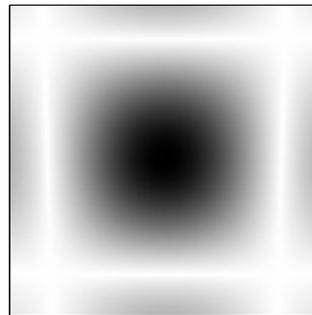
Spatial Ambiguity Function
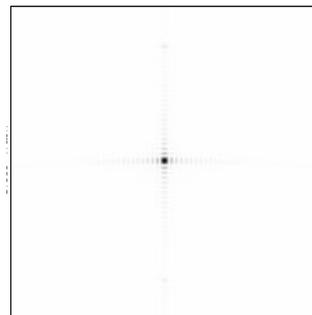
Space-Time Ambiguity Function – No ambiguities

Figure 1:3 Space-Time Ambiguity function [9]

As can be seen by superimposing the spatial pattern on the delay-doppler ambiguity function the energy in the final ambiguity function is reduced. There are also other optimization techniques that work on reducing the sidelobe levels using sequences like Barker, Frank and extended Frank codes [14, 15]. However all these transmit codes just work towards achieving an optimal time-frequency ambiguity function, by either minimizing the peak sidelobe level or pushing out the delay-doppler ambiguities. The total energy in the ambiguity function stays constant. None of these

codes can knock out the time-frequency ambiguities completely; they can just be moved around in the delay-doppler plane to regions where we don't expect our targets to exist.

Efforts have also been made to optimize the ambiguity function in just one dimension, for either a range or doppler resolution radar. In [16] the authors propose polyphase pulse compression transmit sequences, derived from Frank and Extended Frank codes to reduce the sidelobe levels for a range-resolution radar. Such a technique would work excellently if we do not have any moving targets in our target scenario or the doppler associated with each target is precisely zero. But for a remote sensing SAR that is never the case, and hence these techniques find little use. Even if we suppress the sidelobes in range, the ambiguities will move closer in the doppler dimension as the integrated sidelobe energy has to be a constant for plain time-frequency codes.

Nevertheless, this approach does suggest a useful concept of pushing all the ambiguities in a subspace where no targets can exist (here all ambiguities are moved to the non-zero doppler region). For a three dimensional target space, where each target is identified by two dimensions of space and one of radial velocity, we need at least a four dimensions of transmit signal to be able to push our ambiguities in a region where no targets can exist. Such a 4-D transmit signal space can be realized by means of true space-time transmit codes where we have two temporal frequencies (in form of delay and doppler), and two more spatial frequencies - along the horizontal and vertical directions of the plane perpendicular to the direction of radial velocity.

Therefore if we can come up with a radar transmit code that pushes all the ambiguities in one dimension of this 4-dimensional space, then the total available transmit energy can be placed in the remaining three dimensions.

1.2.3 Transmit Signal Design – Illumination Optimization

All the work listed so far has been in the direction of ambiguity optimization. However as pointed before, although interesting, that does not form the objective of this study. Our work deals primarily with the problem of "*space-time illumination optimization*" mentioned earlier.

Related work in this area of illumination optimization has been done by J.R. Guerci of the Defense Advanced Research Projects Agency (DARPA) and others [17-19]. In [17] they propose a method for jointly determining the optimal transmit pulse and receiver impulse response to give the maximum SINR in the presence of signal dependent clutter and noise. However the method is optimized for just a single target, which is characterized by its known impulse response and the characteristics of the surrounding clutter and channel noise are known in terms of their power spectral densities. Using a host of complex signal analysis and mathematical tools, an iterative numerical procedure is developed to come up with the best transmit signal-receiver impulse response pair.

It turns out, that this solution involves finding an eigenfunction solution corresponding to the largest eigen value of an integral equation. This type of eigen analysis is a very powerful tool for our problem (as will be seen later), and is employed repeatedly even in our algorithms to find the best transmit signal code for

different criteria. By modeling linear systems in the form of matrices, the eigen vector–eigen value procedure enables us to find solutions in subspaces most orthogonal to clutter; thus allowing us to place most of the energy in dimensions least aligned with clutter, the kind of idea described earlier. For the problem of [17] the transmit signal turns out to be a critical factor, especially in cases where clutter is significant and often outperforms the standard chirp signal by a great amount.

In other papers like [18] and [19] the authors extend the problem to practical implementations using discrete time signals, so as to search for our optimal transmit signal in finite dimensional vector spaces. The target impulse response can be now be modeled by a matrix and the optimal solution is the eigen vector associated with the minimum eigen value of the correlated noise and clutter correlation matrix. But the underlying idea remains the same - to place maximum energy in the dimensions having minimum interference. Several versions of this approach have been tried - where the transmit vector is either along the best dimension, or is allowed to span several of the better dimensions giving it more flexibility to spread out over the entire band not occupied by clutter. The second approach takes advantage of the rank deficient nature of interference and makes use of all the eigenvectors which have eigenvalues at or below the noise level. A third method where the constructed waveform is made to resemble one of the traditional radar waveforms, like the linear frequency modulated (LFM) chirp is also provided. Such waveforms have a lot of other desirable characteristics besides providing the maximum SINR, and are seen to be more appropriate with respect to other radar parameters. However the fundamental

idea behind each of these approaches does not change, and that is to somehow concentrate all the interference energy in a specific portion of the spectrum. The radar transmit waveform can then be made to occupy a temporal eigen space orthogonal to this interference region, where no clutter can exists. However this may or may not be entirely possible depending on the interference power spread across the spectrum. If the clutter is significant, then there may not be any 'empty' portions in the eigen spectrum for the transmit waveform to fill. But the whole idea can be better exploited, if we opt for space-time codes instead of pure temporal codes. With these codes, we have more space-time degrees of freedom or more flexibility available to confine our clutter to a smaller subspace, or place our transmit energy in subspaces independent of clutter.

Thus we find that although all these methods are useful and potent in their own respect, none of them make use of the real potential of space-time codes as shown in Figure 1.3. Moreover all these algorithms are designed to give optimal code for just one target – point or distributed. In any real life radar scenario there are bound to be multiple targets present at any given time. Thus there is a need to come up with codes which give maximum SINR for multiple scattered targets, or which are optimized with respect to more than one target simultaneously. Also, in all these algorithms there is a tradeoff between SINR improvement and the quality of the radar waveform. As the eigen space used to find the optimal waveform gets smaller, the optimized waveform gets poorer with respect to other characteristics like resolution and ability to control sidelobes. For example in [19] the optimized waveform for

detection of T-72 battle tank turns out to be long duration, narrow band continuous waveform (CW). Although such a long duration CW waveform is consistent with the idea of placing the transmitted energy in a narrow band of spectrum not occupied by clutter, it does not provide the necessary range resolution which is inversely proportional to the signal bandwidth [1].

In addition none of these optimal waveform–matched illumination concepts seem to work well in the cases of high clutter to noise ratio (CNR), which is typically the case for stationary ground targets. As a result these optimized waveforms will find application mainly for a moving target indicator (MTI), rather than a traditional SAR which images stationary objects. All these factors contributed to the motivation for this research - towards finding true and optimal space time codes for improving radar performance in multiple modes. Before we go about describing some of the other advantages of true space-time codes, the topic of the next section, let's briefly touch upon the subject of space time codes and beamforming in the area of wireless communications.

1.2.4 Space-Time Codes for Communications

A lot of work has been done in the field of space-time coding for communications [20-25]. Space-time codes are used in communications mainly to overcome the effects of fading, and also achieve higher data rates. Temporal and spatial correlation is introduced into signals being transmitted from different transmit antennas, which provides diversity at the receiver even with a single receive element - as done in the Alamouti scheme [24, 25]. Thus using space-time codes, more data can

be transmitted over a multi-path fading channel for the same amount of available bandwidth. This effectively means saving time and bandwidth at the expense of extra spatial dimensions, and thus directly translates to coding gain or increased system capacity. Although there are a few similarities between space-time codes for communications and radars, they inherently remain two different problems. To understand this difference, let's once again consider the two fundamental goals of a space-time code or any transmit code for that matter –

- To make all the responses as energetic as possible, so that they stay above the noise level.

- To make all the responses as uncorrelated as possible, so that they can be distinguished at the receiver.

In the case of communication systems, these responses correspond to the various symbols being transmitted over the channel, while for a radar, the responses are from the different targets we are trying to image. Now for a communication system we have a number of different transmit symbols (depending on the modulation scheme), going over the single channel. Hence for each symbol, we are allowed to come up the best space-time code for the same propagation channel. The solution is therefore a code matrix, where each column is the optimum code for one transmitted symbol. This communications space-time problem is illustrated in Figure 1.4. The channel is modeled as a matrix $\overline{\overline{\mathbf{H}}}$, the space-time vectors for each of the transmitted symbol are denoted by $\overline{\mathbf{s}}_1, \overline{\mathbf{s}}_2 \dots \overline{\mathbf{s}}_n$, and the corresponding channel responses

as $\bar{\mathbf{\rho}}_1, \bar{\mathbf{\rho}}_2 \dots \bar{\mathbf{\rho}}_n$. The goal is to form a code matrix $\bar{\bar{\mathbf{S}}} = \left[\, \bar{\mathbf{s}}_1\, \bar{\mathbf{s}}_2 \dots \bar{\mathbf{s}}_n \,\right]$ such that the

matrix $\bar{\bar{\mathbf{P}}} = \left[\, \bar{\mathbf{\rho}}_1\, \bar{\mathbf{\rho}}_2 \dots \bar{\mathbf{\rho}}_n \,\right]$ turns out to be unitary (assuming unit energy for each

transmit code vector).
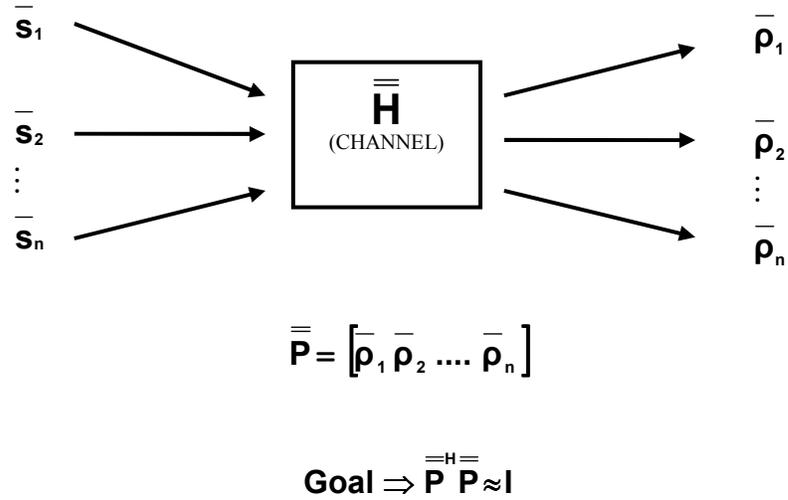
Figure 1:4 Space Time Codes for Communications

Note: The superscript ^{H} stands for conjugate transpose and **I** is the identity matrix.

Contrast this with the space time code problem for radar shown in Figure 1:5 on the

next page.
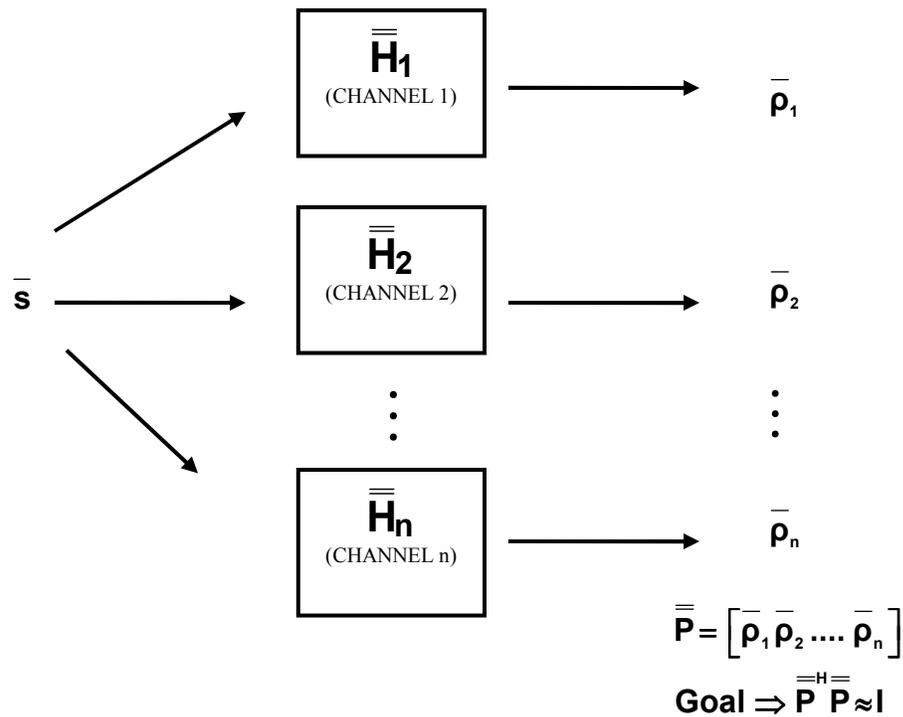
Figure 1:5 Space Time Code for Radar

As can be seen, for the radar problem we have just one space-time transmit signal, and multiple channels as each target has a different location in space. The propagation paths from the transmitter to individual targets, and also back to the receiver make up several independent channels. Also there is no notion of multiple transmit signals, as the radar is not involved in transmission of information unlike a communication system. We just have one transmit code for a given scenario, and need to find that one code which will optimize the performance for several different channels concomitantly. Thus the optimal solution for this problem is a vector - $\overline{\overline{s}}$, and not a matrix like the previous case. Clearly this is a more difficult, more challenging problem than before, and makes up for a really interesting study.

1.2.5 Smart Antennas

A final word about the space-time beamforming techniques employed in wireless communications before moving onto the next section. These techniques employ multiple transmit apertures for controlling the antenna illumination pattern, and can thus be considered as a form of space-time coding (although as will be seen, not the *true space time coding* defined previously). Probably the most prevalent application of this technique in cellular communications is "smart antennas" [26-28].

Smart antennas consist of a number of apertures and can be used to dynamically change or fine tune the coverage pattern based on the changing traffic and RF conditions in the cell. The magnitude and phase associated with each array element can be dynamically controlled, for beam-steering or synthesizing sculpted illumination patterns to suit the topology of a cell or sector (much like the phased array approach). Highly directional beams can be obtained both on the transmit and receive sides, which result in reduced network interference. Since cellular systems are mainly interference limited, this results in higher capacities, improved quality and better coverage. The whole idea of using a narrow beam to track each mobile in the network and minimize interference from unwanted directions, is very analogous to the radar problem, where we want to put energy on only those areas which we wish to detect or estimate, and no energy on areas we are not interested in. Figure 1:6 highlights the concept of a smart antenna system.

Figure 1:6 Smart Antenna concept - Sculpted patterns to fit the topology of the sector. Minimizes transmit power, reduces interference and balances load [28]

Even though it may seem like smart-antennas are the solution to the "space-time illumination optimization" criterion described before, essentially they are just the phased array systems of Figure 1.3. The fact that each array element propagates the same time-frequency signal (just modified in magnitude and phase at each antenna) weans away a lot of power from the transmit array. As seen before, the degrees of freedom available to such an arrangement are far lesser than that to a true space-time structure, which directly affects the effectiveness of these systems in coming up with the desired illumination patterns. Similar work has been done in the field of radars where the spatial pattern is used to place nulls in the direction of maximum disturbance [29]. In all these cases the only unknowns to be determined are

the complex weights on each of the spatial apertures, and thus the transmit vector reduces to a plain spatial code; but that is completely different from what we striving for in this research – "*dissimilar time-frequency signals on each transmit element or true, non-separable space time solutions*". We now move on to the next section, which outlines some of the other propelling factors behind the true space-time code design.

1.3 True Space-Time Codes – Motivation

This topic probably does not require separate categorization as we have already covered many advantages of space-time coding and processing in our earlier sections; but it might still be a good idea to summarize all the points at one place. Like stated before, the true potential of a multi-aperture transmit array is realized only when each antenna propagates a different function of time and frequency – i.e. it acts as a "true space-time transmitter". Since dissimilar signals are present at each transmitter (satellite), the solution is a non-separable code in space and time. Such signals exploit a greater fraction of the available degrees of freedom and thus result in a better radar performance. Here we synopsize some of the major advantages of true space-time codes:

- Better radar performances using the same transmit power and radar resolution.
- Reduced receiver complexity – if the optimal code results in all target responses to be equally energized and uncorrelated, then all linear estimators become equivalent and a simple matched filter can be used.

- Equal distribution of power across all satellites in space-borne radar.

- Improving performance in multiple modes – SAR and GMTI, and also simultaneous mode operation.

- Minimizing vulnerability to jammers, as the signal on each target location is not related by a simple translation in delay and doppler and hence is not predictable.

But coming up with such true space-time signals is much more difficult, as now we need to determine the optimum weights for all the transmitted samples on each of the transmit antennas, and not the weights just for the antennas. Ideally we would like our code to be the perfect code described earlier, i.e. the one which illuminates all targets equally, does not illuminate any clutter, and at the same time makes responses from all targets orthogonal. However such a code does not exist (except for the simplest of problems), and hence we endeavor to find an optimal code for some other optimization criteria. Examples for the different optimization criteria can be:

- Maximize the average energy on all targets

- Minimize the average energy on all clutter objects

- Maximize the ratio of total signal (target) to clutter energy - SCR

- Maximize the SCR for the target receiving the worst SCR

- Minimize the maximum correlation between any two targets

The first four rules come under the purview of this thesis and have been covered in sufficient detail. The fifth has been dealt extensively in [8] as it comes under the

domain of "ambiguity optimization". The objective of this study is thus, to come up with the mathematical and algorithmic knowledge required to construct space-time transmit waveforms, for a high altitude multi-aperture SAR, which are optimal with respect to specific optimization criteria.

1.4 Organization of the Document

In the following chapters of this thesis we describe our work towards the optimal waveform construction. Chapter 2 starts with the description of the space-time radar model used to simulate the radar geometry, propagation physics and target distribution. The model is represented in terms of vector matrix relations. We also introduce a transmit signal model that defines a search space in which to hunt for our best transmit code. Although the search-space can theoretically be infinite dimensional, some constraints are placed on the type of transmit signals we can come up with depending upon our choice of basis functions. This method allows for numeric implementation and application of linear algebraic techniques to our problem, which also forms the core of our design algorithms. Later on we merge the two models, to define one overall composite model. Derivation of some of the numeric model parameters used as default inputs to our model has also been included.

Chapter 3 starts with the actual *space-time illumination optimization* concept. Some of the basic optimization criteria and associated algorithms are introduced. The functioning of these standard algorithms is explained, and results are provided to validate their performance. Few of the early issues that we encountered while

embarking on this path have also been highlighted. The chapter ends with some of the limitations of these basic or standard codes, which call for the design of more advanced algorithms.

Chapter 4 describes the four types of advanced algorithms developed - the Maxi-mins, which enable us to overcome one of the major shortcomings of the standard codes – "*the orphan problem*". We explain how these algorithms are different mathematically, and their success is demonstrated through simulation results for a number of different scenarios. Based on the numerous results we converge to one of these four algorithms, the best or our *champion code*.

In Chapter 5 a more detailed analysis is performed to understand the true nature of these advanced algorithms, and also confirm their optimality. The focus is not on "how well the algorithms work", but more on "why they work". Two new methods for applying the maxi-min criteria are also derived, their operation studied, and performance evaluated.

Chapter 6 is probably the most interesting chapter in this thesis and demonstrates the power of space-time codes for a number of diverse applications. This chapter is full of results showing how space-time codes are different, better and much more versatile than the other kind of spatial codes. Some new discoveries were made along the path, and have also been documented.

Chapter 7 contains a few other approaches that were tried during this study, but do not make up for as big a story as the earlier ones. Nevertheless these approaches brought out some interesting points of their own, and have potential

utility for specific applications. Relevant results are provided to support this claim. The chapter also includes two of the more ambitious ideas that were tried but did not work, more specifically trying to de-correlate the target responses by means of suitable transmit codes, and coming up with optimal transmit solution for the MTI problem. However the chapter does give useful insights into these problems, and provides us with possible pointers towards future work.

Chapter 8 is the last chapter and winds up all the work that has been done in this research. We summarize all the ideas, present conclusions and end by giving possible recommendations for future work.

Chapter 2

Radar Models

2.1 Need for Radar Models

We needed a transmission, target and propagation model [30] to represent our space-time radar and come up with the optimal transmit codes. This software model was implemented in Matlab and in the absence of actual SAR data, allows for the testing and evaluations of various transmit code algorithms. The model was kept fairly simple and is based on the physical assumptions of flat earth, far-field, single polarization and free space. However it is still fairly accurate in its representation of the physics behind a space-time radar illuminating an arbitrary target set, which can consist of any combination of point, distributed, stationary, moving, airborne and surface targets.

In addition we also required a transmit signal model [31] to represent the radar transmit signal as a complex superposition of orthogonal basis functions. This method reduces the problem of finding an optimal transmit signal, to that of finding the complex weights for each of the basis functions. In other words, now we just have to find an optimal transmit vector the complex coefficients of which completely describe the optimal transmit waveform. Therefore these models enable the representation of the space-time radar scenario with vector matrix notations, and thus the application of linear algebraic techniques (eigen analysis) to come up with the solutions.

2.2 Transmission, Target and Propagation Model

This section aims at giving a brief insight into the mathematics behind signal propagation from the radar to a collection of scatterers and then back to the receiver. The readers are referred to [8, 28] for a more detailed description. The radar transmit signal is a function of both space and time and can be modeled as a superposition of N basis functions.

$$s(\bar{z}) = \sum_{n=1}^{N} s_n \, \phi_n(\bar{z}) \tag{2.1}$$

The basis functions ϕ are functions of 3-D space, time and frequency collectively spanning the entire timewidth, bandwidth and the spatial extent of the of the radar array. The vector $\bar{z}$ is therefore a 5-D vector, spanning three dimensions of space - *x, y* and *z,* and one each of slow time *t* and fast frequency *w*.

$$\bar{z} = \begin{bmatrix} x & y & z & t & w \end{bmatrix}^{T} \tag{2.2}$$

One of the simplest ways to represent the transmit signal in terms of basis functions, is to think of each basis function as a time-frequency sample present at one of the spatial transmitters. The vector **s** containing the complex weights s_n for each of the time frequency samples (basis functions) will then represents the transmit signal completely.

$$\mathbf{s} = \begin{bmatrix} s_1 & s_2 & s_3 & \cdots & s_N \end{bmatrix}^{T} \tag{2.3}$$

Note that this is only one of the many possible, and probably the simplest of ways to represent our transmit signal. The choice of the basis functions actually plays a very

important role in the ability of our algorithms to come up with best transmit code (as will be seen in later chapters). The example of using 'samples' as our basis functions is just provided for illustration purposes - the actual basis functions used were very different and form the topic of the next section. The radar transmit signal propagates to the targets where it illuminates a set of scatterers. The joint target scattering response can also be modeled as a combination of N_t orthonormal basis functions, where N_t is the number of targets.

$$\gamma(\bar{y}) = \sum_{t=1}^{N_t} \gamma_t \, \psi_t(\bar{y}) \tag{2.4}$$

The basis functions ψ are functions of 3-D space and radial velocity. Each of them represents a point or distributed target, at different locations and different velocities. The weights γ_t are the complex scattering coefficients associated with each target, and weigh the corresponding basis functions appropriately. The vector $\boldsymbol{\gamma}$ of complex scattering coefficients γ_t then defines the set of illuminated targets completely.

$$\bar{y} = \begin{bmatrix} x & y & z & v_r \end{bmatrix}^T \tag{2.5}$$

$$\boldsymbol{\gamma} = \begin{bmatrix} \gamma_1 & \gamma_2 & \gamma_3 & \cdots & \gamma_{N_t} \end{bmatrix}^T \tag{2.6}$$

Actually for our case i.e. the problem of space-time illumination optimization, we need not go any further while modeling the radar propagation. It is because the illumination problem is concerned only with the propagation from the transmitter to the illuminated targets. In fact even the knowledge of target scattering coefficients is extraneous and is unnecessary for the problem at hand. However for the sake of

completeness, the whole model which was developed for propagation from the transmitter to the targets and back to the receiver will be presented, and then the relevant portion applicable to our case will be pointed out.

Continuing with our discussion, the energy scattered from the targets propagates back to the receiver where the received signal can again be modeled as a function of space and time. More accurately it can be represented as a weighted superposition of M orthonormal space-time basis functions, where M is the total number of received measurements over the entire spatial extent of the array.

$$r(\overline{x}) = \sum_{m=1}^{M} r_m \; \varphi_m(\overline{x}) \tag{2.7}$$

The basis functions φ are again functions of 3-D space, slow time and fast frequency. They describe the receive array aperture and the time frequency sampling function of the receiver. The complex weights r_m can be thought of as the receive A to D samples which weigh these basis functions to result in the complete space-time receive signal. The vector $\overline{x}$ is again a 5-D vector of space and time and the vector $\mathbf{r}$ of complex weights r_m completely defines the received space-time signal.

$$\overline{x} = \begin{bmatrix} x & y & z & t & w \end{bmatrix}^T \tag{2.8}$$

$$\mathbf{r} = \begin{bmatrix} r_1 & r_2 & r_3 & \cdots & r_M \end{bmatrix}^T \tag{2.9}$$

The aim of the whole model was to come up with this receive vector $\mathbf{r}$ for a given space-time transmitter and an arbitrary collection of scatterers, accurately modeling the radar physics and propagation effects. From (2.7), the received complex weights can be expressed as:

$$r_m = \int r(\bar{x})\, \varphi_m(\bar{x})\, d\bar{x} \qquad (2.10)$$

However, the transmitted, target and receive functions are also related by the following convolution integral through the dyadic Green's propagation functions [33].

$$r(\bar{x}) = \int \ddot{H}(\bar{x};\bar{y}).\gamma(\bar{y}).\int \ddot{G}(\bar{y};\bar{z}).s(\bar{z})\, d\bar{z}\, d\bar{y} \qquad (2.11)$$

Where the functions $\ddot{G}(\bar{y};\bar{z})$ and $\ddot{H}(\bar{x};\bar{y})$ are the dyadic Green's functions describing the propagation from the radar transmitter to the targets and back to the receiver respectively. Rest all parameters are as defined earlier. Using (2.11) in (2.10) we get:

$$r_m = \int \varphi_m(\bar{x})\int \ddot{H}(\bar{x};\bar{y}).\gamma(\bar{y}).\int \ddot{G}(\bar{y};\bar{z}).s(\bar{z})\, d\bar{z}\, d\bar{y}\, d\bar{x} \qquad (2.12)$$

And then inserting the expansions of (2.1) and (2.4) we have:

$$r_m = \sum_{t=1}^{N_t} \gamma_t \sum_{n=1}^{N} s_n \int \varphi_m(\bar{x})\int \ddot{H}(\bar{x};\bar{y}).\psi_t(\bar{y}).\int \ddot{G}(\bar{y};\bar{z}).\phi_n(\bar{z})\, d\bar{z}\, d\bar{y}\, d\bar{x}$$

$$= \sum_{t=1}^{N_t} \gamma_t \sum_{n=1}^{N} s_n H_{mn}^t \qquad (2.13)$$

Where the complex value H_{mn}^t is given by:

$$H_{mn}^t = \int \varphi_m(\bar{x})\int \ddot{H}(\bar{x};\bar{y}).\psi_t(\bar{y}).\int \ddot{G}(\bar{y};\bar{z}).\phi_n(\bar{z})\, d\bar{z}\, d\bar{y}\, d\bar{x} \qquad (2.14)$$

The result of (2.13) can be expressed in vector-matrix notation as:

$$r = \sum_{t=1}^{N_t} \gamma_t \, \mathbf{H}_t \, \mathbf{s} + \mathbf{n}$$

$$= \sum_{t=1}^{N_t} \gamma_t \, \rho_t + \mathbf{n} \tag{2.15}$$

where $\mathbf{H}_t$ is a M x N matrix for each target, with the elements H_{mn}^t.

$$\mathbf{H}_t = \begin{pmatrix} H_{11}^t & \cdots & H_{1N}^t \\ \vdots & \ddots & \vdots \\ H_{M1}^t & \cdots & H_{MN}^t \end{pmatrix} \tag{2.16}$$

Vector $\mathbf{n}$ is simply the additive noise in the measurement vector, and vector $\rho_t = \mathbf{H}_t \, \mathbf{s}$ is the normalized response from the tth target (assuming complete reflection).

Thus the matrix $\mathbf{H}_t$ completely characterizes the propagation from the transmitter to the target and back to the receiver for target t. This set of N_t matrices are critical parameters for all our simulations and optimization procedures and need to accurately represent the propagation effects based on the physical scenario, transmitter-receiver geometry, and target distribution. The transmission, target and propagation model was therefore developed [30] and coded in Matlab for this purpose, which takes into account all the factors like radar location, altitude, velocity, look angle, number of transmitters, targets etc. The actual implementation details can be found in [8].

Before moving on to our transmit signal model it would be a good idea to clarify an important point that was mentioned before. For the target illumination problem we just need part of the model which reflects the propagation from the

space-time transmitter to the illuminated targets. As a result only half of the aforementioned model is used for all our optimization algorithms and test cases. More specifically, from [30] it can be seen that when the model is coded or implemented in software, the individual elements of the $\mathbf{H}_t$ matrices are given by:

$$H_{mn}^t = g_h(m,n:t)e^{-j\mathbf{x}_m^{sT}\mathbf{K}_\phi^{sT}\mathbf{y}_t}e^{-j\mathbf{y}_t^T\mathbf{K}_\theta^s\mathbf{z}_n^s}e^{-j\mathbf{y}_t^T(\mathbf{K}_\phi^t+\mathbf{K}_\theta^t)\mathbf{z}_n^t} \qquad (2.17)$$

In this expression $g_h(m,n:t)$ is a complex weighting function that relates the transmit samples to the receive samples for a given target. This function can be split into its spatial and temporal components which relate spatial and time-frequency samples respectively, on both transmit and receive sides. We can think of the spatial function as being made up of additional antenna weighting functions or antenna tapers at the transmitter and receiver, and the temporal function as an interpolation function that takes into account the contribution of multiple time-pulses in one observation window for near and far targets. The two matrices $\mathbf{K}_\theta$ and $\mathbf{K}_\phi$ are real valued frequency matrices which relate the transmit signal space to the target position space and the target position space to the receive signal space respectively. Basically these matrices provide information about the rate of change of phase of the received radar signal with respect to various radar and target parameters. For the exact derivation and interpretation of these matrices the readers are referred to [8, 34]. These matrices can be further partitioned into their spatial and temporal components:

$$\mathbf{K}_\theta = \begin{bmatrix} \mathbf{K}_\theta^s & \mathbf{K}_\theta^t \end{bmatrix} \qquad (2.18)$$

$$\mathbf{K}_\phi = \begin{bmatrix} \mathbf{K}_\phi^s & \mathbf{K}_\phi^t \end{bmatrix} \qquad (2.19)$$

The vectors $\mathbf{z}_n$, $\mathbf{y}_t$ and $\mathbf{x}_m$ are real valued position vectors of the nth transmit sample, t^{th} target and the mth received sample in the transmit, target and receive signal space respectively. Transmit and receive sample position vectors can be further split into their spatial and temporal components as:

$$\mathbf{z}_n = \left[(\mathbf{z}_n^s)^T \quad (\mathbf{z}_n^t)^T \right] \tag{2.20}$$

$$\mathbf{x}_m = \left[(\mathbf{x}_m^s)^T \quad (\mathbf{x}_m^t)^T \right] \tag{2.21}$$

The matrix $\mathbf{H}_t$ is M by N in size where N is the number of transmitted space-time samples and is given by:

$N = J \times K$
$J =$ Number of transmit antennas
$K =$ Number of transmit time-frequency samples on each antenna
$$\tag{2.22}$$

M is the number of received space-time samples and is given by:

$M = I \times K'$
$I =$ Number of receive antennas
$K' =$ Number of receive time-frequency samples on each antenna
$$\tag{2.23}$$

Having explained all the individual terms, it can be seen from (2.17) that the exponential $e^{-j\mathbf{y}_t^T \mathbf{K}_\theta^s \mathbf{z}_n^s} e^{-j\mathbf{y}_t^T (\mathbf{K}_\theta^t)\mathbf{z}_n^t}$ essentially describes the propagation from the transmitter to the target, while the exponential $e^{-j\mathbf{x}_m^{sT} \mathbf{K}_\phi^{sT} \mathbf{y}_t} e^{-j\mathbf{y}_t^T (\mathbf{K}_\phi^t)\mathbf{z}_n^t}$ accounts for the extra path from the targets to the receiver. Since we are just interested in the propagation till the targets, the second term can be left out in the construction of $\mathbf{H}_t$ matrices for our case. Also, we do not have any concept of multiple receive antennas

(*I* receive elements) for the illumination problem. Instead we can think of a single receive antenna being present at each of the targets which receives all the temporal samples of the transmitted signal. Hence the number of receive samples for this case will not be *M* (total space-time receive samples at *I* elements), but will be equal to the number of temporal samples at each of the targets - K'. Thus the $\mathbf{H}_t$ matrices for this case of illumination optimization problem are constructed as:

$$H_{k'n}^t = g_h(k',n:t)e^{-j\mathbf{y}_t^T\mathbf{K}_\theta^s\mathbf{z}_n^s}e^{-j\mathbf{y}_t^T(\mathbf{K}_\theta^t)\mathbf{z}_n^t} \tag{2.24}$$

where $H_{k'n}^t$ are the individual elements and each matrix is K' by N in size. For our optimization algorithms we need the $\mathbf{H}_t$ matrices for all targets, and sometimes also the normalized response $\boldsymbol{\rho}_t$ for evaluating the various algorithm performances. Thus these are the two critical parameters extracted from the transmission, target and propagation model.

2.3 Transmit Signal Model

2.3.1 Introduction

To accomplish our goal of finding optimal transmit signals for different optimization criteria, we write our space-time transmit signal as a weighted superposition of orthonormal basis functions. This warrants a need for a transmit signal model which has been described in this section. The way we expand our transmit signal in terms of various basis functions is very important, as the choice of basis functions has been seen to play a crucial role in extracting good answers from

our optimization algorithms. Significant improvement in performance was observed when the narrow timewidth, narrow bandwidth basis functions (samples or pulses) were replaced by wide timewidth-wide bandwidth functions. Hence this model has been covered in substantial detail in this section, and along with the earlier transmission and propagation model provides a complete structure for determining optimal space-time codes for various criteria.

As mentioned before, if we expand our arbitrary space-time waveform using a set of orthonormal basis functions, then the whole problem of finding an optimal transmit signal reduces to one of finding the optimal weight for each basis function. Finding an optimal set of complex weights is akin to finding the best vector in a multi-dimensional space, and allows for the direct use of linear algebraic techniques like eigen value/eigen vector analysis.

In this section the mathematics describing the construction of a radar signal from a set of wide timewidth-wide bandwidth temporal basis functions distributed across all elements of the transmit array has been proposed. These space-time basis functions can be separated into their spatial and temporal components. Each of the temporal basis functions spans the full timewidth and bandwidth of the radar and is a good radar signal in itself. A methodology of coming up with new basis functions from standard "mother functions", by shifting them in time and frequency has also been presented. Once again, only the salient features of the model have been included here. For a more complete description the readers are referred to [31].

2.3.2 Inputs to the Transmit Signal Model

Let's start our description by defining some of the model inputs:

f_c = carrier frequency (Hz)

B = transmit signal bandwidth (Hz)

f_o = pulse repetition frequency – PRF (Hz)

U = integer number of pulses transmitted as part of the transmit signal (kept odd to simplify the math)

Q = odd number of 'fast-time' basis functions

P = odd number of 'slow-time' basis functions

$g_s(t)$ = a 'mother function' used to generate new slow-time basis functions

$G_f(w)$ = a 'mother function' used to generate new fast-time basis functions

$\{ \tau_q \}$ = Q time delay values used to generate all the fast-time basis functions

$\{ w_p \}$ = P frequency shift values used to generate all the slow-time basis functions

Some other parameters which can be derived from the above set of primary parameters are:

$1/f_o = T_o$ = pulse repetition interval – PRI (sec)

$UT_o = $ T = transmit signal timewidth (sec)

$w_o = 2\pi f_o$ = angular pulse repetition frequency (radians/sec)

$w_c = 2\pi f_c$ = angular carrier frequency (radians/sec)

2.3.3 Signal Construction

We know that any real valued temporal signal can be expressed as:

$$v_s(t) = \text{Re}\{S(t)e^{-jw_ct}\} \tag{2.25}$$

Here $S(t)$ is a complex function describing the magnitude and phase, or the part containing all the real information about our transmit signal. This is the function we are trying to optimize for a number of different optimization criteria. For this purpose, $S(t)$ can be written as a weighted superposition of $R = PQ$ complex basis functions $\psi_{pq}(t)$:

$$S(t) = \sum_p \sum_q S_{pq} \psi_{pq}(t) \tag{2.26}$$

Note that we are just dealing with temporal signals here; there is no concept of space-time yet. The two indices 'p' and 'q' are used as each of these basis functions is in turn written as a product of a slow, and a fast time basis function.

$$\psi_{pq}(t) = s_p(t) \sum_u f_q(t - uT_o)e^{jw_c uT_o} \tag{2.27}$$

The slow and the fast time basis functions cannot exist independently, and are always used in conjunction. From (2.25) – (2.27) it is evident that the set of weights S_{pq} completely describe our transmit signal, and thus the goal of all our optimization algorithms is to come up with the optimal set of values for these weights. These set of PQ weights can be expressed in the form of a vector $\mathbf{S^t}$ of dimension R by 1, where:

$$R = P x Q \tag{2.28}$$

$$\mathbf{S^t} = [S_1 \ S_2 \ S_3 \cdots S_R]^T \tag{2.29}$$

As mentioned before, this approach reduces the problem to searching for the best vector in an *R* dimensional space, and therefore directly calls for the use of linear algebraic tools like eigen analysis; more on that later.

Moving on with our discussion of basis functions, the functions $s_p(t)$ describe a set of *P* slow-time functions having a narrow bandwidth and wide timewidth *T* (i.e. a kind of phase envelope over the entire duration of the transmit signal). Similarly the functions $f_q(t)$ describe a set of fast-time basis functions, each with a narrow timewidth and wide bandwidth B (i.e. like a pulse function). Thus the function $\sum_u f_q(t - uT_o)e^{jw_c uT_o}$ describes a full train of *U* pulses, each coming after the PRI of T_o. The exponential $e^{jw_c uT_o}$ accounts for the carrier phase at the instant of each pulse. For different fast time basis functions - $f_q(t)$, we have different pulse trains. Each of these unique pulse trains weighted by the phase envelope $s_p(t)$ describes a single basis function. It should be obvious then that more are the available choices in terms of the types of pulse trains - $f_q(t)$ and phase envelopes - $s_p(t)$, more are the available degrees of freedom, and more are the chances of coming up with a better transmit signal. This point is validated in one of the later chapters where the performance of our algorithms is seen to improve tremendously with the increase in the number of basis functions.

2.3.4 Fast and Slow Time Basis Function Design

Having expressed the transmit signal in terms of the various fast and slow time basis functions, the next step is to come up with a procedure for generating different basis functions from some kind of a standard function. The different fast and slow time basis functions are derived from a mother function each, by delaying the fast and slow time mother functions in time and frequency respectively. The mother function has to be carefully selected to satisfy the property of narrow time width, wide bandwidth for the fast time and wide timewidth, narrow bandwidth, for the slow time basis functions.

For e.g. the fast time basis functions $f_q(t)$ are just a delayed version of a mother function $g_f(t)$.

$$f_q(t) = g_f(t - \tau_q) e^{j w_c \tau_q}, \text{ where } \tau_q \ll T_o \quad (2.30)$$

For satisfying the earlier stated requirements and also simplifying the math, this mother function is made to have certain properties like – unit energy, even function, narrow timewidth and wide bandwidth.

Similarly the different slow time basis functions $s_p(t)$ are expressed in the frequency domain as a delayed version of the Fourier transform of a mother function $G_s(w)$.

$$S_p(w) = G_s(w - w_p), \text{ where } w_p \ll w_o \quad (2.31)$$

$$S_p(w) = \int_{-\infty}^{+\infty} s_p(t) e^{-jwt} \, dt \quad (2.32)$$

and
$$G_s(w) = S_0(w) \qquad\qquad (2.33)$$

is the non-delayed frequency domain mother function corresponding to the 0th slow-time basis function. The mother function $G_s(w)$ also has similar properties like it's even, has unit energy but is wide timewidth and narrow bandwidth unlike the fast-time mother function.

As an example, the derivation of two fast time basis functions $f_0(t)$ and $f_1(t)$ has been shown from the same mother function in Figure 2:1 on the next page. The mother function $g_f(t)$ in this case is a sinc waveform which satisfies all the above stated requirements. As can be seen the two basis functions are just a time shifted version of each other where the time shift is τ_q.
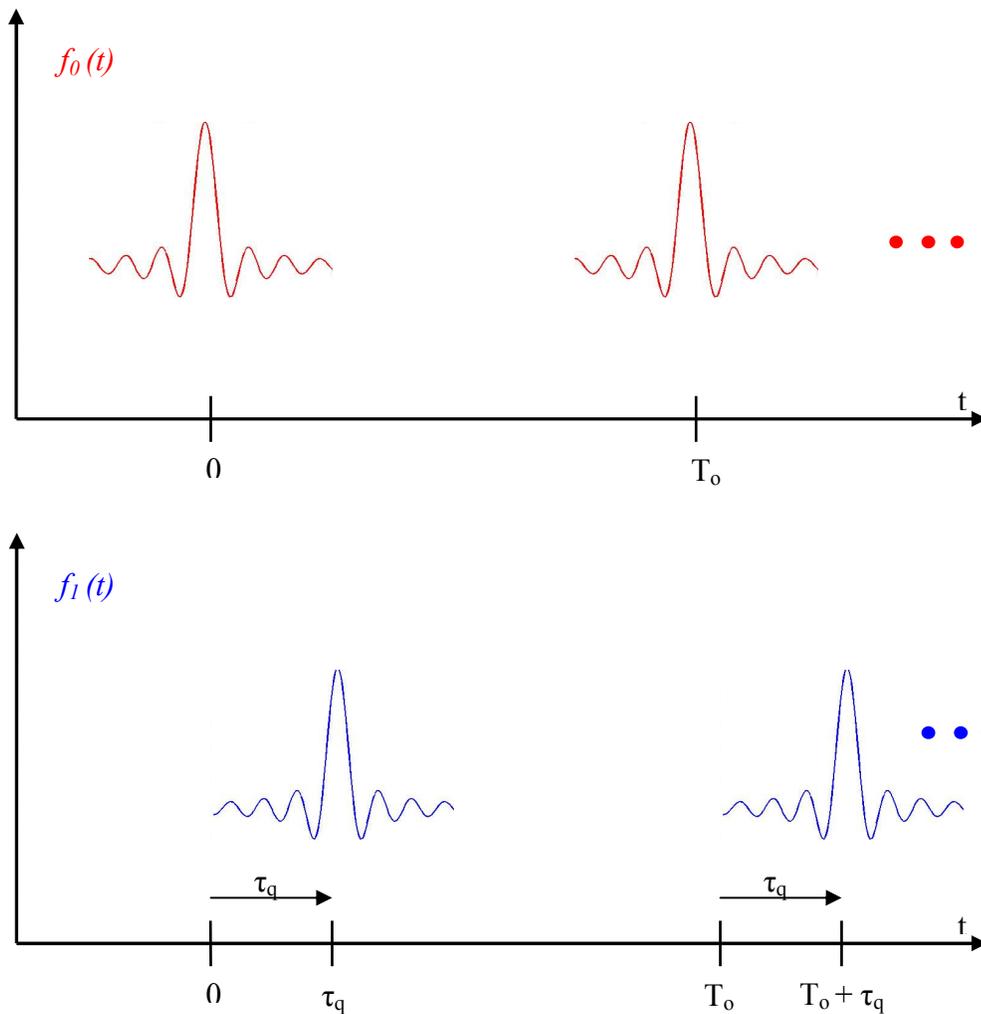
Figure 2:1 Generation of fast time basis functions from the time domain sinc mother function

Similarly the different slow time basis functions can be visualized in the frequency domain as the frequency shifted version of the same mother function $G_s(w)$. Once again the frequency domain mother function is considered to be a sinc. The two basis functions are separated by a translation w_p in the frequency domain which metamorphizes into a phase shift in the time domain.
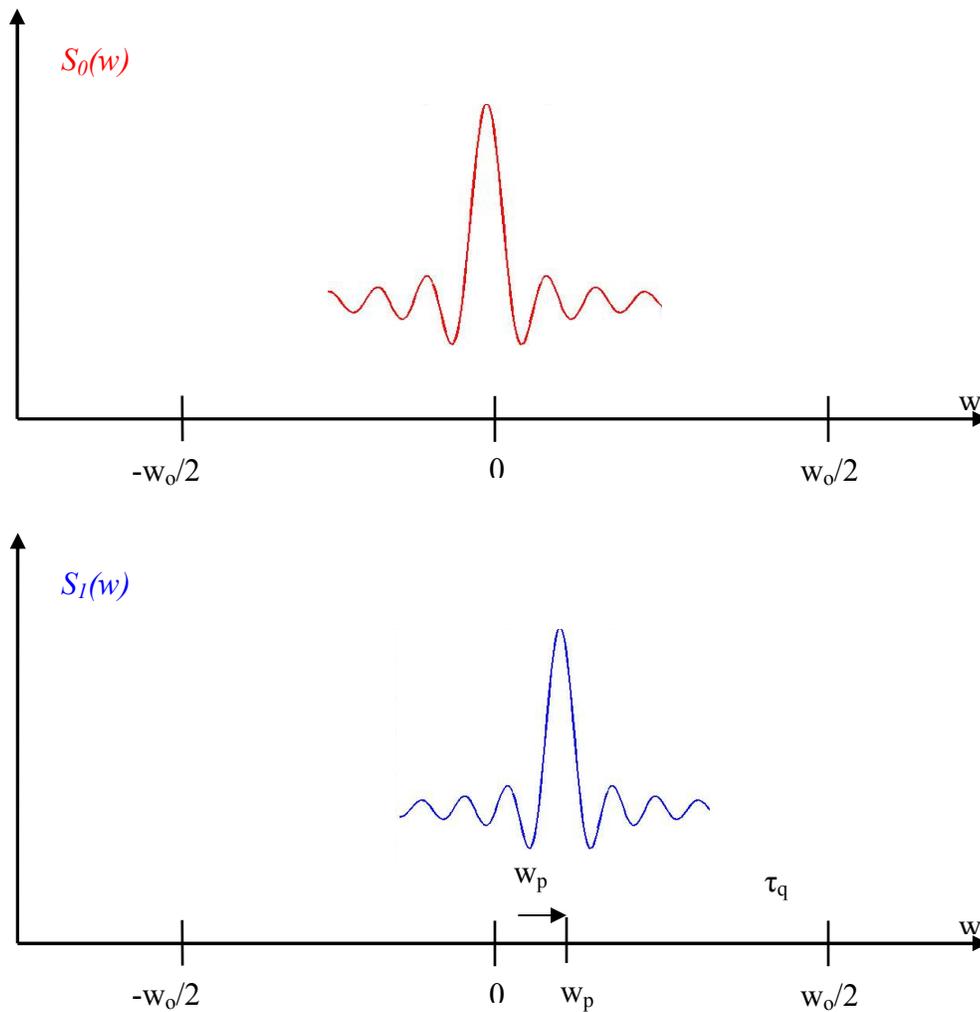
Figure 2:2 Generation of slow time basis functions from the frequency domain sinc mother function

An important point which comes out from this illustration is the constraint on the values of P and Q, or the number of slow and fast time basis functions we can have. Although more number of basis functions means more degrees of freedom and thus more flexibility in constructing our transmit signal, the number of basis functions cannot be increased arbitrarily. Besides the obvious downside of increasing the length

of the simulation (more basis functions is equal to a larger dimensional search space) the number of basis functions are limited by the PRF of the radar. As can be seen from Figures 2:1 and 2:2 the values of P and Q are limited by the following two inequalities:

$$Q\tau_q \leq T_0 \tag{2.34}$$

$$Pw_p \leq w_0 \tag{2.35}$$

For higher values of P and Q the fast and slow time basis functions would leak into the next time and frequency window, and would essentially wrap around to result in the same basis functions as before. Thus increasing the number of basis functions beyond a point does not yield any additional advantage. The PRF along with the radar time and bandwidth, sets an upper limit on the number of slow and fast time basis functions that can be used.

2.3.5 Sampled Windowed Fourier Transform of *S (t)*

Now that we have the definitions of our slow and fast time basis functions, we can use them in (2.26)-(2.27) to come up with our complete expression for the radar transmit signal. Noting that:

$$s_p(t) = \frac{1}{2\pi} \int_{-\infty}^{+\infty} S_p(w) e^{jwt} \, dw \tag{2.36}$$

And using this with (2.27) in (2.26), we get:

$$S(t) = \sum_p \sum_q S_{pq} \frac{1}{2\pi} \int_{-\infty}^{+\infty} S_p(w) e^{jwt} \, dw \sum_u f_q(t - uT_o) e^{j\omega_c uT_o} \tag{2.37}$$

43

After some simplifications and using the earlier expressions from (2.31) – (2.33), it can be shown that:

$$S(t) = \sum_p \sum_q S_{pq} \, e^{j\omega_p t} \, g_s(t) \sum_u f_q(t - uT_o) e^{j\omega_c uT_o} \tag{2.38}$$

where $g_s(t)$ is the inverse Fourier transform of the frequency domain slow time mother function.

$$g_s(t) = \frac{1}{2\pi} \int_{-\infty}^{+\infty} G_s(w) e^{jwt} \, dw \tag{2.39}$$

We would like to express our transmit signal as a vector of independent time-frequency samples. For this purpose we take a windowed Fourier transform of the time domain signal of (2.38), and then sample the frequency spectrum at each time window. The window function is made to have certain properties like – even function, timewidth of one PRI i.e. T_o and unit value at the center (i.e. at $t = 0$). Thus the window function effectively selects one pulse at a time from the train of U time pulses, and the Fourier transform of the resulting time domain signal is evaluated. Skipping a lot of messy math, it can be shown that the windowed Fourier transform of our signal has the following form:

$$s(uT_o, \omega) = \sum_p g_s(uT_o) e^{ju\omega_p T_o} \sum_q S_{pq} G_f(\omega) e^{-j\omega uT_o} e^{-j(\omega - \omega_c)\tau_q} \tag{2.40}$$

where $G_f(\omega)$ is the Fourier transform of the fast time mother function $g_f(t)$

$$G_f(w) = \int_{-\infty}^{+\infty} g_f(t) e^{-jwt} \, dt \tag{2.41}$$

The next step is to sample the frequency spectrum at each of the pulse locations i.e. uT_0. Since the time extent of the window is T_0 (i.e. from $-T_0/2$ to $+T_0/2$), we just need to sample at a rate:

$$\Delta w = \frac{2\pi}{T_0} = w_o \qquad (2.42)$$

to satisfy Nyquist criteria. However we choose to oversample with

$$\Delta w = w_o/2 \qquad (2.43)$$

so as to increase the observation period in the time domain from $-T_o$ to $+T_o$. This is done to capture the leakage effect of the previous and next pulses for the near and far targets respectively, in the observation window of the current pulse (as our observation window in time, is specified with respect to the target exactly at the centre of the illuminated area). The assumption is that the only extra energy that leaks into the window of the current pulse is from the adjacent pulses. Hence we need to map the whole time range from $-T_o$ to $+T_o$ unambiguously before applying our windowing function, which extends from $-T_o/2$ to $+T_o/2$, and thus the oversampling in frequency. At the receiver, or even at the targets to compute the normalized responses, we throw out the extra frequency samples (as they do not contain additional information); again effectively sampling the spectrum at $\Delta w = w_o$.

Sampling the windowed frequency response and defining a complex value s_{uv}, we can simplify (2.40) as (intermediate steps again left out for simplicity):

$$s_{uv} = \sum_p g_s(uT_o) e^{ju\omega_p T_o} \sum_q S_{pq} G_f(\frac{v\omega_o}{2}) e^{-j(\frac{v\omega_o}{2} - \omega_c)\tau_q} \qquad (2.44)$$

This complex value s_{uv} essentially describes *the vth frequency sample of the uth time pulse*. Thus there are a total of U transmit pulses and V frequency samples for each pulse. The value of V is given as:

$$V \approx \frac{2\pi B}{w_o / 2} + 1 = 2BT_0 + 1 \text{ (To make } V \text{ odd)} \tag{2.45}$$

Multiplying by the number of pulses we get the total number of time frequency samples as:

$$UV = 2B(UT_0) + 1 = 2BT + 1 \approx 2BT \tag{2.46}$$

Thus the number of spectrum samples we have, are twice than what are required i.e. *BT*. And thus at the receiver we can decimate and throw out the extra frequency samples to come up with our received vector, or even the normalized responses for each target. We define another complex value:

$$\psi_{uv}^{pq} = g_s(uT_o) e^{ju\omega_p T_o} \ G_f(\frac{v\omega_o}{2}) e^{-j(\frac{v\omega_o}{2} - \omega_c)\tau_q} \tag{2.47}$$

which enables us to write the complex transmit signal samples more compactly as:

$$s_{uv} = \sum_p \sum_q \psi_{uv}^{pq} S_{pq} \tag{2.48}$$

Thus each and every time-frequency sample of the transmit signal can be written in terms of the basis function weights S_{pq} and the complex terms ψ_{uv}^{pq}. These terms ψ_{uv}^{pq} get established once we select our basis functions, PRF, signal timewidth, bandwidth etc, and the only parameters remaining that define our transmit signal are the weights of the $R \ (= PQ)$ basis functions. This vector of the basis function weights is what we intend to find. A vector matrix model has been developed for this purpose which is

described in the next subsection. It involves extending the present model to space-time signals, as well as an interfacing it with the previous transmission and propagation model.

2.3.6 A Vector/Matrix Signal Model and Extension to Space-Time Transmit Signals

After a little re-indexing of the data samples, (2.48) can be rewritten as:

$$s_k = \sum_r \psi_{kr} S_r \tag{2.49}$$

where $k = (uV + v) + \left(\dfrac{UV+1}{2}\right)$ and $r = (pQ + q) + \left(\dfrac{PQ+1}{2}\right)$. Hence the vector of all s_k values $\mathbf{s}^t = \begin{bmatrix} s_1 & s_2 & s_3 \cdots s_K \end{bmatrix}^T$ describes the transmit signal completely in terms of the $2BT$ time frequency samples. It can be determined from the vector of all S_r values $\mathbf{S}^t = \begin{bmatrix} S_1 & S_2 & S_3 \cdots S_R \end{bmatrix}^T$ or the basis function weights. As mentioned before $R = P \, x \, Q$, and $K = U \, x \, V$. If the KR values ψ_{kr} are written in matrix form:

$$\boldsymbol{\psi} = \begin{bmatrix} \psi_{11} & \psi_{12} & \psi_{13} & \cdots & \cdots & \cdots & \psi_{1R} \\ \psi_{21} & \psi_{22} & \psi_{23} & \cdots & \cdots & \cdots & \psi_{2R} \\ \psi_{31} & \psi_{32} & \psi_{33} & \cdots & \cdots & \cdots & \psi_{3R} \\ \vdots & & \ddots & & & & \\ \vdots & & & \ddots & & & \\ \vdots & & & & \ddots & & \\ \psi_{K1} & \psi_{K2} & \psi_{K3} & & & & \psi_{KK} \end{bmatrix} \tag{2.50}$$

then our model simply reduces to:

$$\mathbf{s}^t = \boldsymbol{\psi} \mathbf{S}^t \tag{2.51}$$

47

All the equations up till now have been for a single transmit element, i.e. we have been dealing with purely temporal signals. If we wish to extend this model to represent true space time signals, then we have to consider a similar transmit signal at each of the transmit elements.

Let J be the number of spatial transmit elements, then there will be a total of $N = J \times K$ transmit samples with K time-frequency samples on each of the J elements. Similarly there will be a total of $W = J \times R$ basis function weights. We can arrange the time-frequency samples and the basis functions weights in terms of the following two vectors:

$$\mathbf{s}_k^s = [s_{1k}, s_{2k}, s_{3k}, \cdots, s_{Jk}]^T \tag{2.52}$$

$$\mathbf{S}_r^s = [S_{1r}, S_{2r}, S_{3r}, \cdots, S_{Jr}]^T \tag{2.53}$$

where $\mathbf{s}_k^s$ essentially contains the kth time-frequency sample, and $\mathbf{S}_r^s$ contains the rth basis function weight for all the transmit elements. Thus two composite vectors can be formed, that contain all the time-frequency samples and basis function weights from the individual $\mathbf{s}_k^s$ and $\mathbf{S}_r^s$:

$$\mathbf{s} = [(\mathbf{s}_1^s)^T, (\mathbf{s}_2^s)^T, (\mathbf{s}_3^s)^T, \cdots, (\mathbf{s}_K^s)^T]^T \tag{2.54}$$

$$\mathbf{S} = [(\mathbf{S}_1^s)^T, (\mathbf{S}_2^s)^T, (\mathbf{S}_3^s)^T, \cdots, (\mathbf{S}_R^s)^T] \tag{2.55}$$

It can be shown that these two vectors are related as [31]:

$$\mathbf{s} = \mathbf{F}\,\mathbf{S} \tag{2.56}$$

where $\mathbf{F}$ is an N by W matrix and is given as:

$$\mathbf{F} = \mathbf{\psi} \otimes \mathbf{I}_J \tag{2.57}$$

$\otimes$ indicates the *kronecker* product. The matrix $\boldsymbol{\psi}$ calculated using (2.50), contains only the temporal characteristics of the transmit signal and does not depend on the number of transmit elements. The matrix $\mathbf{F}$ contains the complete space-time attributes of the transmit signal and essentially becomes the output of the transmit signal model.

Once we have the matrix $\mathbf{F}$, the only thing that remains is the application of this matrix to the earlier transmission and propagation model. It turns out that this interfacing is very simple and is explained below. From the earlier propagation model we know that:

$$\boldsymbol{\rho}_t = \mathbf{H}_t\,\mathbf{s} \tag{2.58}$$

$\mathbf{s}$ contains the actual time-frequency samples of our transmit signal. Using (2.56) of the transmit signal model we have,

$$\boldsymbol{\rho}_t = \mathbf{H}_t\,(\mathbf{FS})\text{, or} \tag{2.59}$$

$$\boldsymbol{\rho}_t = \mathbf{H}_t'\mathbf{S} \tag{2.60}$$

Here $\mathbf{H}_t'$ is an M x W matrix and is defined as:

$$\mathbf{H}_t' = \mathbf{H}_t\,\mathbf{F} \tag{2.61}$$

Therefore from (2.60) the illumination optimization problem can be concisely stated as - for a given collection of $\mathbf{H}_t'$ matrices find the optimal vector $\mathbf{S,}$ which would result in the best set of vectors $\boldsymbol{\rho}_t$, for a particular optimization criterion. We call

these transmit vectors as transmit codes, and from now on both the terms would be used inter-changeably within this document.

2.3.7 Default Values for the Signal Model

In section 2.2 we saw that each basis function can be defined by a 5-D position vector $\overline{z}$, which can be further split into a spatial and temporal vector. Hopefully after the discussion on the transmit signal model, it should be evident that the temporal position vectors $\mathbf{z}_k^t = \begin{bmatrix} t_{k,} & w_k \end{bmatrix}^T$ occupy pre-determined points on the time-frequency plane that have been established by our choice of the PRF, signal timewidth and bandwidth..

$$\mathbf{z}_k^t = \begin{bmatrix} u\,T_o, & v\,w_o/2 \end{bmatrix}^T \tag{2.62}$$

The spatial position vectors $\mathbf{z}_j^s = \begin{bmatrix} x_j, y_j, z_j \end{bmatrix}$ describe the location of the various antenna elements in 3-dimensionsal space, or the arrangement of the radar transmit array. Some other simplifying assumptions were made with respect to our transmit signal model. For e.g. unit energy sinc functions were considered for the fast and slow time mother functions - $g_f(t)$ and $G_s(w)$ respectively. These waveforms satisfy all the properties of the mother functions stated before. The incremental time shifts τ_q used to generate new fast-time basis functions were selected to be:

$$\tau_q = \frac{q}{B} \tag{2.63}$$

And the small frequency shifts for generating the slow time basis functions were kept as:

$$w_p = 2\pi \left(\frac{p}{T} \right)$$
(2.64)

It should be clear that these expressions satisfy the earlier constraints of $\tau_q \ll T_o$ and $w_p \ll w_o$. In addition the carrier frequency f_c was made an integer multiple of the bandwidth B, and the bandwidth an integer multiple of the PRF f_o (thus $f_c \gg B \gg f_o$). Although all these assumptions greatly simplify our computation of the $\boldsymbol{\psi}$ matrix, it should be noted that the model also contains provisions for using any other values for the aforementioned parameters. The default values have been selected, only to simplify the various expressions without loosing out on any generality.

2.4 Numeric Parameters for the Radar Models

This section describes the radar geometry that was considered for all our simulations, and also the basis for selecting the values of various numeric parameters that are required for the two radar models [32]. Simplifying constraints have been placed on several values, which results in many parameters being dependent on the others. Typical values for a low earth orbiting spaceborne radar have been used for the remaining independent parameters. The geometry for a standard side-looking case was assumed, which has been shown in Figure 2.3 on the next page.
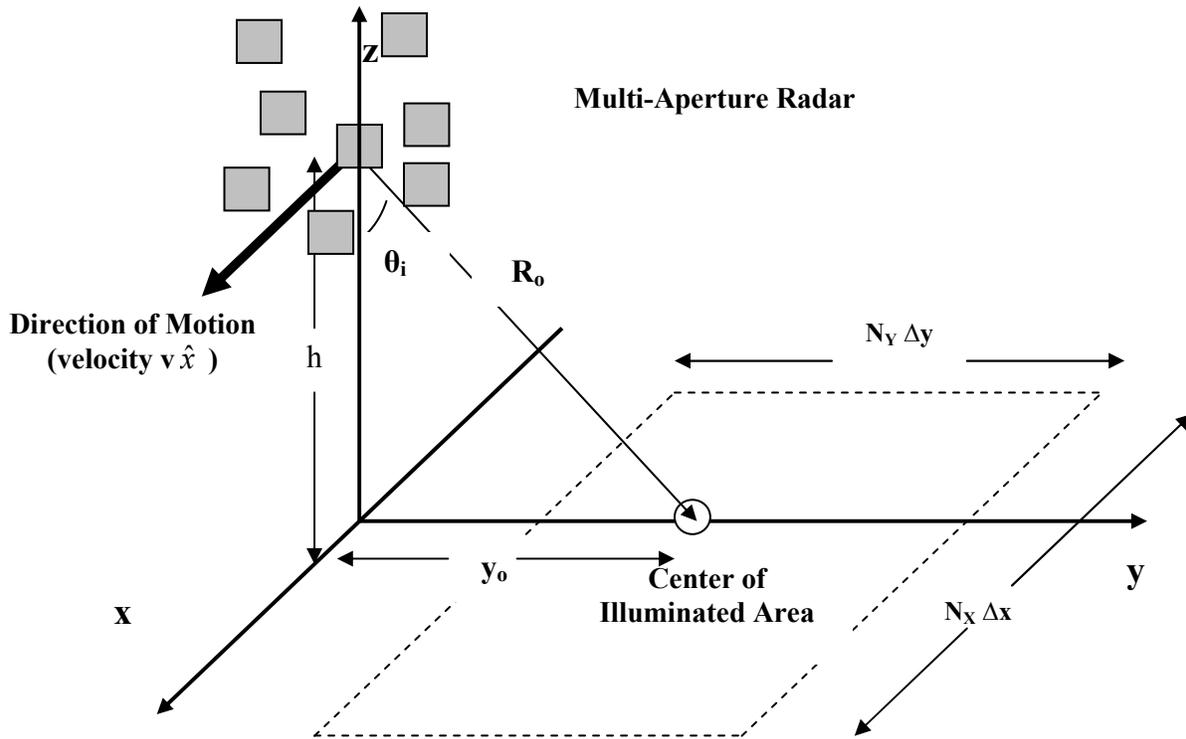
Figure 2:3 Side-looking Multi-Aperture Radar Geometry

Following points can be observed from Figure 2.3:

- The radar is flying in the $\hat{x}$ direction with velocity $v\hat{x}$.

- The center of the radar (transmit array) is $x = 0$, $y = 0$, $z = h$, i.e. the radar is at an altitude h.

- The center of the illuminated area is at $x = 0$, $y = y_o$, $z = 0$, i.e. a standard side-looking case.

The following two equalities follow from the figure:

$$y_o = R_o \cos\theta_i \qquad (2.65)$$

$$h = R_o \sin \theta_i \qquad (2.66)$$

It turns out that for this geometry we can derive default values for the matrix $\mathbf{K}_\theta$ which is required in (2.24) for the computation of the $\mathbf{H}_t$ matrices. The $\mathbf{K}_\theta$ matrix [34] turns out to be:

$$\mathbf{K}_\theta = \frac{\omega_c}{c} \begin{bmatrix} \dfrac{-1}{R_o} & 0 & 0 & \dfrac{-v}{R_o} & 0 \\[2ex] 0 & \dfrac{-h^2}{R_o^3} & \dfrac{-hY_o}{R_o^3} & 0 & \dfrac{Y_o}{\omega_c R_o} \\[2ex] 0 & \dfrac{-hY_o}{R_o^3} & \dfrac{-Y_o^2}{R_o^3} & 0 & \dfrac{-h}{\omega_c R_o} \\[2ex] 0 & 0 & 0 & 0 & -1 \end{bmatrix} \qquad (2.67)$$

Here c is the velocity of propagation or the velocity of light. From (2.5) we know that each target is described by a position vector of the form $\bar{y}_t = \begin{bmatrix} x_t & y_t & z_t & v_t^r \end{bmatrix}^T$. Targets are assumed to be distributed across a two dimensional grid (size N_x by N_y) on the x-y plane. The target spacing in the x direction is denoted by Δx and that along the y direction is denoted by Δy. The radial velocity v_t^r is considered positive if the target is moving towards the radar. With these assumptions the target position vector can be rewritten as:

$$\mathbf{y}_t = \begin{bmatrix} n_x \Delta x, & n_y \Delta y, & z_t, & v_t^r \end{bmatrix}^T \qquad (2.68)$$

For the sake of simplicity, the target spacings in the x and y directions are set to be equal to the radar resolution in the along and cross track directions respectively: Thus each resolution cell is one target for our radar.

$$\Delta x = \frac{cR_o}{2UT_o v f_c} \qquad (2.69)$$

$$\Delta y = \frac{cR_o}{2BY_o} \qquad (2.70)$$

It would be prudent to mention an important here. Recall that the target model was developed for the full propagation from transmitter to the targets and back to the receiver. Hence the above expressions are taking into the account the phase shift that occurs in both the forward and reverse paths. However as mentioned before, for the illumination optimization problem we just consider the propagation from the transmitter to the targets. Therefore the actual resolution will be double of what is given by (2.69) and (2.70), and thus for our case targets immediately adjacent to each other will not be resolvable. Only the targets which are two or more cells apart will be discernable in our case, for propagation from the transmitter to the targets. This point is not of much consequence as far as the various simulations are concerned, but will assume significance in Chapter 6 when we describe one of the potential applications of true space-time codes – reducing the main lobe width of the radar ambiguity function.

Thus our default case is completely described by that following set of inputs:

1. *To, B, w_c,* c

2. *v, R_o, y_o*

3. *U, V, J*

4. *N_x, N_y*

5. $\mathbf{y}_t$ for all targets t

6. $\mathbf{z}_j^s$ for all transmit antennas j

It turns out that after a few other simplifying assumptions; some of the above parameters become dependent on the others. These assumptions, the resulting dependence between the various parameters, and standard values for the remaining independent parameters has been described next.

The following parameters are selected to be the fundamental parameters describing the radar physics and the side-looking scenario:

$$c, h, \theta_i, v, f_c$$

Their value does not depend on any other factor, and all the other parameters are derived from these. Using these values in (2.65) and (2.66) we can get:

$$R_o = \frac{h}{\cos\theta_i} \tag{2.71}$$

$$y_o = h\tan\theta_i \tag{2.72}$$

as well as the transformation matrix $\mathbf{K}_\theta$. From (2.69) and (2.70) the two new expressions for the radar resolution can be determined as:

$$\Delta x = \frac{cR_o}{2UT_o v f_c} = \frac{cR_o}{2Tv f_c} \tag{2.73}$$

$$\Delta y = \frac{cR_o}{2BY_o} = \frac{c}{2B\sin\theta_i} \tag{2.74}$$

We assume the resolution in the along and cross track dimensions to be equal, which gives us our first expressions for the signal bandwidth and timewidth [32]:

$$B = \sqrt{\frac{N_x N_y v f_c}{\beta Y_o}} \tag{2.75}$$

$$T = \sqrt{\frac{N_x N_y Y_o}{\beta v f_c}} \qquad (2.76)$$

We define a new parameter β - the ratio of the total number of resolution cells to the radar time-bandwidth product. For single aperture radar the number of targets should be less than the number of independent time frequency samples or the time-bandwidth product. Thus β should be less than one. However for multi-aperture radar we can have additional spatial samples on the receive side due to the multiple receive apertures and hence this value can be greater than one. In other words, the total number of space-time receive samples can still be greater than the number of targets even if $\beta > 1$.

$$\beta = \frac{N_x N_y}{BT} \qquad (2.77)$$

In section 2.3.5 we saw that the total number of transmit time-frequency samples were equal to twice the time-bandwidth product of the radar i.e. $UV \approx 2BT$ (2.46). Using this equation with (2.77) we can show that $UV \approx 2\dfrac{N_x N_y}{\beta}$. Separating further into two non-unique product terms, we come up with the following two values:

$$U = \frac{N_x}{\sqrt{\beta}} \qquad (2.78)$$

$$V = \frac{2N_y}{\sqrt{\beta}} \qquad (2.79)$$

This division is not as irrational as it may seem. It should be noted that N_x along track resolution cells can be resolved only with $U > N_x$ independent time samples. Similarly

N_y cross track resolution cells can be unambiguously resolved only if $V/2 > N_y$ (as we oversample in the frequency domain on the transmit side).

The value of the PRI is easily determined once the signal timewidth T and the number of transmit pulses U is known:

$$T_o = \frac{T}{U} \tag{2.80}$$

Finally we have to make sure that the spatial extent of the transmit array is small enough so as to not affect the radar resolution. It is because for very large arrays, the spatial resolution may become too fine and ultimately set the limit on the range and doppler resolutions. All along we have assumed that the along and cross track resolution are decided by the temporal values of signal timewidth and bandwidth. A very fine spatial resolution will thus be a direct violation of our previous assumptions. To ensure this condition, we first determine the spatial resolution of radar with spatial extent L_x in any one direction. This value is given by:

$$\Delta X_s \approx \frac{c R_o}{f_c L_x} \tag{2.81}$$

Thereafter, we define another parameter η which is the ratio of the spatial (main beam width) to the temporal resolution:

$$\eta = \frac{\Delta X_s}{\Delta x} \tag{2.82}$$

This parameter can be set to any value greater than 1. From (2.81) and (2.82) we get an expression for the spatial extent of the transmit array in each direction (assuming equal spatial resolution in both directions):

$$L_x = \frac{c\, R_o}{f_c\, \eta\, \Delta x} \tag{2.83}$$

Thus in the end, we find that for the following set of independent radar parameters,

$$c, h, \theta_i, v, f_c, N_x, N_y, \beta, \eta$$

we can determine the remaining set of dependent values:

$$B, T, T_o, U, V, L_x, \mathbf{K}_\theta$$

The following default values were assumed for the independent parameters. These values have been selected to be consistent with those of a typical low earth orbiting spaceborne radar.

$c = 3 \times 10^8$ m/s

$h = 183$ km

$v = 7.8$ km/s

$f_c = 10$ GHz

$\theta i = 45°$

and thus,

$y_o = 183$ km

$R_o = 258.8$ km

Additionally the target grid was kept square with $N_x = N_y = 2^i - 1$ (i is an integer > 1), so that the number of resolution cells in both along and cross track directions are almost a power of 2 - {3, 7, 15, 31, 63...}. The other values selected were:

$\beta = 4.2$

$\eta = 5$, and

$\sigma_x = L_x/2$, for a random (Gaussian) distribution of elements - sparse array

The last point to be made in this section is that the values provided here are just representative default values to simplify our simulations. By no means are they the only values that can be used in these models. The software code for all our models has been kept modular enough to accommodate any further changes, or set of values that may be required in the future. The size of the simulation depends on the integer value i, which in-turn decides the size of our target grid and most other dependent parameters. This value is selected as per the goal of our simulation, or on what are we trying to achieve. Usually it is kept small enough (2 or 3) for debugging cases and larger (4 or 5) for getting more representative results. All other values were selected depending on the value of i or N_x and N_y. Table 2:1 on the next page demonstrates the calculation of various parameter values for different N_x and N_y.

Table 2:1 Radar simulation parameter worksheet

f_c (Hz)	θ_i (rad)	β	η	R_o (m)	c (m/s)	h (m)	v (m/s)
1.00E+10	0.785398163	4.2	2.5E+00	2.59E+05	3.00E+08	1.83E+05	7.80E+03

Nx	Ny	B/T	BT	U	V	B (Hz)	T (sec)	T_o (sec)	f_o (Hz)	Δx (m)	Δy (m)	Lx
3	3	4.262E+08	2.143E+00	1.464E+00	2.928E+00	3.022E+04	7.090E-05	4.844E-05	2.065E+04	7.019E+03	7.019E+03	2.212E-01
7	7	4.262E+08	1.167E+01	3.416E+00	6.831E+00	7.052E+04	1.654E-04	4.844E-05	2.065E+04	3.008E+03	3.008E+03	5.162E-01
15	15	4.262E+08	5.357E+01	7.319E+00	1.464E+01	1.511E+05	3.545E-04	4.844E-05	2.065E+04	1.404E+03	1.404E+03	1.106E+00
31	31	4.262E+08	2.288E+02	1.513E+01	3.025E+01	3.123E+05	7.327E-04	4.844E-05	2.065E+04	6.793E+02	6.793E+02	2.286E+00
63	63	4.262E+08	9.450E+02	3.074E+01	6.148E+01	6.347E+05	1.489E-03	4.844E-05	2.065E+04	3.342E+02	3.342E+02	4.646E+00
127	127	4.262E+08	3.840E+03	6.197E+01	1.239E+02	1.279E+06	3.002E-03	4.844E-05	2.065E+04	1.658E+02	1.658E+02	9.365E+00
255	255	4.262E+08	1.548E+04	1.244E+02	2.489E+02	2.569E+06	6.027E-03	4.844E-05	2.065E+04	8.258E+01	8.258E+01	1.880E+01
511	511	4.262E+08	6.217E+04	2.493E+02	4.987E+02	5.148E+06	1.208E-02	4.844E-05	2.065E+04	4.121E+01	4.121E+01	3.768E+01

Now that we have described both our radar models and laid down a clear foundation of the problem at hand, we are ready to dive into the actual process. We start exploring the *space time illumination optimization problem* by first looking at some of the basic algorithms.

Chapter 3

Illumination Optimization - Basic Algorithms

Now that we are ready to delve into the space time illumination optimization problem, the first question to be asked is what optimization criteria should be used, and once selected how practical it is to realize that criterion. In other words, can the optimal solution actually be found using that criterion, and if yes what are the processing costs and other issues involved. From an illumination optimization point of view, an ideal transmit signal should put all the energy on the scatterers we are interested in, and none on the scatterers we do not wish to illuminate. We call the first class of scatterers - 'target objects' or 'targets' and the second class as 'clutter objects'. In addition to not wasting any energy on the clutter objects, we would also like to distribute the transmit energy as fairly or uniformly as possible on the remaining targets. This will ensure that the probability of correct estimation for even the worst case target is maximized. However such an ideal radar signal is normally impossible to construct, except for the most trivial of radar problems. Instead we define specific optimization criteria, and try to find a transmit signal that satisfies these criteria to the greatest possible extent. In this chapter we start our discussion with some of these basic optimization criteria, like maximizing the overall target illumination energy, minimizing the overall clutter illumination energy or maximizing the ratio between the two i.e. the *signal to clutter ratio* or the *SCR*. Thereafter we move on to more advanced algorithms like maximizing the minimum *SCR* received

by any of the targets, i.e. the Maxi-min algorithms, which are covered in the subsequent chapters.

3.1 Setting up the Target Illumination Problem

Like stated before all scatterers can be classified into two sets:

Set a: Scatterers we wish to illuminate or estimate - 'Targets'.

Set b: Scatterers we do not wish to illuminate - 'Clutter Objects'.

This segregation of targets and clutter essentially describes the radar mode of operation. For e.g. in a GMTI, all moving scatterers will be classified as targets and all stationary ones as clutter. Also note that this demarcation does not require knowledge about the actual scatterers or their scattering coefficient values γ_t. All it requires is a demarcation of the two measurement spaces where given targets and clutter objects may exist. In other words just another reiteration of the earlier point - for the illumination optimization problem we only need to concern ourselves with the propagation from the transmitter to the scatterers, and not beyond. Anyway continuing with our classification process, we can define another set of scatterers as:

Set c: Scatterers we do not care about - 'Don't Cares'.

What this means is that we are not concerned about illuminating, or not illuminating the scatterers in this set. From a practical point of view these 'don't cares' don't make much sense, as we would always like to either illuminate or not illuminate each scatterer depending upon our estimation goals. Any illumination energy not falling on the target objects is just a waste of available energy and needs to be minimized.

But this classification proves quite interesting just from an academic point of view, and also results in 'more realizable' target-clutter geometries. The 'don't cares' allow for a physical separation between the objects of *sets a* and *b* i.e. the targets and clutter, and hence make it easier to realize the desired illumination solutions. For real world cases, the *set c* objects can be thought of as regions with very low back-scattering coefficients (like. water bodies), such that the reflected energy from these objects does not interfere with returns from the scatterers which we wish to estimate – the targets.

Let us define a *W x W* hermetian, non-negative definite matrix **A** representing all target objects as:

$$\mathbf{A} = \sum_{i \in a} \mathbf{H}''_i \mathbf{H}'_i \text{ , or} \tag{3.1}$$

$$\mathbf{A} = \sum_{i \in a} \mathbf{A}_i$$

where $\mathbf{H}'_i$ is the same matrix as described in (2.61), and $\mathbf{H}''_i$ denotes the conjugate transpose of the matrix. As can be noted

$$\mathbf{A}_i = \mathbf{H}''_i \mathbf{H}'_i \tag{3.2}$$

is the matrix for each individual target.

Similarly we can define another *W* by *W* hermetian, non-negative definite matrix **B** representing all clutter objects as:

$$\mathbf{B} = \sum_{i \in b} \mathbf{H}''_j \mathbf{H}'_j \text{, or} \tag{3.3}$$

$$\mathbf{B} = \sum_{j \in b} \mathbf{B}_j$$

64

Again,

$$\mathbf{B}_j = \mathbf{H}''_j \, \mathbf{H}'_j \qquad (3.4)$$

is the matrix representing each individual clutter object.

From (2.60) the total illuminated energy on all targets is given as:

$$E_a = \sum_{i \in a} \boldsymbol{\rho}'_i \, \boldsymbol{\rho}_i \qquad (3.5)$$

$$= \mathbf{S}' \left(\sum_{i \in a} \mathbf{H}''_i \mathbf{H}'_i \right) \mathbf{S}$$

$$= \mathbf{S}' \left(\sum_{i \in a} \mathbf{A}_i \right) \mathbf{S}$$

$$= \mathbf{S}' \mathbf{A} \, \mathbf{S}$$

Where it is obvious that the individual energy on any of the targets is:

$$E_a^i = \mathbf{S}' \mathbf{A}_i \, \mathbf{S} \qquad (3.6)$$

Similarly the total illuminated energy on all clutter objects is given as:

$$E_b = \sum_{j \in b} \boldsymbol{\rho}'_j \, \boldsymbol{\rho}_j \qquad (3.7)$$

$$= \mathbf{S}' \left(\sum_{j \in b} \mathbf{H}''_j \mathbf{H}'_j \right) \mathbf{S}$$

$$= \mathbf{S}' \left(\sum_{j \in b} \mathbf{B}_j \right) \mathbf{S}$$

$$= \mathbf{S}' \mathbf{B} \, \mathbf{S}$$

Once again it is apparent that the illuminated energy for any one clutter object is:

$$E_b^j = \mathbf{S}' \mathbf{B}_j \mathbf{S} \qquad (3.8)$$

Once the different matrices have been formed, and their physical significance and the relation between various entities understood, we are ready to define our basic illumination optimization algorithms.

3.2 Maximum Target Energy

It turns out that each of these basic codes is very easy to find. For the maximum target energy solution, we first write matrix $\mathbf{A}$ in terms of its eigen vectors $\hat{e}_n^a$ and eigen values λ_n^a:

$$\mathbf{A} = \sum_n \lambda_n^a \, \hat{e}_n^a \, \hat{e}_n^{a\prime} + \mathbf{K}_{noise} \tag{3.9}$$

Here $\mathbf{K}_{noise}$ is a diagonal matrix which represents the effect of noise in the measurements. Since all eigen vectors are unit vectors, signal energy ≈ 1, and the value of diagonal terms in this matrix was kept of the order of 0.0001 (40 dB below the signal level). Although addition of noise may seem unnecessary at this stage, this step assumes significance when we go to the Maxi-min algorithms in the later chapters (more about it then). Since matrix $\mathbf{A}$ is non-negative definite, all its eigen values λ_n^a are real and positive. Therefore it follows from (3.5) that the transmit code which maximizes the total or average illumination energy on the targets of *set a*, is nothing but the eigen vector associated with the largest eigen value $(\lambda_n^a)_{max}$.

$$\therefore \mathbf{S} = \hat{e}_n^a \text{ associated with } (\lambda_n^a)_{max} \tag{3.10}$$

3.3 Minimum Clutter Energy

This time we write the **B** matrix in terms of its eigen vectors and eigen values:

$$\mathbf{B} = \sum_n \lambda_n^b \, \hat{e}_n^b \, \hat{e}_n^{b\prime} \qquad (3.11)$$

Note that the noise matrix is not added in this case, the reason for which will become clear in the subsequent chapters. Once again since matrix B is non-negative definite, it follows from (3.7) that the transmit code which minimizes the total or average illumination energy on the clutter objects of *set b*, is simply the eigen vector associated with the smallest eigen value $(\lambda_n^b)_{\min}$.

$$\therefore \ \mathbf{S} = \hat{e}_n^b \ \text{associated with} \ (\lambda_n^b)_{\min} \qquad (3.12)$$

3.4 Maximum SCR

Although the earlier two codes are interesting in their own standing, from a practical point of view the criterion that makes more sense is maximizing the ratio of the illuminated target and clutter energies. We call this quantity the signal to clutter ratio or the *SCR*, and this term will be used henceforth to reference this value. The code which maximizes the overall target energy might not be one which minimizes the clutter energy as well, and hence we seek to find a code which maximizes the ratio of these two quantities, the SCR:

$$\frac{E_a}{E_b} = \frac{\mathbf{S}'\mathbf{A}\mathbf{S}}{\mathbf{S}'\mathbf{B}\mathbf{S}} \qquad (3.13)$$

Note that we have two non-negative definite matrices in the above expression. To get an expression in terms of a single matrix, we rewrite (3.13) as:

$$\frac{E_a}{E_b} = \frac{\mathbf{S}'\mathbf{A}\mathbf{S}}{\mathbf{S}'\mathbf{B}\mathbf{S}}$$

$$= \frac{\mathbf{S}'(\mathbf{B}^{-1/2}\,\mathbf{B}^{1/2})'\,\mathbf{A}(\mathbf{B}^{-1/2}\,\mathbf{B}^{1/2})\mathbf{S}}{\mathbf{S}'(\mathbf{B}^{1/2}\,\mathbf{B}^{1/2})\mathbf{S}}$$

$$= \frac{\mathbf{S}'(\mathbf{B}^{1/2})'(\mathbf{B}^{-1/2})'\,\mathbf{A}(\mathbf{B}^{-1/2})(\mathbf{B}^{1/2})\mathbf{S}}{\mathbf{S}'(\mathbf{B}^{1/2})'(\mathbf{B}^{1/2})\mathbf{S}} \tag{3.14}$$

$$= \frac{\tilde{\mathbf{S}}'(\mathbf{B}^{-1/2})'\,\mathbf{A}(\mathbf{B}^{-1/2})\tilde{\mathbf{S}}}{\tilde{\mathbf{S}}'\tilde{\mathbf{S}}}$$

The following equalities have been used to simplify the above expression:

$$\mathbf{I} = \mathbf{B}^{-1/2}\mathbf{B}^{1/2}$$

$$\mathbf{B} = \mathbf{B}^{1/2}\mathbf{B}^{1/2}, \text{and} \tag{3.15}$$

$$\mathbf{B}^{1/2} = (\mathbf{B}^{1/2})' \text{ as } \mathbf{B} \text{ is hermetian}$$

Also we have defined another vector as,

$$\tilde{\mathbf{S}} = \mathbf{B}^{1/2}\mathbf{S} \tag{3.16}$$

Now if we define another matrix $\mathbf{C}$:

$$\mathbf{C} = (\mathbf{B}^{-1/2})'\,\mathbf{A}(\mathbf{B}^{-1/2}) \tag{3.17}$$

then (3.14) reduces to,

$$\frac{E_a}{E_b} = \frac{\tilde{\mathbf{S}}'\mathbf{C}\tilde{\mathbf{S}}}{\tilde{\mathbf{S}}'\tilde{\mathbf{S}}} \tag{3.18}$$

This matrix can also be written in terms of its eigen vectors and values:

$$\mathbf{C} = \sum_n \lambda_n^c \, \hat{e}_n^c \, \hat{e}_n^{c\prime} \qquad (3.19)$$

And then the vector $\tilde{\mathbf{S}}$ which maximizes the SCR of (3.18) is simply the eigen vector associated with the largest eigen value of $\mathbf{C}$, i.e. $(\lambda_n^c)_{\max}$

$$\therefore \; \tilde{\mathbf{S}} = \hat{e}_n^c \;\; \text{associated with} \;\; (\lambda_n^c)_{\max} \qquad (3.20)$$

The corresponding transmit vector $\mathbf{S}$ can then be found from:

$$\tilde{\mathbf{S}} = \mathbf{B}^{1/2}\,\mathbf{S}, \;\; \text{as}$$

$$\qquad (3.21)$$

$$\mathbf{S} = \mathbf{B}^{-1/2}\tilde{\mathbf{S}}$$

Note that although vector $\tilde{\mathbf{S}}$ is an eigen vector and has unit magnitude, the vector $\mathbf{S}$ obtained from the transformation of (3.21) will most probably not be a unit vector. In such cases it needs to be normalized, so that we stay consistent with our assumption of unit transmit energy.

Another important to be made here is regarding the calculation of matrix $\mathbf{B}^{-1/2}$. Many a times when the number of clutter objects is less, matrix $\mathbf{B}$ will have zero eigen values. In such cases taking a direct inverse of the matrix would result in numerical errors, and thus grossly atrocious results. Therefore the inverse of this matrix has to be determined very carefully using only the non-zero eigen values λ_n^b:

$$\mathbf{B}^{-1/2} = \sum_n (\lambda_n^b)^{-1/2} \, \hat{e}_n^b \, \hat{e}_n^{b\prime} \qquad (3.22)$$

Here λ_n^b represent only the non-zero eigen values of **B**. Typically each eigen value is compared with the maximum value $(\lambda_n^b)_{max}$, and the values smaller by a factor of 10^{-5} or less are left out in the computation (i.e. if $\lambda_n^b / (\lambda_n^b)_{max} <= 10^{-5}$, the value is considered to be zero). Also the number of non-zero eigen values in the eigen-spectrum of **B,** is equal to the number of clutter objects times the number of basis functions. Thus if there are n_b clutter objects, then the total number of non-zero eigen values is $n_b \times R$, where $R = P \times Q$ is the number of basis functions. This point can be better understood with the following explanation.

Suppose there is just one clutter object, then the number of orthogonal ways in which energy can be placed on this object is equal to the number of basis functions ($R = P \times Q$). It is because all the basis functions are orthogonal to each other and any one of them can be used to put some energy on the clutter object, or a target object for that matter. The amount of energy received by the object would obviously depend on the choice of the basis function, as each function potentially results in a different illumination pattern on the object. Hence for this case, the matrix **B** or **B**ⱼ as there is only one object would have a rank R, or there will be R non-zero eigen values in the eigen spectrum of **B**. The eigen values give the value of energy received by the object if the corresponding eigen vector is selected as the transmit code.

This behavior can be directly extended to a multiple object case. For multiple clutter objects the composite **B** matrix consists of all the individual n_b **B**ⱼ matrices, and hence the total number of non-zero eigen values will simply be $n_b \times R$ (till a

maximum of W as that is the total number of values in the spectrum). This point is more clearly demonstrated by Figure 3:1 on the next page.

1 Objects   **2 Objects**

5 Objects   **224 Objects**
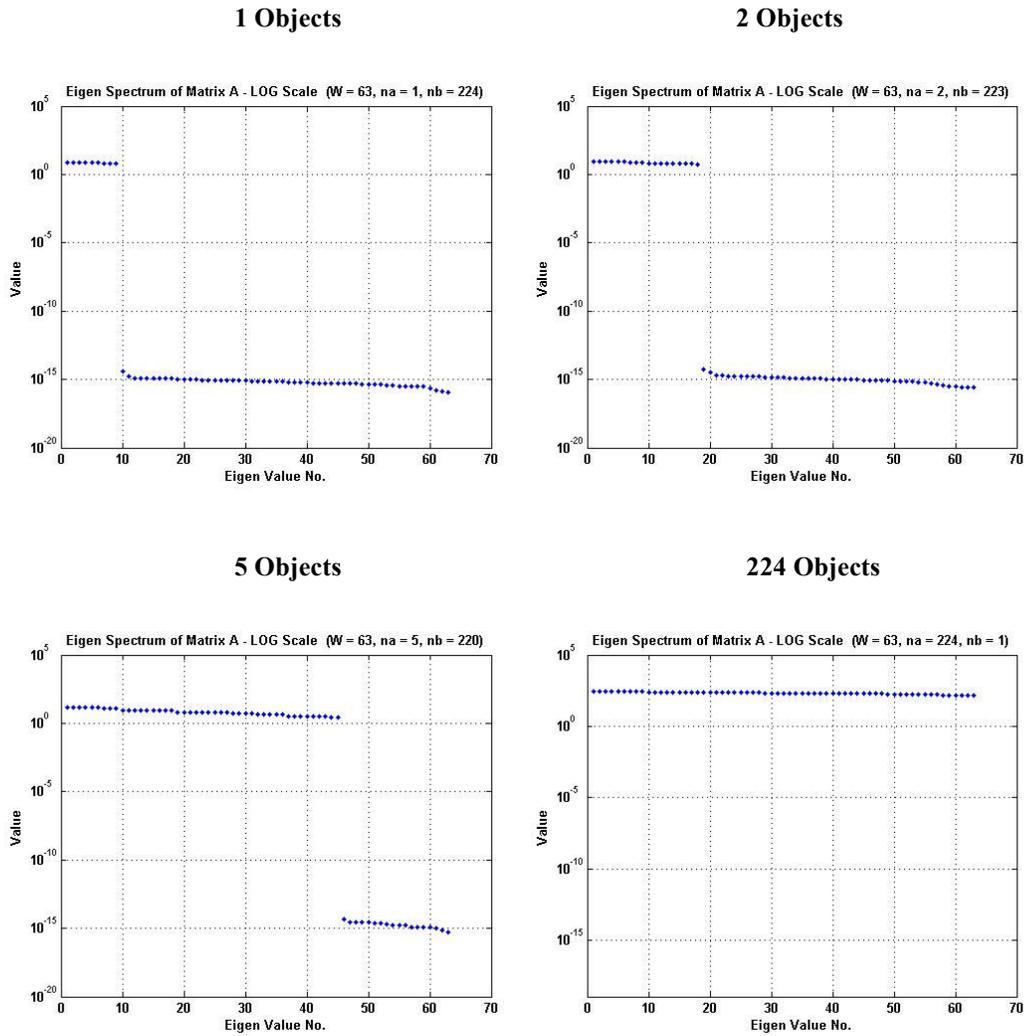
Figure 3:1 Non-zero eigen values in the spectrum of matrix A for different no. of target objects

This figure shows the eigen spectrum of matrix **A** for different number of target objects. The number of transmit antennas $J = 7$, and total number of basis functions $R = 9$ ($P = 3$ and $Q = 3$). Therefore the dimension of the transmit signal space $W = J \times R$

71

= 63. As the number of objects increase from 1 to 2 to 5, the number of non-zero

eigen values correspondingly increase from 9 to 18 to 45. For more than 7 objects all

eigen values in the spectrum are non zero as shown by the last figure for 224 objects.

3.5 Results and Observations

Let us now look at some of the results for each of these algorithms. Figures

3:2–3.4 show the illumination patterns resulting from all the three basic codes, for the

same target-clutter distribution. Note that the location of target objects is shown by

triangles▲, and that of clutter objects by circles◯. The received energy at each

resolution cell is the integrated energy over time i.e. the entire duration of the transmit

signal.

Maximum Target Energy

Average SCR = 6.92 dB
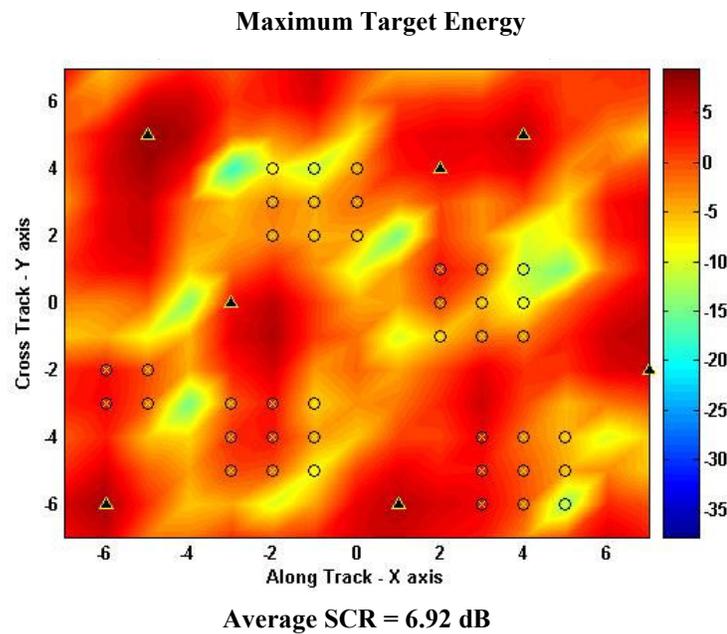
Figure 3:2 Illumination energy across a surface area for the Maximum Target Energy Code

Minimum Clutter Energy

Average SCR = 13.18 dB
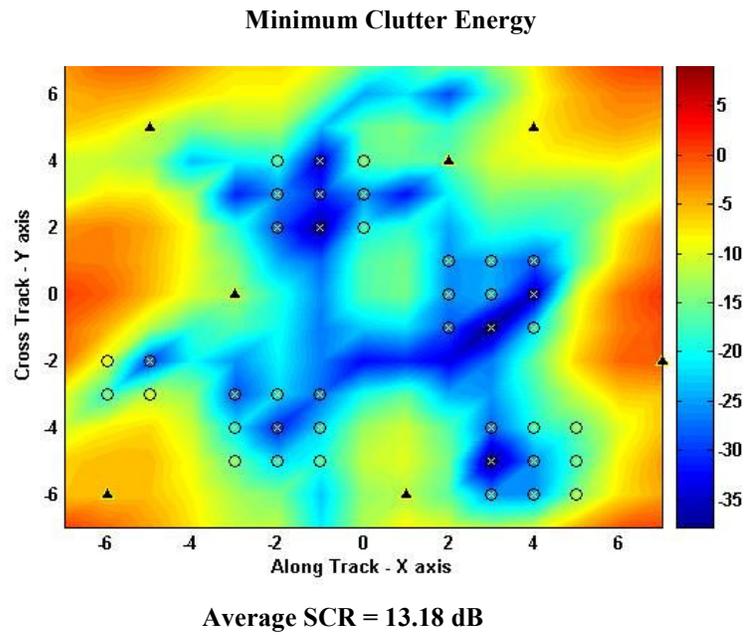
Figure 3:3 Illumination energy across a surface area for the Minimum Clutter Energy Code

Maximum SCR

Average SCR = 14.99 dB
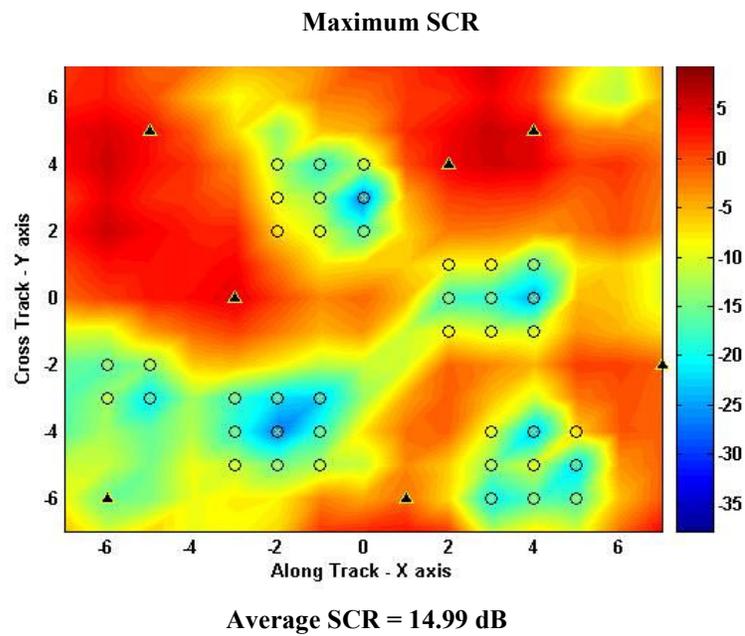
Figure 3:4 Illumination energy across a surface area for the Maximum SCR Code

As can be seen each code tries to optimize its own criteria. The above case is for a 15×15 grid size or $N_x = N_y = 15$. The number of time-frequency basis functions were kept as 9 ($P = Q = 3$) and there were $J = 14$ transmit elements. This combination gives a transmit vector dimension of $W = 126$ ($J \times P \times Q$), and therefore we need to search for our best vector in a 126 dimensional search space. Later, results for more number of basis functions or a larger dimensional search space have also been presented. The 14 element transmit array used for most of our simulations is a sparse distributed array, the spatial extent for which was determined using (2.83). The individual element locations were then picked from a gaussian distribution using $\sigma_x = L_x/2$. This sparse array is shown in Figure 3.5.
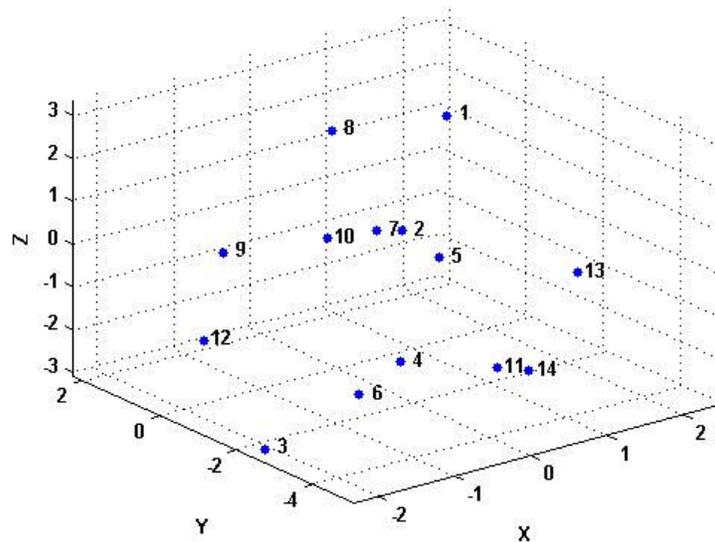
Figure 3:5 Fourteen element sparse distributed transmit array used for the simulations

Another example of the standard code performance has been shown in Figure 3:6 on the next page.

Maximum Target Energy
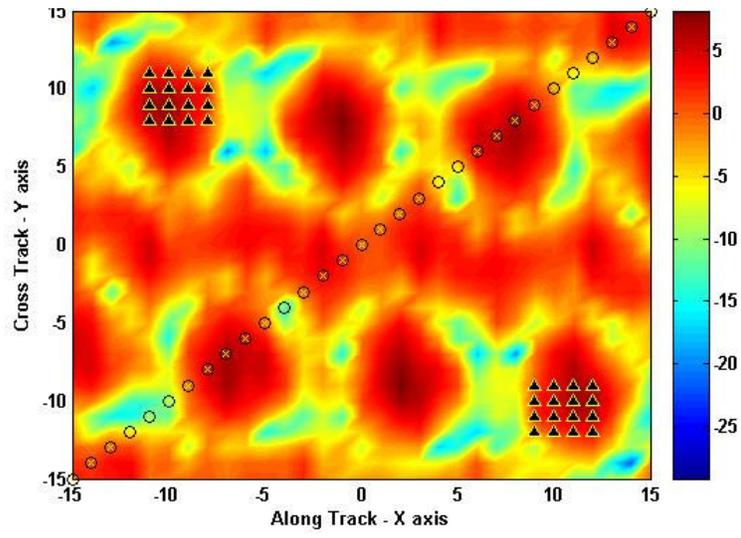
Average SCR = 2.85 dB

Maximum SCR
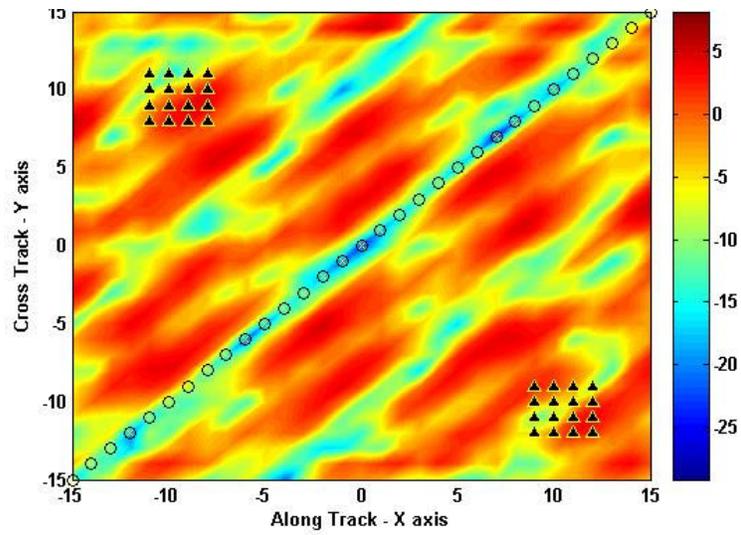
Average SCR = 14.47 dB

Figure 3:6 Another example of the standard code performance

On first impression it may seem as if Maximum SCR can provide us with really good radar solutions; and this might in fact be true for some of the more simple cases. The average SCR value for the Maximum SCR is typically much higher as compared to the other standard codes, and it could have indeed made a very good radar solution, but for a small issue - the *'orphan problem'*.

3.6 The Orphan Problem and the need for Alternate Criteria

From a radar point of view all targets are equally important. Hence even though the 'selective optimization' approach of standard codes may come up with good numerical answers, from a practical point of view they do not be considered good radar solutions. As seen in the earlier plots, the Maximum SCR maximizes the total or average SCR received by all targets by sacrificing some of the 'hard' targets. We call them hard targets, as probably they are the most difficult to place energy on. Thus these targets get left out (*are orphaned*) in the process, and the effect is compensated by putting more energy on the relatively 'easier' targets.

However this approach is not acceptable for remote sensing radars. There is no way of knowing beforehand, which targets are more important and it may very well turn out that the orphaned targets were the ones most critical to our objective. We need to keep all targets equally happy and in the words of Dr. James Stiles, *"A socialist approach has to be adopted rather than a capitalist one"*. The orphan problem for our earlier examples along with some more cases has been illustrated in Figure 3.7. All examples shown are for the Maximum SCR.

Maximum SCR
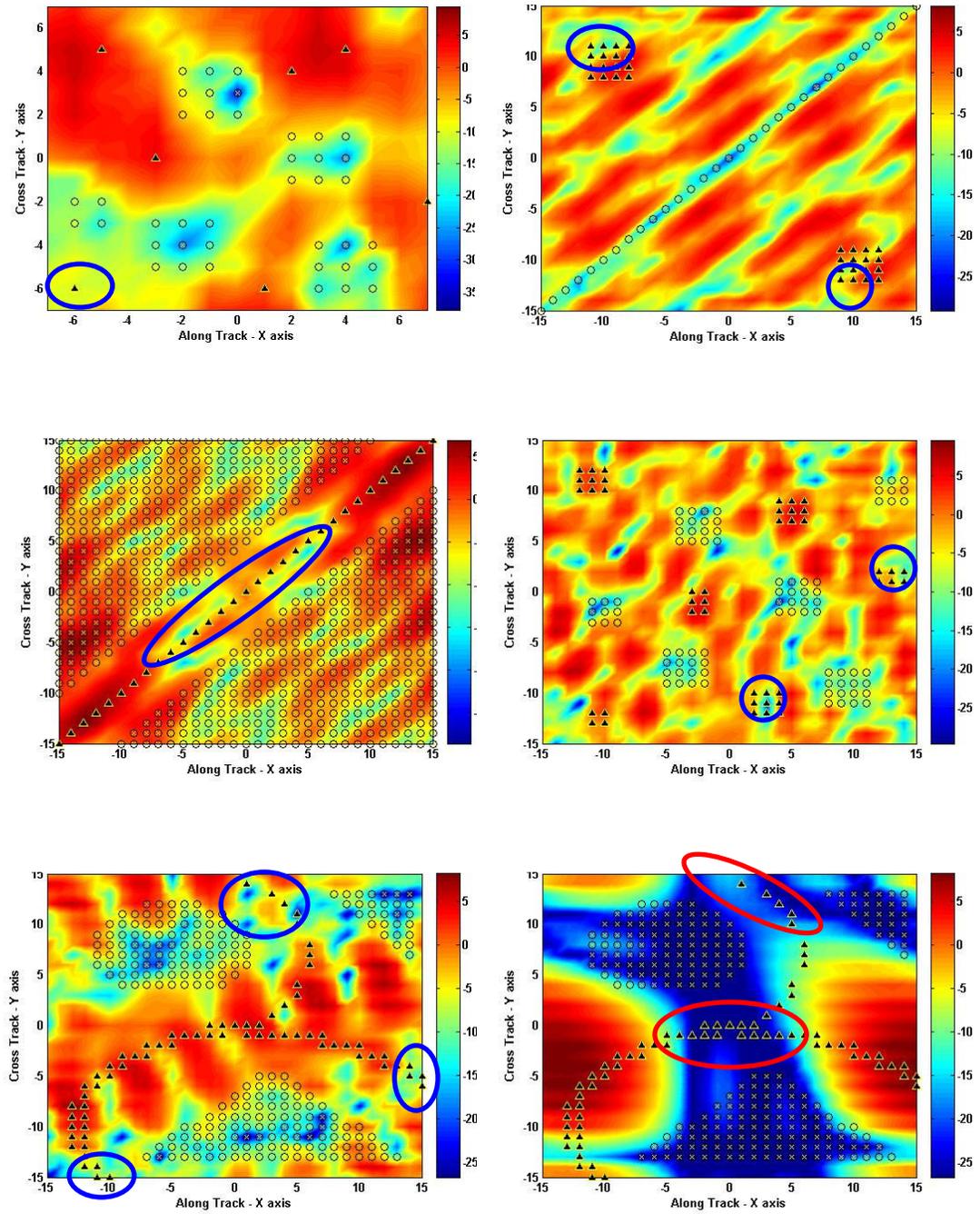
Figure 3:7 The Orphan Problem for Maximum SCR algorithm

It should be obvious from these plots, that a good numeric value of average SCR does not necessarily imply a good answer.

Note that the last two plots on the previous page have identical target-clutter geometries but different illumination patterns for the same transmit code, i.e. the Maximum SCR. It is because these plots are for two different transmit arrays. While the one on the left is for the standard 14 element sparse array shown earlier, the one on the right is for a 16 element regularly spaced 4×4 array. The sparse arrays, like the one described earlier for the spaceborne constellation have a number of advantages. In essence a sparse array provides us with a lot more flexibility – large spatial extent for fine resolution, minimum separation between any two elements decide the position of grating lobes, and the size of each antenna element controls the total illuminated area. Therefore even though almost all the results presented in this document are for the 14 element sparse array case, towards the end we also decided to test our algorithms for a more standard regular antenna array. The 16 element regular 4×4 array has been shown in Figure 3.8. It can be seen that the equivalent 4 by 4 array occupies a much smaller volume than the random sparse array.
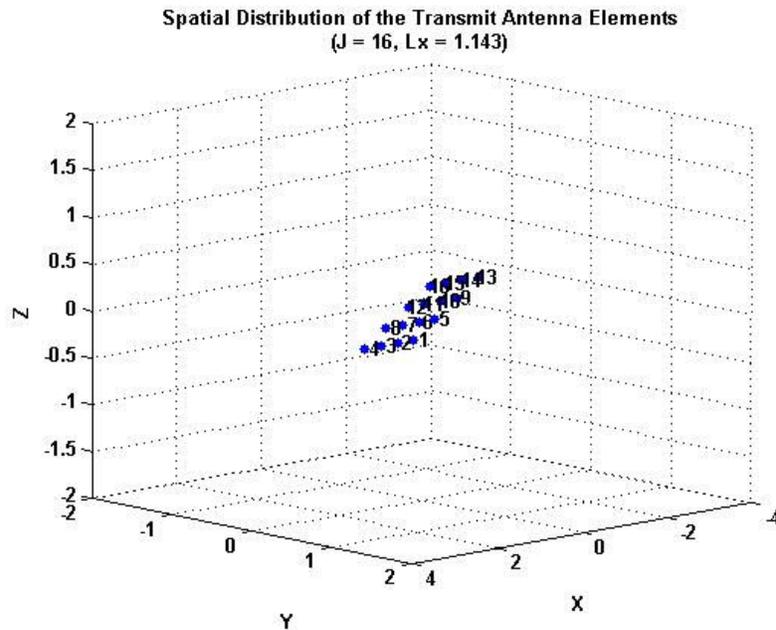
Figure 3:8 Sixteen element regularly distributed 4 × 4 transmit array

Having looked at the standard optimization criteria and the problems associated with them, it should be now clear that these criteria are often inadequate for many radar problems. Thus there is a need for new optimization algorithms which can tackle the orphan problem more effectively. This leads us into our next chapter on the "Maxi-min" algorithms, but before that one last point needs to be made about the standard codes.

Recall that the whole idea behind opting for a space-time transmitter was to come up with true space-time codes, i.e. independent time-frequency signals on each of the transmit elements. The amount of correlation between the temporal signals of different transmit antennas, gives a good indication of how close we reach towards our goal of realizing true space-time codes. The correlation coefficient values

between the signals on different antennas can be shown by a 2-D matrix or a 2-D colored plot as shown in Figure 3:9. This plot is for the Maximum SCR code of the last case in Figure 3.7, i.e. the illumination plot for the regular 4×4 array.
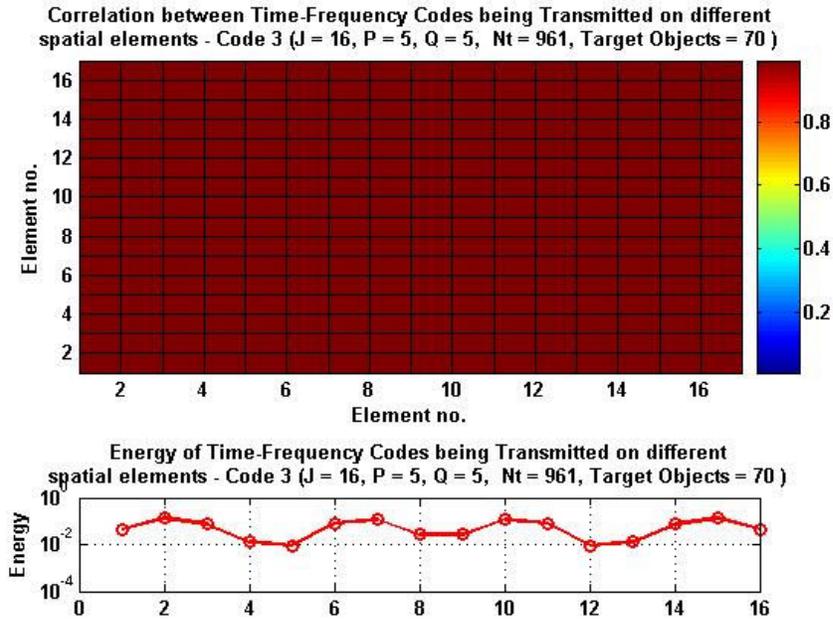
Figure 3:9 Correlation coefficients between temporal signals of different elements, and distribution of energy on different antennas for a standard code – Maximum SCR

Note that henceforth we will be calling these plots as the correlation matrix plots. Actually it turns out that the correlation matrix plot shown above is representative of almost all the standard code solutions we ever come up with. In this case we have 25 time-frequency basis functions, or enough degrees of freedom to come up with different temporal signals on each of the transmit antennas. But as can be seen from the figure, the transmit signals on the different antennas are perfectly correlated or have a correlation coefficient value of 1. It means is that the same time-frequency signal is propagated on each of the antennas, with just an additional

weighting on top. This additional weighting can be partly be seen in the lower part of the figure, where the curve shows the energy of the temporal signals on the different transmit elements (indicative of just the magnitude, and not the phase part).

Summarizing, the whole point of this discussion is to demonstrate that even though a valid structure exists, most of the time standard codes do not provide us with true or non-separable space-time solutions. Thus the real potential of space-time codes is not realized, and the solutions essentially become beamforming solutions - the form of the time-frequency signal obviously being inconsequential in such cases. With this assertion we move onto the next chapter on the Maxi-min codes, which are more advanced in character and thus attempt to exploit the full potency of the space-time transmitter.

Chapter 4

Illumination Optimization: Advanced Algorithms

4.1 The Maxi-min Criteria

This chapter is all about the 'new and improved' criteria – the Maxi-min or the Mini-max, which would make more applicable radar signals. We can actually have a number of different definitions for the maxi-min or the mini-max:

- The code which maximizes the smallest energy received by any target
- The code which minimizes the largest energy received by any clutter object
- The code which maximizes the SCR for the target with the worst SCR

Extending the same reasoning as for the standard codes, the last criterion makes most sense and was thus adopted as our primary maxi-min criterion. However finding solutions for these more appropriate criteria is not as direct as the standard codes, and requires a considerably greater computational effort.

From (3.13), the SCR received by each individual target can be mathematically defined as:

$$SCR_i = \frac{E_a^i}{E_b} = \frac{\mathbf{S'A}_i\mathbf{S}}{\mathbf{S'BS}} = \frac{\tilde{\mathbf{S}}'\mathbf{C}_i\tilde{\mathbf{S}}}{\tilde{\mathbf{S}}'\tilde{\mathbf{S}}} \tag{4.1}$$

where,

$$\mathbf{C}_i = \mathbf{B}^{-1/2}\,\mathbf{A}_i\,\mathbf{B}^{-1/2} \tag{4.2}$$

The aim of our algorithms is to find a transmit vector $\mathbf{S}$ which would maximize the smallest of these values i.e. the worst SCR or $SCR_{\min}$:

$$SCR_{\min} = \min\left\{\lambda_1^{min}, \lambda_2^{min}, \lambda_3^{min}, \cdots \lambda_{N_t}^{min}\right\} \qquad (4.3)$$

$N_t = N_x \times N_y$ is the total number of targets, and thus the total number of individual $\mathbf{C}$ matrices. Note there is no way to determine this value of $SCR_{\min}$, or know our weakest target beforehand. If it could be done, then we could have just focused our efforts on making that weakest target as strong as possible, but this weakest target and the value of $SCR_{\min}$ are very dependent on the transmit signal itself. Putting it another way, there is no way of directly finding a transmit vector $\mathbf{S}$ that would maximize the SCR on our worst target, as the worst target and the SCR it receives are themselves dependent on the transmit vector $\mathbf{S}$ - kind of like a chicken and egg problem. One line of action is to use numerical search methods like genetic algorithms. However such methods do not have much mathematical basis, and are essentially just a means for 'guessing intelligently'. As a result the processing costs associated are huge, and the answers not always satisfactory. In this chapter we propose methods that are more algebraic in nature, are computationally less expensive, and perform reasonably well under most circumstances.

4.2 Implementation – Different types of Maxi-mins

4.2.1 True Maxi-min

As mentioned before finding the optimal maxi-min solution is not easy, however finding the worst maxi-min solution is much simpler. Since all matrices $\mathbf{C}_i$

are non-negative definite, the smallest eigen value λ_i^{min} provides the value of the worst SCR that the ith target can receive, and the corresponding eigen vector $\tilde{\tilde{e}}^{min}$ is the worst SCR solution for that particular target. The overall worst solution for all the targets is then simply the eigen vector associated with the smallest of all minimum eigen values, i.e. the eigen vector $\tilde{\tilde{e}}^{min}$ associated with:

$$\lambda^{min} = \min\left\{\lambda_1^{min}, \lambda_2^{min}, \lambda_3^{min}, \cdots \lambda_{N_t}^{min}\right\} \le SCR_{min} \tag{4.4}$$

This eigen value thus provides a lower bound on SCR_{min}, or the worst SCR our weakest target can receive. No transmit vector except $\tilde{\tilde{e}}^{min}$ can result in a SCR_{min} value as small as λ^{min}. It logically follows that if we project out this worst dimension (i.e. the one associated with $\tilde{\tilde{e}}^{min}$) from our search space, we would raise the lower bound for SCR_{min}. For this purpose a projection matrix $\mathbf{P}_\perp(l)$ is formed as:

$$\mathbf{P}_\perp(l) = \mathbf{I} - \tilde{\tilde{e}}^{min}\,\tilde{\tilde{e}}^{min\prime} \ , \tag{4.5}$$

and this projection matrix is then used to update all the $\mathbf{C}_i$ matrices for individual targets:

$$\mathbf{C}_i(l+1) = \mathbf{P}_\perp{}'(l)\,\mathbf{C}_i(l)\,\mathbf{P}_\perp(l) \tag{4.6}$$

The solution space for our transmit vector $\mathbf{S}$ is now restricted to a subspace orthogonal to the worst vector $\tilde{\tilde{e}}^{min}(l)$, where l represents the iteration index. We can again find the worst solution in this new subspace and then project orthogonal to this new worst solution $\tilde{\tilde{e}}_{l+1}^{min}$. Since all the projections are orthogonal to the previous ones, our lower bound monotonically increases with each iteration. We continue with this

process until we are left with a solution space of just one dimension – a vector, which then becomes our optimal maxi-min solution **S**. Note that this method just claims to maximize the lower bound on SCR_{min}, it does not say that it will provide us with the best maxi-min solution possible. There might be better solutions present, but due to the inherent complex nature of the problem there is no way of knowing where they lie in our multi-dimensional search space. The assumption is that the lower bound solution still provides us with a pretty good if not the best answer, and the nice thing is that we now have a structure or mathematical procedure for arriving at that answer.

We call the algorithm described above - the "*True Maxi-min*", because of the way it's organized. It has a clear mathematical foundation, and every projection is mathematically guaranteed to raise the lower bound. The solution after every iteration is as good if not better than the last one, and there is no ambiguity involved. We have another class of algorithms called the "*Heuristic Maxi-mins*" which although not as sound mathematically, are quite effective in their own way. Before we move on to this new algorithm, we first need to point out two variations of the True Maxi-min.

4.2.2 Maxi-min SCR and Maxi-min Energy Convergence

Note that the projection step of (4.5–4.6) can be performed in either of the two ways.

$$\tilde{\mathbf{P}}_{\perp}{}' \, \mathbf{C}_i \, \tilde{\mathbf{P}}_{\perp} \text{ where,}$$

$$\tilde{\mathbf{P}}_{\perp} = \mathbf{I} - \tilde{\tilde{e}}^{min} \, \tilde{\tilde{e}}^{min\prime} \tag{4.7}$$

or,

$$(\mathbf{P}_\perp'\mathbf{B}\mathbf{P}_\perp)^{-1/2} \ (\mathbf{P}_\perp'\mathbf{A}_i\mathbf{P}_\perp) \ (\mathbf{P}_\perp'\mathbf{B}\mathbf{P}_\perp)^{-1/2}) \text{ where,}$$

<div align="right">(4.8)</div>

$$\mathbf{P}_\perp = \mathbf{I} - \hat{e}^{min}\,\hat{e}^{min\prime}, \text{ and } \hat{e}^{min} = \mathbf{B}^{-1/2}\,\tilde{\hat{e}}^{min}$$

In the first case we stay in the squiggle domain throughout (i.e. directly deal with the eigen vectors of $\mathbf{C}$ matrix), and convert back to the non-squiggle domain right at the end - using (3.21). We thus call this approach as the '*True Maxi-min Squiggle*'. While in the second case we convert back and forth between the squiggle and non-squiggle domains after every iteration. More specifically, we find our worst projection vector in the squiggle domain (which is one of the eigen vectors of one of the $\mathbf{C}$ matrices), convert it back to the non-squiggle domain using (3.21), and form our projection matrix $\mathbf{P}_\perp$ in the non-squiggle domain. We then use $\mathbf{P}_\perp$ to update the $\mathbf{B}$ and all individual $\mathbf{A}_i$ matrices and again form our new $\mathbf{C}_i$ matrices. As the projection operation is performed in the non-squiggle world, this approach is understandably called the '*True Maxi-min Non-Squiggle*'. Both the above approaches are valid but inherently different, and hence yield different results.

The reason behind this difference lies in the fact that two orthogonal vectors in one domain (squiggle) may no longer stay orthogonal in another domain (non-squiggle) after a projection. The projection essentially implies a change of the coordinate space. This point clearly illustrated by the following equations:

If
$$\tilde{\mathbf{S}}_1'\,\tilde{\mathbf{S}}_2 = 0,$$

then
$$\mathbf{S}_1'\mathbf{S}_2 = \tilde{\mathbf{S}}_1'\,\mathbf{B}^{-1/2}\,'\,\mathbf{B}^{-1/2}\,\tilde{\mathbf{S}}_2 = 0 \text{ , only if}$$

$$\mathbf{B^{-1/2}}' \, \mathbf{B^{-1/2}} = \mathbf{I} \, ,$$

which is not true (generally) and especially if $\mathbf{B}$ is not full ranked.

It turns out that due to this reason, both the algorithms take completely different paths to the final solution and converge to two independent answers. In fact for the trivial case of a single target, the *squiggle* algorithm ($\tilde{\mathbf{P}}_\perp$) converges to the Maximum SCR solution as would be normally expected but the *non-squiggle* algorithm ($\mathbf{P}_\perp$) converges to the Maximum Energy solution instead. The convergence for the "true" algorithms is illustrated in Figure 4.1 on the next page.

True Maxi-min Energy Convergence

Maxi-min Non-Squiggle $\mathbf{P}_\perp$ **Maximum Energy**

True Maxi-min SCR Convergence

Maxi-min Squiggle $\tilde{\mathbf{P}}_\perp$ **Maximum SCR**
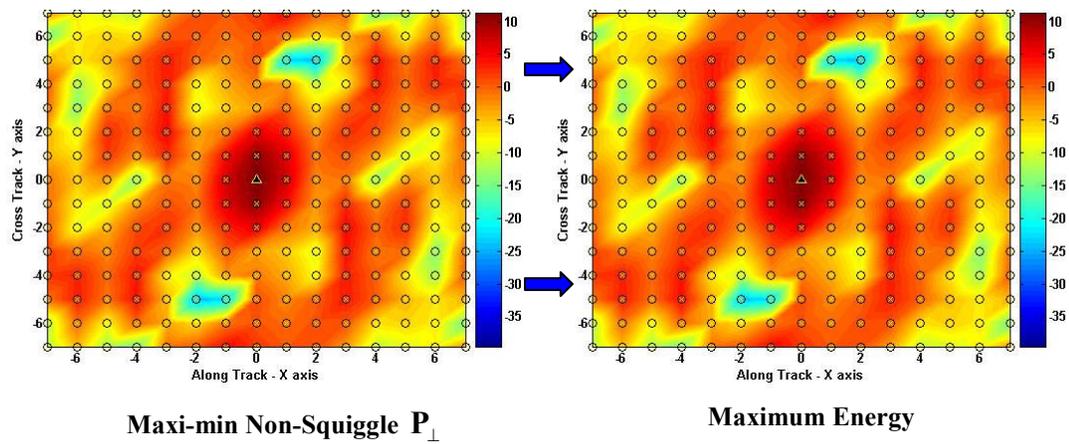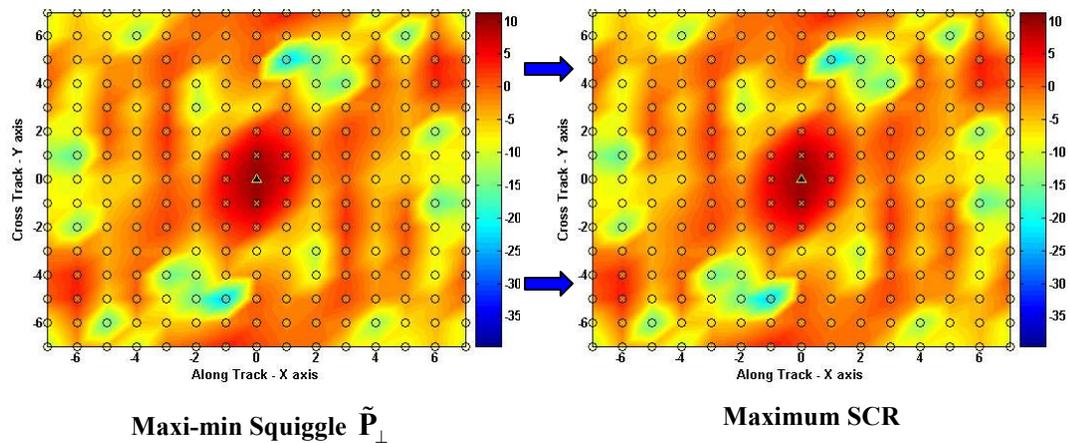
Figure 4:1 Convergence of the True Squiggle and Non-Squiggle Maxi-mins

This behavior is explained as follows. For the single target case there is just one matrix $\mathbf{C}$, and in the squiggle domain we are trying to maximize the quantity $\tilde{\mathbf{S}}' \mathbf{C} \tilde{\mathbf{S}}$. Therefore we find the codes which would put the least SCR on our target, i.e. the vectors corresponding to the smallest eigen values of $\mathbf{C}$ and form our projection

matrix $\tilde{\mathbf{P}}_\perp$ in the squiggle domain. Thus we always stay orthogonal to the largest eigen vector of **C**, and in the end converge to this code or the Maximum SCR solution.

For the non-squiggle domain algorithm we again try to stay orthogonal to the vector corresponding to the largest eigen value of **C** in the squiggle domain, but as mentioned before, once we transform out of the squiggle to the non-squiggle world that orthogonality is lost. Instead the problem now becomes of maximizing the ratio $\dfrac{\mathbf{S}'\,\mathbf{A}\,\mathbf{S}}{\mathbf{S}'\,\mathbf{B}\,\mathbf{S}}$, and the worst vector which minimizes the SCR on our target (say by putting zero or very little energy on the target in the non-squiggle domain) need not be orthogonal to the Maximum SCR vector (in the squiggle domain). It can just be orthogonal to the vector corresponding to the largest eigen value of **A** (Maximum energy code) and still satisfy the math in the non-squiggle domain. However our Maximum SCR code typically has some component which is not in the same direction as the Maximum Energy code, and with each projection we knock down part of this component. Thus we are just guaranteed to stay in the direction of the Maximum Energy and not the Maximum SCR, and this is the reason why the non-squiggle algorithm converges to the Maximum Energy vector in the end.

This would be a good time to mention one other point about the squiggle domain or SCR convergence maxi-min algorithm. Note that henceforth the *squiggle domain maxi-min* will be known as the *SCR convergence maxi-min* and the *non-squiggle domain maxi-min* will be known as the *energy convergence maxi-min* in this

document. And although not exactly precise, the eigen vector corresponding to the largest eigen value will be referred to as the *largest eigen vector* and the one corresponding to the smallest eigen value - the *smallest eigen vector*. In reality all eigen vectors have the same unit magnitude but this terminology greatly simplifies the language, making it easier to explain the main concepts instead of unduly worrying about the semantics. Continuing with the important point on the SCR convergence maxi-min - the main reason it works, or the fact that we can stay in the squiggle domain and convert back right at the end, is because we have a matrix **B** which is constant for all targets. If it were not so, then this method could not have been employed and we would have been short of one algorithm. This point is better explained with the following equations:

For the sake of simplicity let's assume that there are only two projections or we are searching for the best vector in a 3-dimensional space. Then in the end we would be looking for a vector $\tilde{\mathbf{S}}$ that would maximize the quantity:

$$\frac{\tilde{\mathbf{S}}'(\tilde{\mathbf{P}}'_{\perp 2}\,\tilde{\mathbf{P}}'_{\perp 1}\,\mathbf{C}\,\tilde{\mathbf{P}}_{\perp 1}\,\tilde{\mathbf{P}}_{\perp 2})\tilde{\mathbf{S}}}{\tilde{\mathbf{S}}'\tilde{\mathbf{S}}}$$

in the squiggle domain. The equivalent expression in the non-squiggle domain would be:

$$= \frac{\tilde{\mathbf{S}}'(\tilde{\mathbf{P}}'_{\perp 2}\,\tilde{\mathbf{P}}'_{\perp 1}\,\mathbf{B}^{-1/2'}\mathbf{A}\,\mathbf{B}^{-1/2}\,\tilde{\mathbf{P}}_{\perp 1}\,\tilde{\mathbf{P}}_{\perp 2})\tilde{\mathbf{S}}}{\tilde{\mathbf{S}}'\tilde{\mathbf{S}}}\text{ , or}$$

$$= \frac{(\tilde{\mathbf{P}}_{\perp 1}\,\tilde{\mathbf{P}}_{\perp 2}\,\tilde{\mathbf{S}})'\,\mathbf{B}^{-1/2}\mathbf{A}\,\mathbf{B}^{-1/2}\,(\tilde{\mathbf{P}}_{\perp 1}\,\tilde{\mathbf{P}}_{\perp 2}\,\tilde{\mathbf{S}})}{\tilde{\mathbf{S}}'\tilde{\mathbf{S}}}$$

Comparing with (3.14), and then using (3.21) we find that the corresponding non-squiggle domain vector should be:

$$\mathbf{S} = \mathbf{B}^{-1/2}(\tilde{\mathbf{P}}_{\perp 1}\,\tilde{\mathbf{P}}_{\perp 2}\,\tilde{\mathbf{S}})$$

Since all projections are orthogonal to each other, our final squiggle domain vector $\tilde{\mathbf{S}}$ would pass through unscathed i.e.

$$\tilde{\mathbf{P}}_{\perp 1}\,\tilde{\mathbf{P}}_{\perp 2}\,\tilde{\mathbf{S}} = \tilde{\mathbf{S}},\text{ and}$$

$$\therefore \mathbf{S} = \mathbf{B}^{-1/2}\,\tilde{\mathbf{S}}$$

just like the normal case, and therefore we can find our non-squiggle domain vector right at the end. Note that this method would not have worked had the matrix $\mathbf{B}$ been different for each target, as is the case in some conditions (for e.g. finding a code to minimize correlation between 2 objects [8]). Fortunately for our problem that is not the case, and we get an extra algorithm that is not only computationally faster (the extra projections from squiggle to non-squiggle domain at every step are done away with), but also more effective than the non-squiggle algorithm in most cases.

To wrap up this section let's present a formal, mathematical step by step description of the two True Maxi-min algorithms:

True Maxi-min SCR convergence

1. Find the minimum eigen value λ_i^{min} for each individual $\mathbf{C}_i$ matrix.

2. Determine the absolute minimum of the lot, or our lower bound on SCR_{min}

    $: \lambda_{smallest}^{min} = \min\left\{\lambda_1^{min}, \lambda_2^{min}, \lambda_3^{min}, \cdots \lambda_{N_t}^{min}\right\}$

3. Use the corresponding eigen vector $\tilde{\hat{e}}^{min}$ to form the projection matrix:

$$\tilde{\mathbf{P}}_\perp(l) = \mathbf{I} - \tilde{\hat{e}}_l^{min} \tilde{\hat{e}}_l^{min\prime}$$

4. Update all individual $\mathbf{C}_i$ matrices in the squiggle domain:

$$\mathbf{C}_i(l+1) = \tilde{\mathbf{P}}_\perp{}'(l) \, \mathbf{C}_i(l) \, \tilde{\mathbf{P}}_\perp(l)$$

5. Again find the minimum eigen value of the set and repeat the process till the time only one non zero value remains in the eigen spectrum of each $\mathbf{C}_i$ matrix, i.e. repeat for W-1 iterations where W is the transmit signal dimension.

6. Use the last surviving vector in the squiggle domain to find our optimal transmit code as $\mathbf{S} = \mathbf{B}^{-1/2} \tilde{\mathbf{S}}$

True Maxi-min Energy convergence

1. Find the minimum eigen value λ_i^{min} for each individual $\mathbf{C}_i$ matrix.

2. Determine the absolute minimum of the lot, or our lower bound on SCR_{min}

$$: \lambda_{smallest}^{min} = \min\left\{\lambda_1^{min}, \lambda_2^{min}, \lambda_3^{min}, \cdots \lambda_{N_t}^{min}\right\}$$

3. Use the corresponding eigen vector $\tilde{\hat{e}}^{min}$ to determine the projection vector in the non-squiggle domain: $\hat{e}^{min} = \mathbf{B}^{-1/2} \tilde{\hat{e}}^{min}$

4. Form the projection matrix: $\mathbf{P}_\perp(l) = \mathbf{I} - \hat{e}_l^{min} \hat{e}_l^{min\prime}$.

5. Update the individual $\mathbf{A}_i$ matrices and the $\mathbf{B}$ matrix in the non-squiggle domain: $\mathbf{A}_i(l+1) = \mathbf{P}_\perp{}'(l) \, \mathbf{A}_i(l) \, \mathbf{P}_\perp(l)$, and $\mathbf{B}(l+1) = \mathbf{P}_\perp{}'(l) \, \mathbf{B}(l) \, \mathbf{P}_\perp(l)$.

6. Find the new $\mathbf{C}_i$ matrices: $\mathbf{C}_i(l+1) = \mathbf{B}(l+1)^{-1/2} \, \mathbf{A}_i(l+1) \, \mathbf{B}(l+1)^{-1/2}$

7. Again find the minimum eigen value of the set and repeat the process till the time only one non zero value remains in the eigen spectrum of each $\mathbf{C}_i$ matrix, i.e. repeat for W-1 iterations where W is the transmit signal dimension.

8. Use the last surviving vector in the squiggle domain to find our optimal transmit code as $\mathbf{S} = \mathbf{B}^{-1/2} \tilde{\mathbf{S}}$.

In this section we saw the two "True" algorithms, which try to come up with an optimal answer by maximizing the lower bound on $SCR_{\min}$. It turns out that there can be one more approach to the maxi-min problem, i.e. by trying to preserve the upper bound and keeping it as high as possible. We call this algorithm the "Heuristic" algorithm, and it is the topic of our next section.

4.2.3 Heuristic Maxi-min

The first thing to be pointed out about this algorithm is the name "heuristic". This name is kind of misleading as the algorithm is not completely heuristic. It has quite a bit of mathematical teeth to it, and only a small portion of it can really be treated as abstract. This algorithm is quite similar in structure to the "true" algorithm, but at the same time has one major difference associated with itself.

In case of the 'true' algorithms we focused our attention on the smallest of all minimum eigen values: $\lambda^{min} = \min\left\{\lambda_1^{min}, \lambda_2^{min}, \lambda_3^{min}, \cdots \lambda_{N_t}^{min}\right\}$, or the lower bound on our $SCR_{\min}$. Likewise we can also focus our attention on the smallest of all maximum eigen values, which gives us the upper bound on $SCR_{\min}$ i.e.

$$\lambda_{\text{smallest}}^{max} = \min\left\{\lambda_1^{max}, \lambda_2^{max}, \lambda_3^{max}, \cdots \lambda_{N_t}^{max}\right\} \geq SCR_{\min} \tag{4.9}$$

The eigen vector associated with each of these values is the best solution for that particular target respectively. No solution vector **S** can result in a $SCR_{\min}$ better than $\lambda_{\text{smallest}}^{max}$. It will be seen later in Chapter 5, that this upper bound is a critical parameter for all our optimization procedures and kind of sets the limit on how much the lower bound can be increased. It is because with every projection as the lower bound increases, we also throw out some component for our individual best vectors and thus the upper bound also falls. Even at its maximum value during the last iteration, the lower bound is still smaller than the upper bound value of any and every previous iteration. Therefore the upper bound, in a way sets the limit on how close our lower bound can converge to the maximum $SCR_{\min}$ solution.

The "true" algorithms seen before, however just work to provide the maximum increase in the value of lower bound after each step. They do not care about preserving the upper bound at all. It's quite possible that the lower bound increases slightly, but the upper bound falls substantially during the same iteration. Just as an example Figure 4.2 shows the convergence of the lower and upper bounds (monotonic rise and fall respectively), for one of the "true" algorithms. This example is again for 14 transmit antennas and 9 time-frequency basis functions, and hence a total transmit signal dimension of $W = 126$.

True Maxi-min SCR Convergence
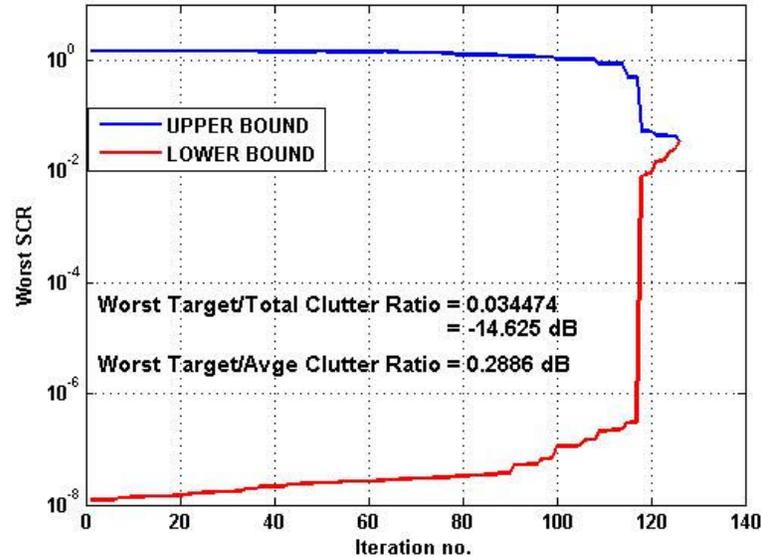
Figure 4:2 Convergence of upper and lower bounds with iteration number

Here also it seems that it is the lower-bound which tries to rise and meet the upper bound. This once again emphasizes the importance of preserving the upper bound, and as mentioned before the upper bound can be thought of putting an indirect limit on how close the lower bound can reach the maximum SCR_{min} solution. This also signals a need for an algorithm which can raise the lower bound "floor" while at the same time preserve the upper bound "ceiling", and here's where our "Heuristic Maxi-min" finds application.

For this algorithm, we first find the target 't' with the minimum largest eigen value, $\lambda^{max}_{smallest}$ of (4.9). This is the target which sets the upper bound on our SCR_{min} i.e. the potentially best SCR it can receive is the least amongst all targets. We thus call it our weakest target and try to take special care of it. The next step is therefore to

determine the eigen spectrum of the corresponding matrix $\mathbf{C}_t$, and select the worst solution for this target $\tilde{\tilde{e}}_t^{min}$ as our projection vector, i.e. the vector associated with λ_t^{min}. The selection of this vector ensures that the upper bound on SCR_{min} does not fall any further. Since all eigen vectors are orthogonal to each other, the projection vector $\tilde{\tilde{e}}_t^{min}$ turns out to be orthogonal to the best solution vector for our weakest target - $\tilde{\tilde{e}}_t^{max}$. Thus there is no reduction in the maximum eigen value λ_t^{max} for this target, as the best solution vector for the weakest target is still part of the new projected subspace. The projection obviously reduces the maximum eigen values for other targets, but since these values were anyway larger than λ_t^{max} to begin with, the overall reduction in the upper bound is minimized.

But here's where the name "heuristic" comes from. Although we are trying to keep the upper bound up, there is no assurance that a projection will not cause the maximum eigen value of some other target to drop drastically, and hence result in complete decimation of our upper bound. For the numerous simulation cases tried such a behavior was never encountered, but even then there is nothing in the math which says that this "cannot" happen. This algorithm is clearly not as defensible (mathematically) as the earlier "true" algorithm, but is still seen to outperform it in most cases. Hopefully it should also be clear to the readers that although this algorithm is called "heuristic", it is not exactly so; it is completely unlike a random or numerical search method where we just try to make intelligent guesses. There is a definite mathematical rationale behind it wherein we try and uphold the upper bound,

but at the same time we also have the possibility of running into pitfalls by going down the wrong search paths.

Anyhow, the remaining steps are exactly identical to the "true" algorithms. We form our projection matrix in the squiggle or non-squiggle domain depending on the algorithm version (SCR or energy convergence) and proceed in exactly the same fashion. We stop after W-1 projections when we are left with a single dimension – our optimal Maxi-min solution $\mathbf{S}$. For a single target case, the "heuristic" algorithms also converge to the Maximum energy and SCR solutions as shown in Figure 4.3.

Heuristic Maxi-min Energy Convergence

Maxi-min Non-Squiggle $\mathbf{P}_\perp$ **Maximum Energy**

Heuristic Maxi-min SCR Convergence

Maxi-min Squiggle $\tilde{\mathbf{P}}_\perp$ **Maximum SCR**
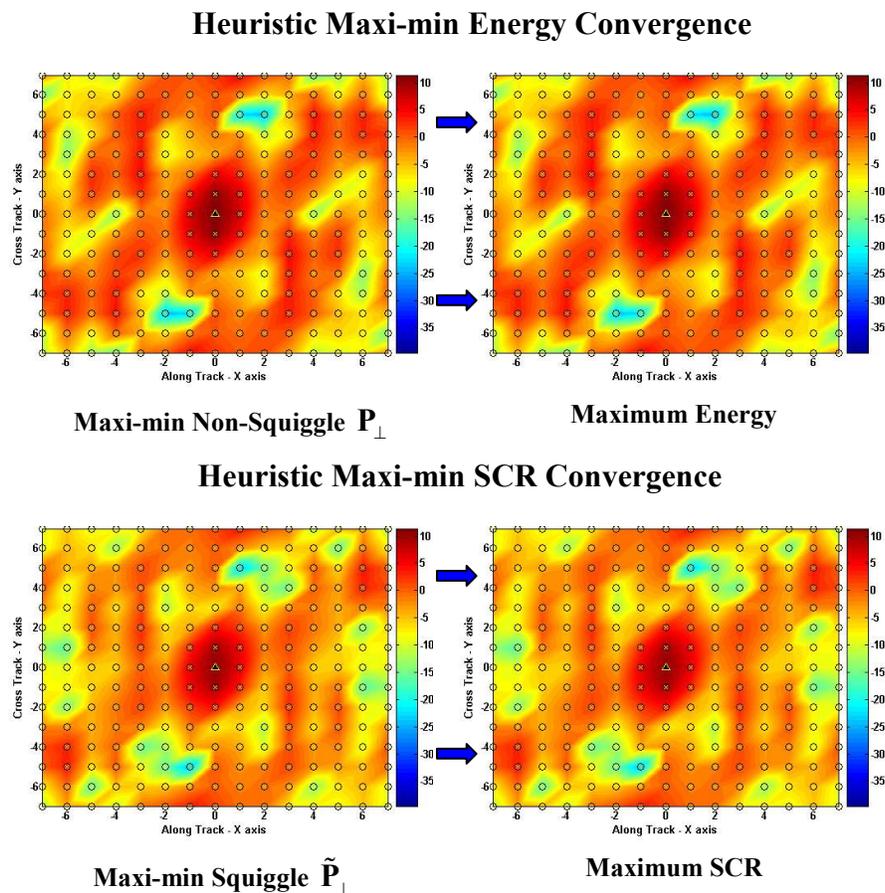
Figure 4:3 Convergence of the Heuristic Squiggle and Non-Squiggle Maxi-min

97

The two variants of this algorithm have been described in a mathematical step by step form below.

Heuristic Maxi-min SCR convergence

1. Find the maximum eigen value λ_i^{max} for each individual $\mathbf{C}_i$ matrix.

2. Determine the absolute minimum of the lot (upper bound on SCR_{min}) as

   $$\lambda_{smallest}^{max} = \min\left\{\lambda_1^{max}, \lambda_2^{max}, \lambda_3^{max}, \cdots \lambda_{N_t}^{max}\right\}$$, and thus the weakest target 't' so that

   $$\lambda_t^{max} = \lambda_{smallest}^{max}.$$

3. Find the minimum eigen value for the weakest target 't' - λ_t^{min}

4. Use the corresponding eigen vector $\tilde{e}^{min}$ to form the projection matrix:

   $$\tilde{\mathbf{P}}_{\perp}(l) = \mathbf{I} - \tilde{e}_l^{min} \tilde{e}_l^{min\prime}$$

5. Update all individual $\mathbf{C}_i$ matrices in the squiggle domain:

   $$\mathbf{C}_i(l+1) = \tilde{\mathbf{P}}_{\perp}{}'(l) \, \mathbf{C}_i(l) \, \tilde{\mathbf{P}}_{\perp}(l)$$

6. Again find the minimum eigen value of the set and repeat the process till the time only one non zero value remains in the spectrum of each matrix, i.e. repeat for W-1 iterations where W is the transmit signal dimension.

7. Use the last surviving vector in the squiggle domain to find our optimal transmit code $\mathbf{S} = \mathbf{B}^{-1/2}\, \tilde{\mathbf{S}}$.

Heuristic Maxi-min Energy convergence

1. Find the maximum eigen value λ_i^{max} for each individual $\mathbf{C}_i$ matrix.

2. Determine the absolute minimum of the lot (upper bound on $SCR_{\min}$) as

$$\lambda_{\text{smallest}}^{max} = \min\left\{\lambda_1^{max}, \lambda_2^{max}, \lambda_3^{max}, \cdots \lambda_{N_t}^{max}\right\} ,\text{ and thus the weakest target `t' so that}$$

$$\lambda_t^{max} = \lambda_{\text{smallest}}^{max} .$$

3. Find the minimum eigen value for the weakest target `t' - λ_t^{min}

4. Use the corresponding eigen vector $\tilde{e}^{min}$ to determine the projection vector in

   the non-squiggle domain: $\hat{e}^{min} = \mathbf{B}^{-1/2}\, \tilde{\hat{e}}^{min}$

5. Form the projection matrix: $\mathbf{P}_\perp(l) = \mathbf{I} - \hat{e}_l^{min}\, \hat{e}_l^{min\prime}$.

6. Update the individual $\mathbf{A}_i$ matrices and the $\mathbf{B}$ matrix in the non-squiggle

   domain: $\mathbf{A}_i(l+1) = \mathbf{P}_\perp{}'(l)\, \mathbf{A}_i(l)\, \mathbf{P}_\perp(l)$, and $\mathbf{B}(l+1) = \mathbf{P}_\perp{}'(l)\, \mathbf{B}(l)\, \mathbf{P}_\perp(l)$.

7. Find the new $\mathbf{C}_i$ matrices: $\mathbf{C}_i(l+1) = \mathbf{B}(l+1)^{-1/2}\, \mathbf{A}_i(l+1)\, \mathbf{B}(l+1)^{-1/2}$

8. Again find the minimum eigen value of the set and repeat the process till the

   time only one non zero value remains in the spectrum of each matrix, i.e.

   repeat for W-1 iterations where W is the transmit signal dimension.

9. Use the last surviving vector in the squiggle domain to find the optimal

   transmit code as $\mathbf{S} = \mathbf{B}^{-1/2}\, \tilde{\mathbf{S}}$.

That completes our discussion on the types of Maxi-mins. So in all we have four

different maxi-min algorithms – the 'true' and 'heuristic' *SCR convergence* and the

'true' and 'heuristic' *energy convergence*. All four are designed for the same

objective, but perform differently as will be seen in the next section.

Before we go on to see the actual maxi-min performance results, one look at the processing costs involved. For a typical simulation case we use a 31×31 grid, 14 antenna elements and 25 time-frequency basis functions, i.e.:

$N_x = N_y = 31$

$J = 14$, and

$P = Q = 5$

The transmit signal dimension comes out to be 350 (W), and for the default parameter inputs the dimensions of $\mathbf{H}''$ matrices are 255×350 ($K' \times W$). Similarly each individual $\mathbf{A}_i$ and $\mathbf{C}_i$ matrix is 350×350 in size ($W \times W$).

Thus we are dealing with almost 1000 complex matrices of the above dimensions, and all operations – projections, multiplications, eigen value / vector decomposition have to be performed on these matrices. Moreover all the processes have to be repeated 349 times for the W-1 iterations. If we look at all these factors together, the processing times involved do not stay trivial. As an example for the above case, just one of the maxi-min algorithms (*Heuristic SCR convergence*) takes about 36 hours to come up with an answer. This is using a Pentium 4 - 2.8 GHz machine with 3 GB RAM, and 7200 rpm Hard Disk. The algorithm run requires a lot of data (mainly the $\mathbf{H}''$ and /or the $\mathbf{A}_i$ matrices) to be initially dumped on the Hard Disk, and then used as and when required. The processing time obviously goes up due to the high frequency of disk access, but is unavoidable as the large volume of generated data is too big to fit in the finite main memory.

The point to be made after describing the non-trivial computational costs associated with these advanced algorithms, is that these large processing times limit our options; the options of exploring new theories and/or trying new ideas. For example, we started out with an idea of retaining more than one projection vector after each iteration. Hence, instead of using only the worst or most promising vector for our projection matrix, we tried using two, three and even more number of most promising vectors to form different projection matrices. The same numbers of most promising "worst" vectors were retained after each iteration. The conjecture was that if instead of following a single path towards the optimal solution, the algorithm is given more flexibility in terms of the number of paths it can explore, then it will come up with much better solutions. And the hypothesis did seem to work for the smaller cases that were tried, but the idea had to be eventually abandoned due to the large amounts of processing cost involved. Similarly, more number of basis functions directly translate to more power to the algorithms and the possibility of coming up with better answers. However once again due to the constraints on the computation time, we could not try our algorithms for very large number of time-frequency basis functions. This point is covered later in greater detail.

It's time now to move on and look at some of the actual results for our Maxi-min algorithms. The results have been presented for several different scenarios, and the algorithm performance (and dependence) was studied for a number of criteria.

4.3 Maxi-min Results and Observations

4.3.1 Orphan Problem Solution

Before comparing the performance of all our algorithms, let's take a quick first glance on the efficacy the maxi-mins in resolving the orphan problem. Figures 4.4- 4.5 on the next two pages show the maxi-min performance for the orphan cases of Figure 3.7. All maxi-min plots shown are for the "Heuristic SCR convergence", which generally turns out to be our best algorithm (as will be seen later).

Maximum SCR   **Heuristic SCR Convergence**

SCR_{min} = -2.73 dB SCR_{min} = 11.38 dB

SCR_{min} = -2.21 dB SCR_{min} = 8.84 dB
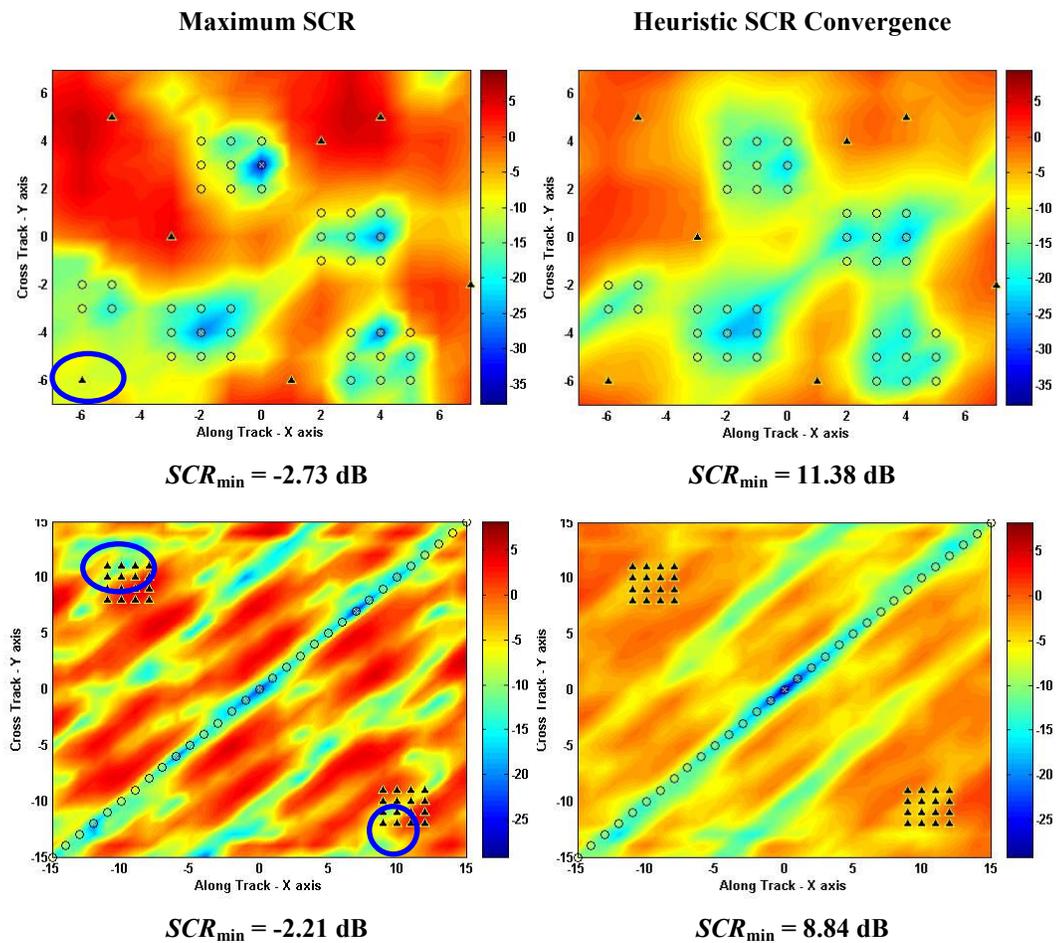
Figure 4:4 Maxi-min solution to the orphan problem – Heuristic SCR convergence

Maximum SCR ⟶ Heuristic SCR Convergence

SCR_{min} = -4.54 dB SCR_{min} = 1.35 dB

SCR_{min} = -10.68 dB SCR_{min} = 2.50 dB

SCR_{min} = -13.82 dB SCR_{min} = 6.96 dB
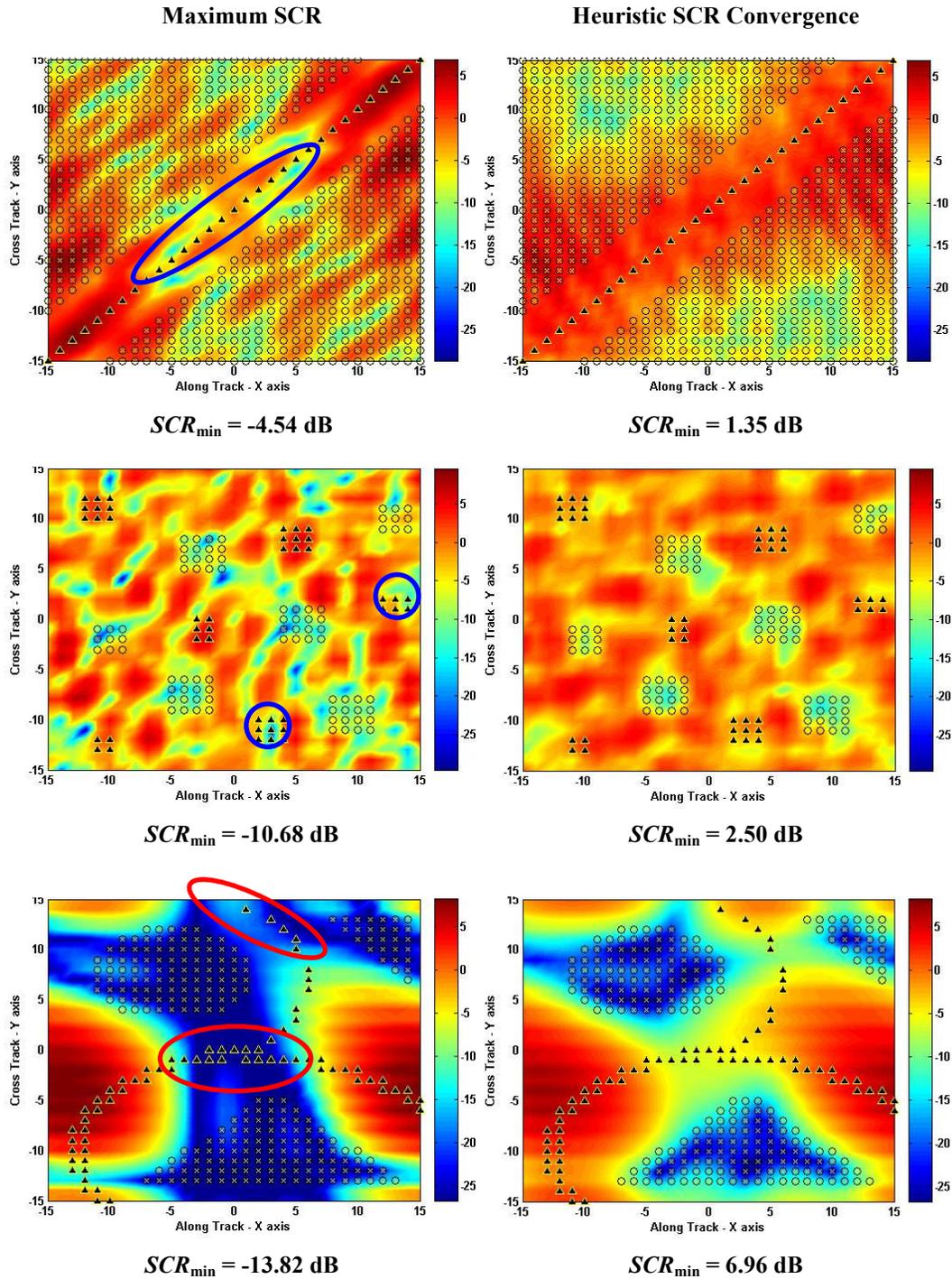
Figure 4:5 Maxi-min solution to the orphan problem – Heuristic SCR convergence

As can be seen, significant improvement in the worst SCR or SCR_{min} for our weakest target is achieved. For the cases shown this improvement is anywhere between 6 to 20 dB, or to 4 to 100 times. The gain in SCR_{min} is usually achieved at the cost of some loss in the average target energy or average SCR; but then the slight reduction in accuracy while detecting some targets is still far better than completely loosing out the others.

4.3.2 Comparison of the 4 Maxi-mins

The performance of all algorithms for a few cases, which also serve as good examples for the purpose of comparison, is shown next in Figures 4.6 - 4.7.
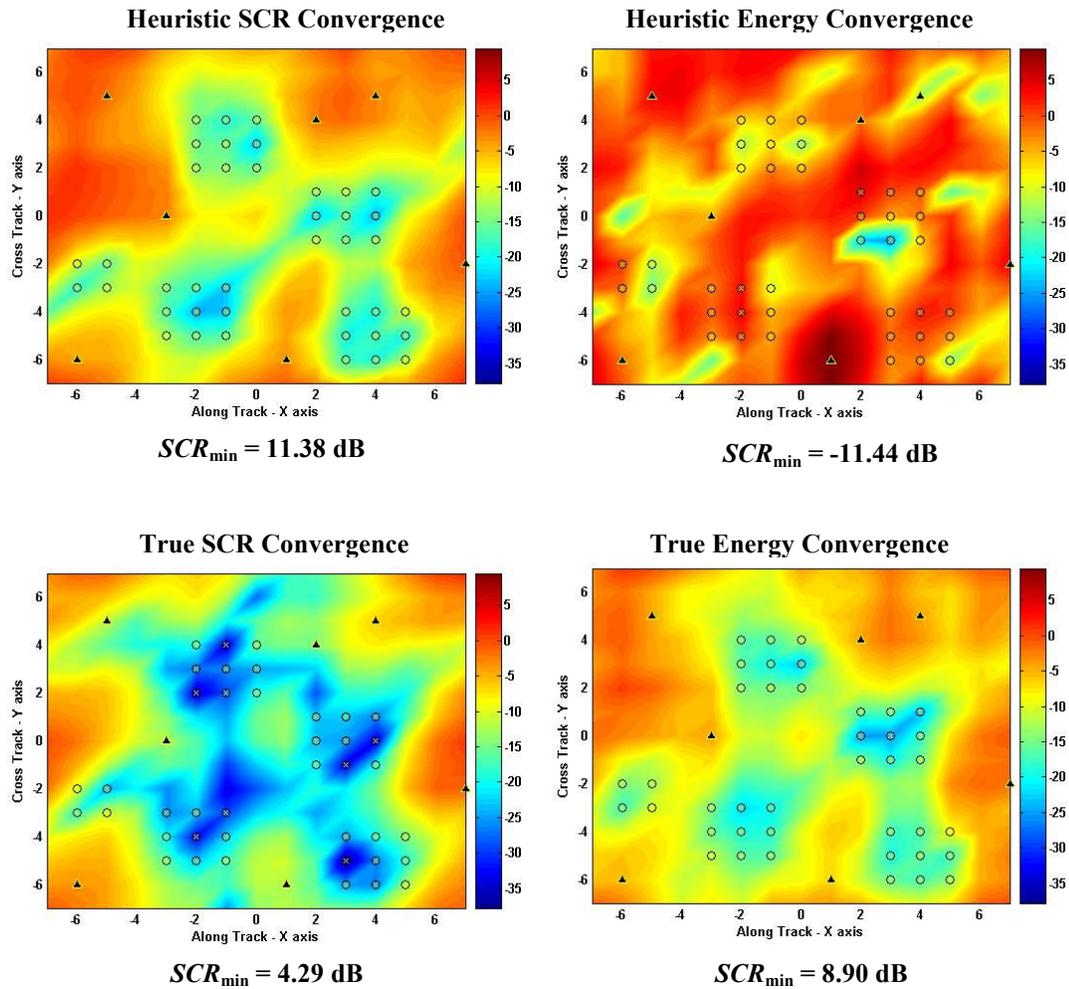
Figure 4:6 Performances of all 4 Maxi-min algorithms – Example I

The above case is for 9 time frequency basis functions. Note that although majority of the algorithms perform well here (three out of four), the "Heuristic Energy convergence" results in a terrible SCR_{min} value of -11.44 dB, i.e. it performs poorly than even the standard "Maximum SCR" for which SCR_{min} was -2.73 dB. This shows that there are no definite rules to predict when a particular algorithm will perform well, and when it will not. All algorithms search for the best answer in a huge multi-dimensional vector space, which is also full of lots and lots of bad solutions.

Therefore once in a while the possibility of ending up with one of these bad solutions is always there, but to predict when exactly this occurs is a very difficult proposition, probably near to impossible.

Certain observations can still be made about our algorithms. Under some circumstances all of them perform well, for other cases few of them do well and in rare cases none of them work at all. However, the "Heuristic SCR convergence" seems to perform reasonably under most conditions. Not only that, for the cases when most or all algorithms perform well, usually it's still the pick of the lot. This point is further illustrated in Figure 4.7 where all maxi-mins are again compared for a different target-clutter pattern, and for more number of basis functions.

Maximum SCR
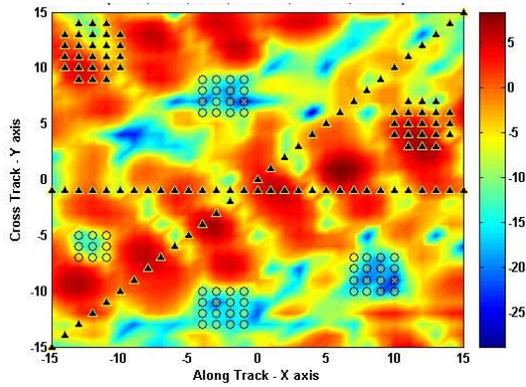
SCR_{min} = -3.5 dB

Heuristic SCR Convergence
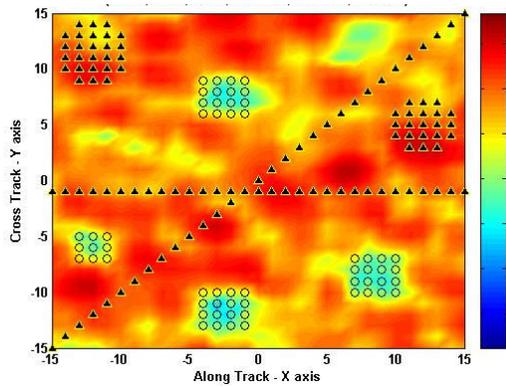
SCR_{min} = 2.51 dB

Heuristic Energy Convergence
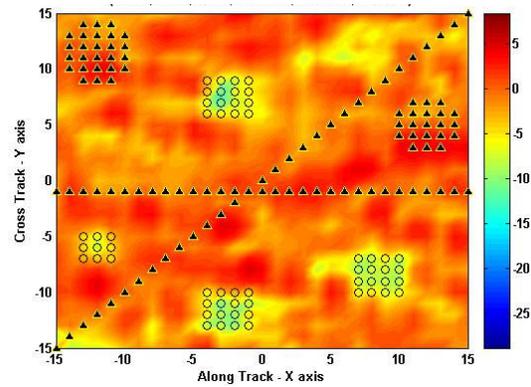
SCR_{min} = 1.29 dB

True SCR Convergence
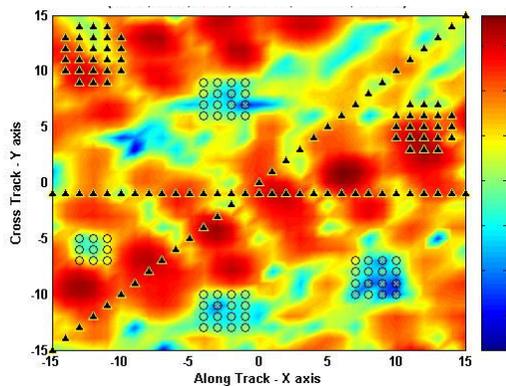
SCR_{min} = -1.47 dB

True Energy Convergence
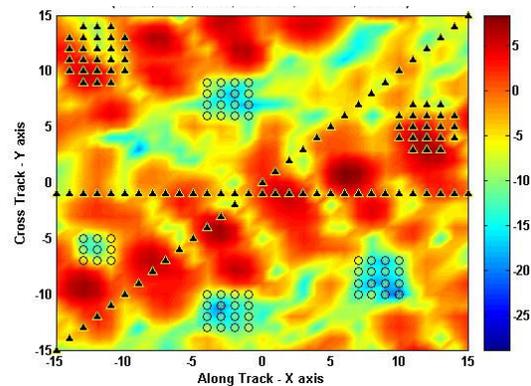
SCR_{min} = -0.19 dB

Figure 4:7 Performances of all 4 Maxi-min algorithms – Example II

The plots shown in Figure 4.7 are for 25 time-frequency basis functions (the effect of basis functions on algorithm performance is covered later). Once again the "Heuristic SCR convergence" is seen to give the best results. Also note the greatly improved performance of "Heuristic energy convergence" in this example. In fact both the heuristic algorithms are better than the "true algorithms" for this case. This is consistent with our earlier statement about the unpredictable nature of these algorithms. We never know which ones will perform better than the others, although most often the competition is limited to only three out of the four algorithms – the "Heuristic SCR convergence" being our unrivalled champion in most cases. Note that this conclusion was made after running a lot of different simulations and not just the above two examples. It's not possible to present all of those results here, but for majority of those cases "Heuristic SCR convergence" emerged as the undisputed victor over other maxi-mins. One way to probably explain this is by going back to our earlier discussion on the upper and lower bounds; we saw how the upper bound kind of sets the limit on lower bound improvement. Since the "Heuristic SCR" focuses on this upper bound preservation (which turns out to be the more important of the two bounds), and also resembles the "Maximum SCR" in its inherent nature (recall the trivial case of one target), intuitively it makes sense that it should turn out to be our best code.

Although the plots of Figure 4.7 may once again indicate that *"Heuristic SCR convergence"* is most likely our *champion code*, making other definite conclusions about the maxi-mins is still a risky proposition. Their performance though

understandable in many cases is not always explainable. Let's look at some more cases for the "Heuristic SCR convergence" performance, and try to understand its dependence on some of the key parameters.

4.3.3 Dependence on orphan occurrence

We saw cases where the Maxi-mins improved the SCR for the orphan targets. That is nice as that is what the maxi-mins are intended for, but what about the cases when there are no orphans at all? In other words, the illumination optimization problem is so simple that the standard codes themselves provide good solutions. We find that in such cases the maxi-mins are unable to improve the performance any further and often end up giving worse solutions. This point is demonstrated in Figure 4.8.

SCR_{min} = 1.4 dB SCR_{min} = 0.7 dB
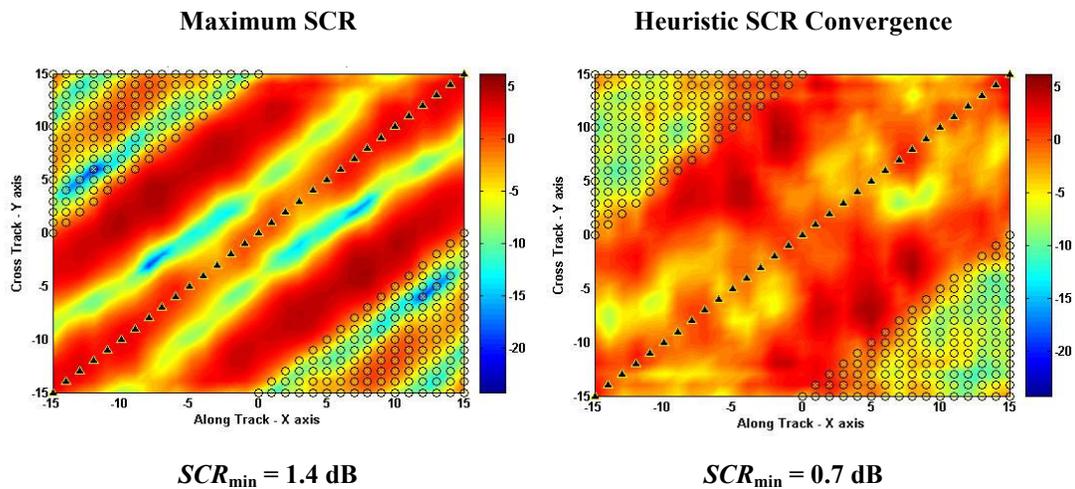
Figure 4:8 Maxi-min performance – Dependence on orphan occurrence I

The reason can again be attributed to the capricious behavior of the maxi-mins, and the way they search for good answers in the big search subspace. They may

try to come up with the best solution from their side, but it is always possible that they are not able to converge to the exact same standard code solution, which was so easy to find in the first place. However the solution they come up with is typically not much worse than the one for standard codes. Now let us compare the illumination pattern and SCR_{min} values of Figure 4.8 above, with the ones of Figure 4.9 where we do have some orphans in the solution for "Maximum SCR".

Maximum SCR	Heuristic SCR Convergence
SCR_{min} = -4.54 dB	SCR_{min} = 1.35 dB
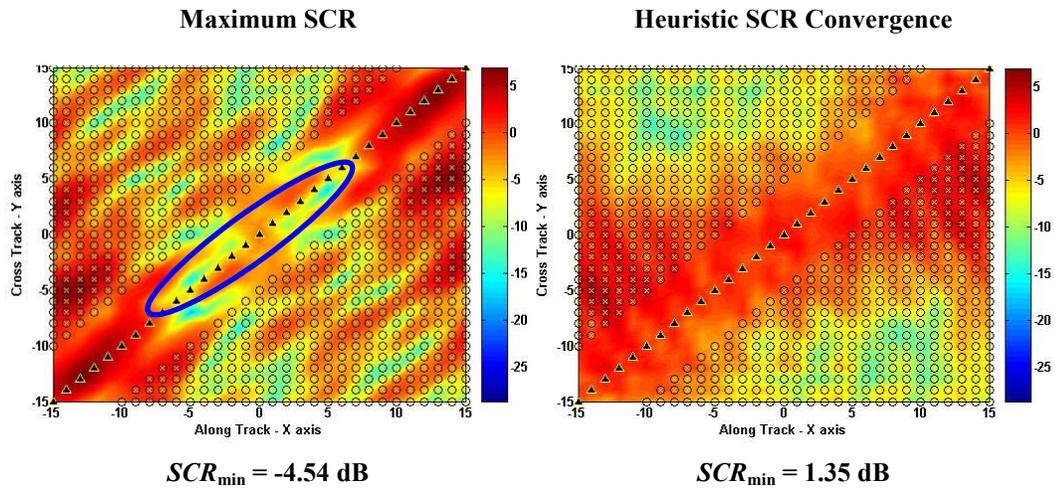
Figure 4:9 Maxi-min performance – Dependence on orphan occurrence II

Actually this is one of the earlier cases shown before. A good strategy that exhorts itself from these observations is to use the standard solutions like "Maximum SCR" for simple problems, and the exotic "Heuristic SCR" for the more difficult ones.

4.3.4 Dependence on target scenario

We just saw that the maxi-mins may not work (as expected) if the target-clutter scenario is too simple. The same thing happens if the target scenario is too complex. In fact if there are lots of target and clutter objects too close to each other,

110

then no code including the standard algorithms would result in a good solution. This
point is illustrated in Figure 4.10.

Maximum SCR   **Heuristic SCR Convergence**

SCR_{min} = -20 dB SCR_{min} = -8.4 dB
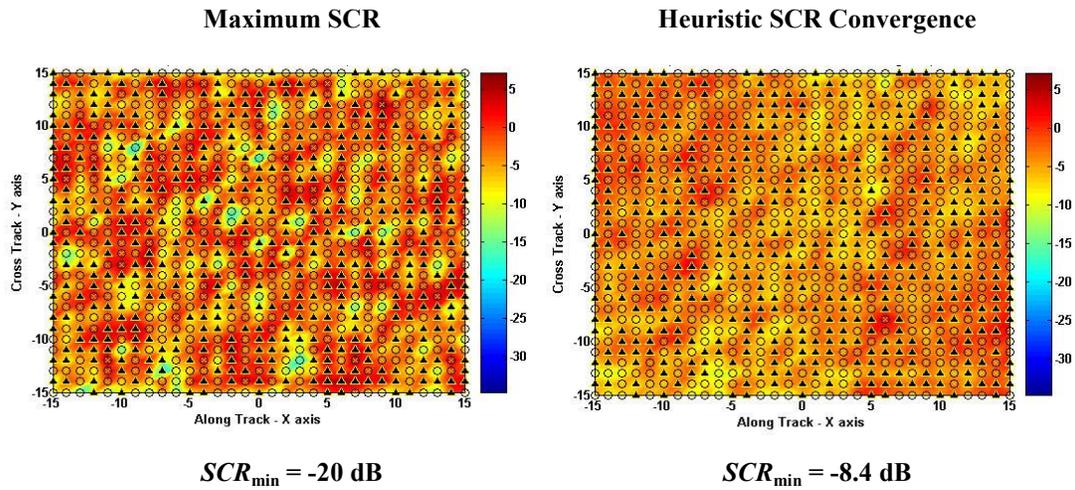
Figure 4:10 Maxi-min performance – Dependence on target scenario I

On the other hand if the target and clutter objects are sparse and disjoint, the solutions
can be exceptional. Figure 4.11 shows one such example.

Maximum SCR   **Heuristic SCR Convergence**

SCR_{min} = -23.64 dB SCR_{min} = 7.19 dB
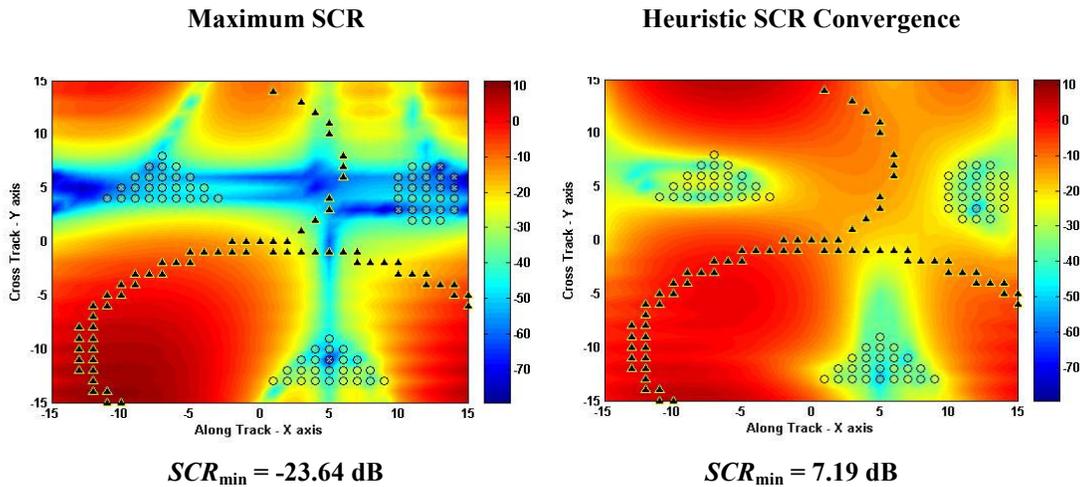
Figure 4:11 Maxi-min performance – Dependence on target scenario II

4.3.5 Dependence on the number of Basis Functions

This probably is the most important dependence to consider and really tells us a lot about the personality of our maxi-min algorithms. As seen in Chapter 3, the standard codes essentially provide us with spatial beamforming or separable space-time solutions. They do not make use of the available temporal degrees of freedom, and thus their performance is fairly insensitive to the number of basis functions. The maxi-mins on the other hand result in true non-separable space-time solutions, and are therefore very dependent on the number of time-frequency basis functions. The dependence of all maxi-mins on the number of basis functions can be seen from Figures 4.12 – 4.15, where results for single and multiple basis functions have been provided. It should be noted that the single basis function case essentially implies a spatial code, or the fact that the same temporal signal propagates on each of the transmit elements.

1 Basis Function   **25 Basis Functions**

SCR_{min} = -13.1 dB SCR_{min} = 2.5 dB

Heuristic SCR Convergence

Figure 4:12 Dependence on the number of basis functions – Heuristic SCR Convergence

1 Basis Function   **25 Basis Functions**

SCR_{min} = -13.3 dB SCR_{min} = 1.3 dB
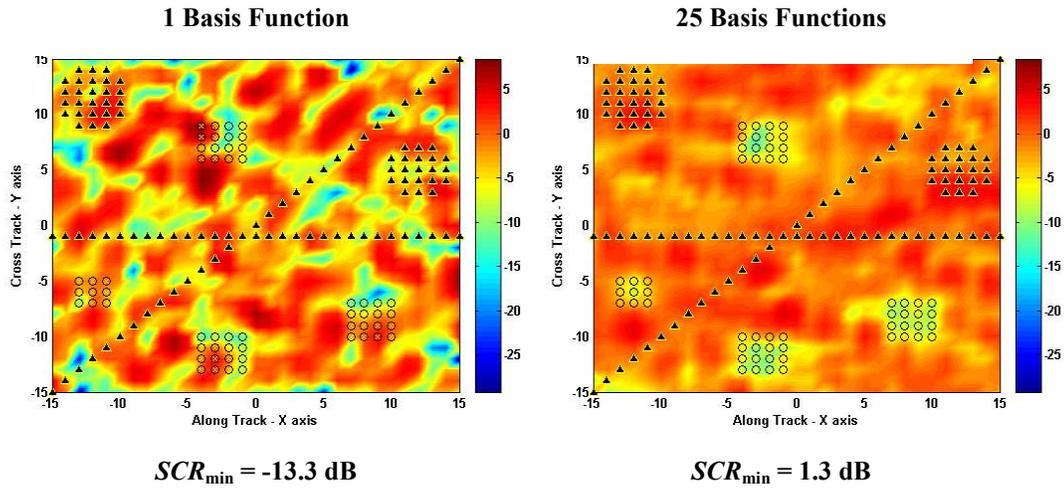
Heuristic Energy Convergence

Figure 4:13 Dependence on the number of basis functions – Heuristic Energy Convergence

1 Basis Function   **49 Basis Functions**

SCR_{min} = -5.4 dB SCR_{min} = -0.5 dB
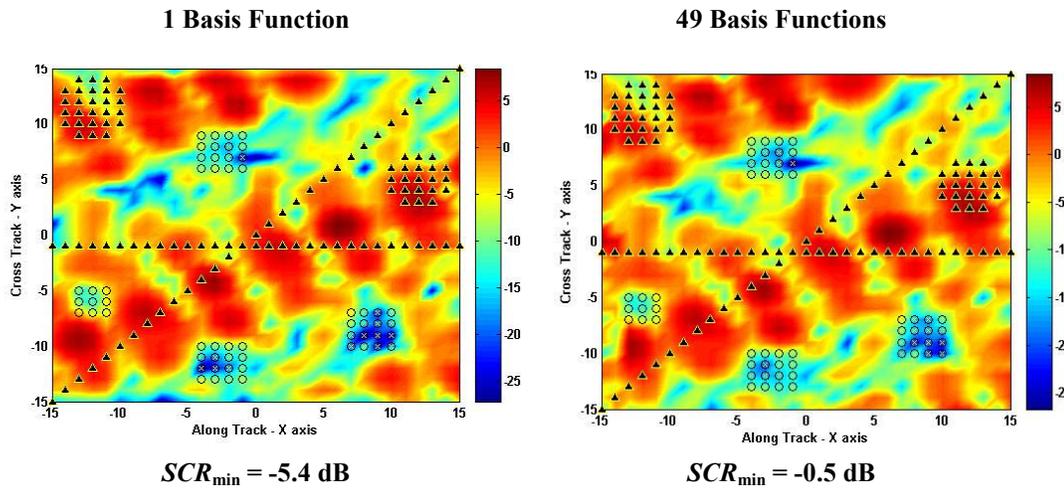
True SCR Convergence

Figure 4:14 Dependence on the number of basis functions – True SCR Convergence

113

1 Basis Function   **49 Basis Functions**
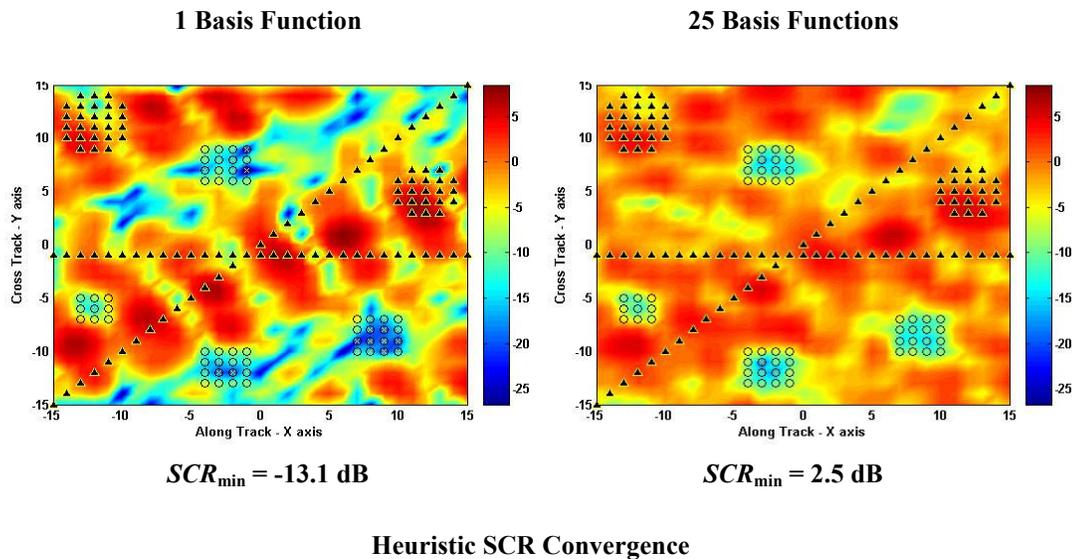
SCR_{min} = -6.3 dB SCR_{min} = 0.2 dB
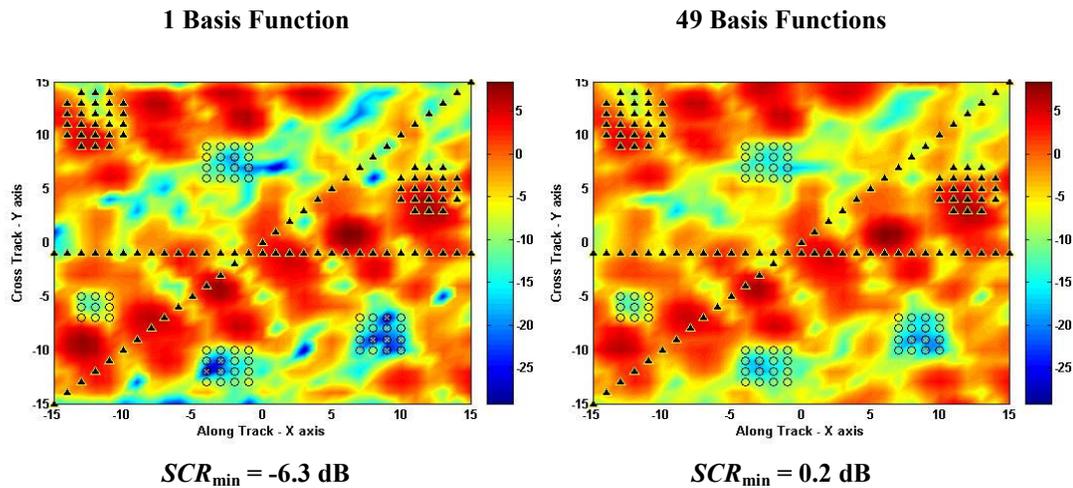
True Energy Convergence

Figure 4:15 Dependence on the number of basis functions – True Energy Convergence

As can be seen all codes give better results for more number of basis functions. The effect is particularly prominent for "Heuristic" algorithms where we get an improvement of around 15 dB for both versions. Also note that even with 25 basis functions, the "heuristic" codes outperform the "true" algorithms with 49 basis functions; thus they seem to be more responsive to the increase in basis functions.

The reason we show results up till 25 and 49 basis functions only, is because of the processing overhead described earlier. Considerable amount of time and effort was devoted to make our programs both time and memory efficient. Several resource saving techniques were employed in the software, but describing them here will take the focus away from the main issues (and will just end up filling extra pages). In any case, these methods would probably be of more interest to a programming person or a software engineer, and have therefore been left out of the scope of this thesis.

One important point that needs to be mentioned though is about the application of the time-saving techniques. It turns out that because of the way the algorithms are structured, one of our very effective time-saving methods can only be applied to the "true", and not the "heuristic" algorithms. This enables us to run larger simulations only for the "true" procedures, and that is why we were able to show results for 49 basis functions for the true algorithms and only 25 basis functions for the "heuristic" ones. Note that even with all the time-saving techniques this was the highest we could go in terms of our basis functions. And even though we can make the "true" algorithms run much faster, this does not turn out to be of great application as for most cases the champion code is still the "Heuristic SCR", and thus that is the one we are most interested in finding.

Let us now look at the performance of the various algorithms with respect to specific parameters, for increasing number of basis functions. The individual parameters considered are a*verage target energy, average clutter energy, average SCR, and worst SCR*. The idea is to see how the performance of different algorithms changes with more number of basis functions. All the plots are for the same target-clutter geometry as shown before in Figures 4.12-4.15.

Average Target Energy
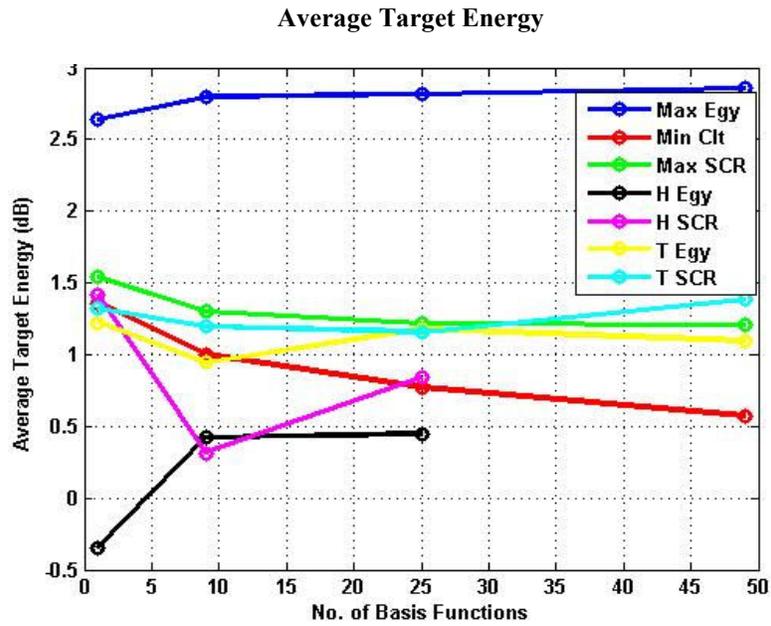
Figure 4:16 Average target energy for different codes for increasing number of basis functions

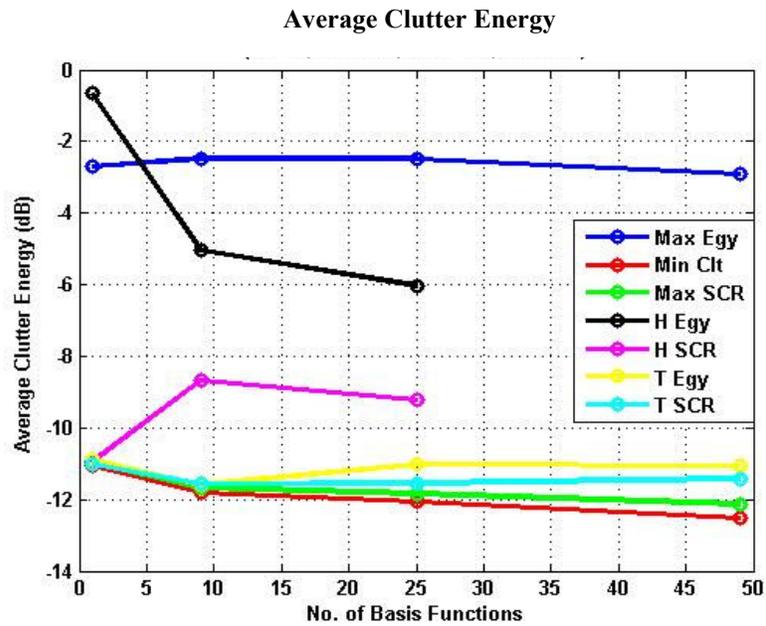**Average Clutter Energy**

Figure 4:17 Average clutter energy for different codes for increasing number of basis functions
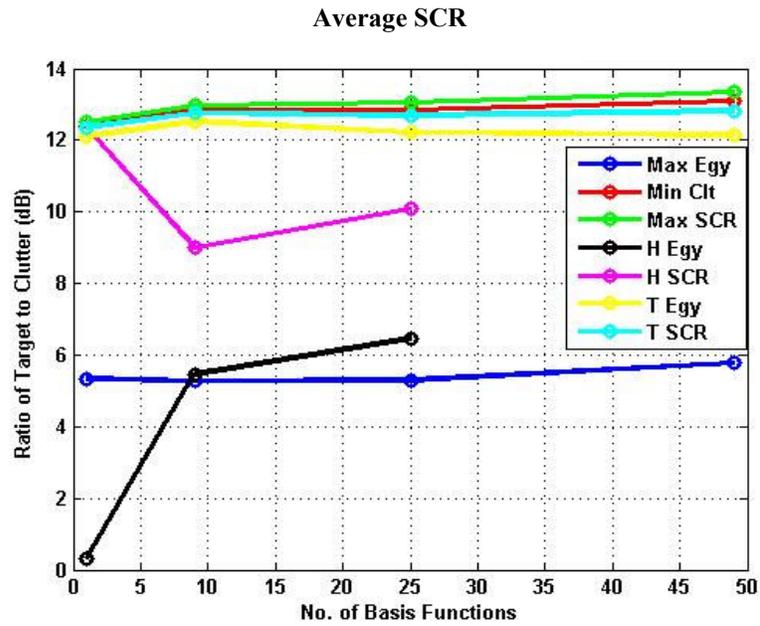
Average SCR

Figure 4:18 Average SCR for different codes for increasing number of basis functions

SCR~min~
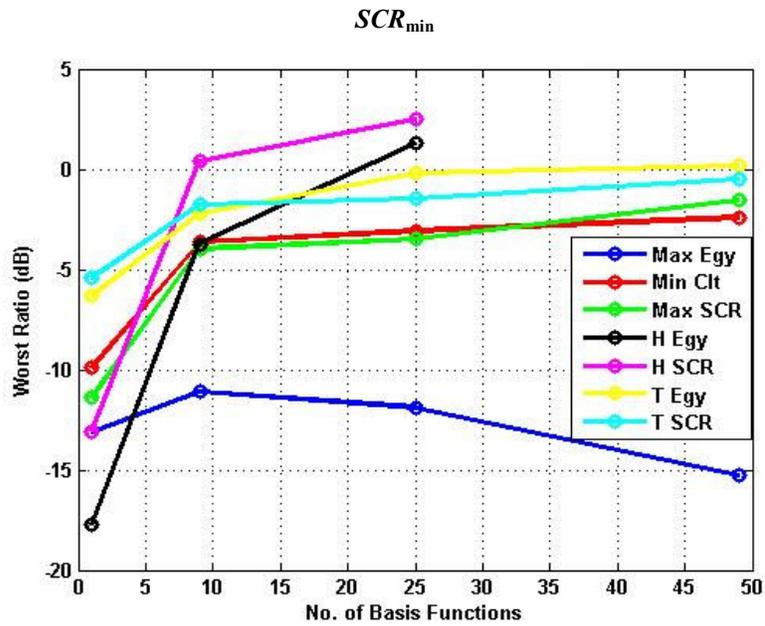
Figure 4:19 *SCR* ~min~ for different codes for increasing number of basis functions

For the first three figures i.e. Figures 4.16 to 4.19, each of the standard codes designed to optimize a particular criterion can be seen to perform best with respect to that criterion. For e.g. in Figure 4.16 the "Maximum Energy" code (Max Egy) or the blue trace stays higher than all other codes. Similarly in Figure 4.17 the "Minimum Clutter" code (Min Clt) or the red trace stays the lowest (minimizes the average clutter energy), and in Figure 4.17 the "Maximum SCR" or the green curve again stays the highest. Also note that for each of these criteria, the other curves (especially the maxi-mins) bounce around randomly with increase in number of basis functions. The pattern should not surprise us as the other codes have nothing to do with the particular criteria of those plots; these codes are not optimized for them and are thus free to result in any value of that optimization parameter, irrespective of the number of basis functions. Only the codes optimized for a particular criterion are expected to show consistency in performance with the increase in the number of basis functions

The best performance of the standard codes for their respective criterion is kind of expected, and reinforces our contention that for the simple criteria standard codes are the best codes. But also note that the three best curves in Figures 4.16 to 4.19 stay very flat throughout. This clearly indicates that their performance is typically unaffected by the number of basis functions and thus spatial beamforming would yield almost comparable solutions for these criteria. Most interesting results are however observed for the maxi-mins in Figure 4.19. Note that the traces for the maxi-mins – "H SCR", "H Egy", "T SCR" and "T Egy" rise monotonically with increase in the number of basis functions. However this rise is more substantial for

118

the "heuristic" codes as indicated by the black and magenta traces. These curves start at much lower starting points (indicating poorer spatial solutions) as compared to the "true" algorithms, but rapidly catch up and then even overshoot the "true" code curves for higher number of basis functions; i.e. the curves rise quite sharply as we go from 1 to 9 and 9 to 25 basis functions. In fact as indicated before, even with 25 basis functions they reach a higher point than what the "true" curves achieve for 49 basis functions - thus indicating their higher responsiveness to the increase in the number of basis functions. On the contrary, the "true" curves rise moderately as we go from 1 to 9 basis functions and then kind of flatten out, indicating that any space-time solution after that is equally good and more number of basis functions do not create a real difference.

On the whole, these plots indicate the true space-time nature of maxi-min codes and directly convey that spatial beamforming is not an equally effective solution for this criterion. They also reiterate a point made very early in this thesis – more number of basis functions directly translates to a greater flexibility in construction of our transmit signal and hence better final solutions. This rule however seems to apply to only the maxi-min solutions though; probably because the standard criteria turn out to be so trivial, that it becomes possible to find the best solutions using just spatial degrees of freedom. Also note that in each of the figures the plots for the "heuristic" codes are limited till 25 basis functions only (for reasons explained before).

4.4 Form of the Maxi-min transmit signal

We are pretty much at the end of this chapter, but before moving on lets take a quick look at the form of the maxi-min signals just as we did for the standard codes in Chapter 3. Actually this topic comes more under the purview of Chapter 6 where we discuss some of the other potentials of space-time codes, but a small mention here would make up good reading just for the sake of comprehensiveness.

Recall that for the standard codes the final solutions turn out to be purely spatial solutions (generally), as indicated by the 2-D correlation matrix of Figure 3.9. This correlation matrix plot corresponds to the "Maximum SCR" solution for the last case of Figure 3.7. The "Heuristic SCR convergence" solution for the same target-clutter geometry is shown as the last plot of Figure 4.5. For the sake of lucidity both these plots have been again reproduced here:
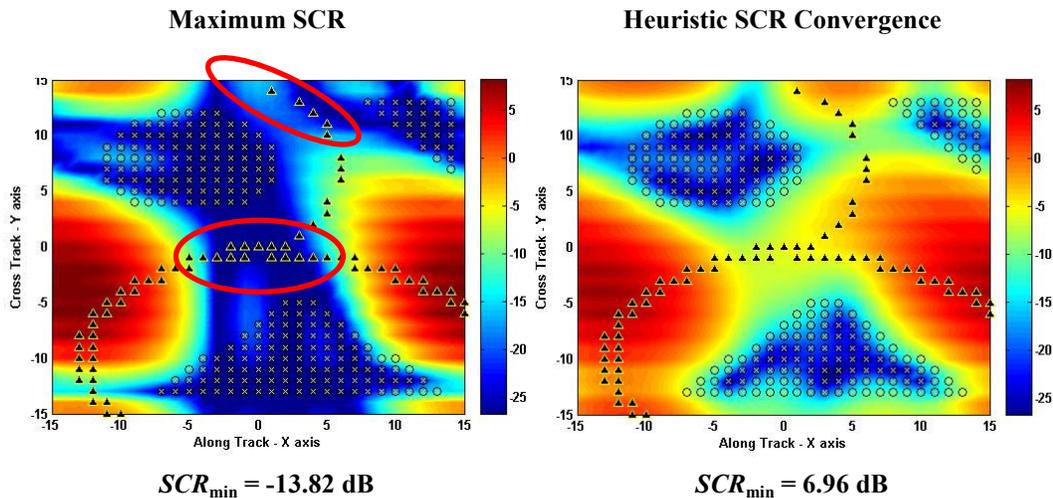
Figure 4:20 Target-clutter geometry and the two solutions – "Maximum SCR" and "Heuristic SCR Convergence", for which the temporal signal correlation matrices have been shown

120

The corresponding 2-D correlation matrices for both the codes – "Maximum SCR" and the "Heuristic SCR Convergence" solution have also been shown below.
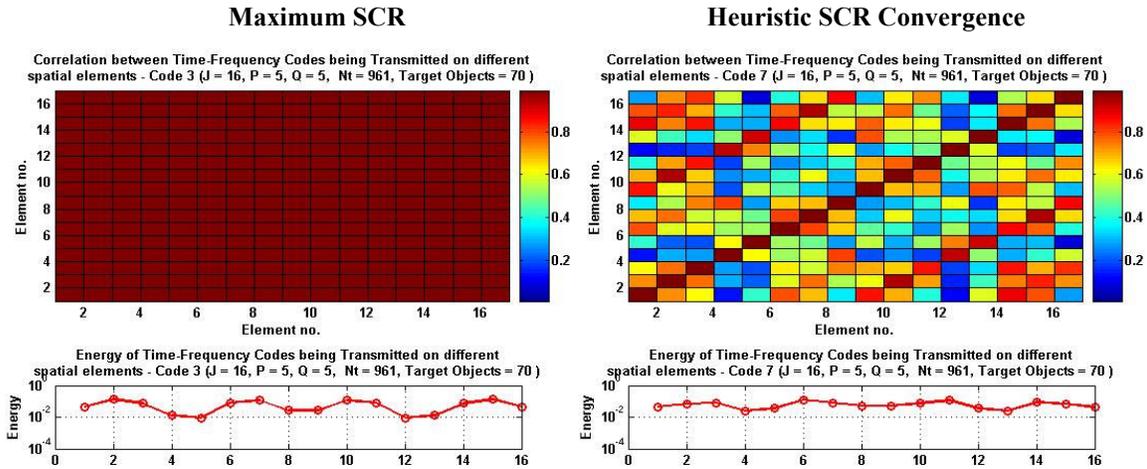
Figure 4:21 Correlation coefficients between temporal signals of different elements, and distribution of energy on different antennas for both codes – Maximum SCR and Heuristic SCR convergence

We have already seen the correlation matrix for the standard "Maximum SCR" solution (one on the left) in Chapter 3. However the one on the right for the maxi-min solution turns out to be more interesting. As is evident from the multi-colored checkerboard plot, the temporal signals on different transmit elements are reasonably uncorrelated with each other; thus indicating that fairly dissimilar temporal signals propagate on each antenna, unlike the standard code solutions of Chapter 3.

Contrast this plot with the one for "Maximum SCR" solution. For the "Maximum SCR" each square in the checkerboard is completely 'red', indicating a correlation coefficient value of 1 or perfect similarity between all individual signals. These plots are for 25 basis functions, and thus reflect how the maxi-min truly utilizes

121

the full potential of the additional temporal dimensions. Also note that the energy distribution for the temporal signals on the different transmitter elements, is much more uniform for the maxi-min solution case as compared to the "Maximum SCR" solution.

To summarize, the maxi-mins not only provide us with good solutions but also true and non-separable space time solutions. We have already seen how these solutions are useful from an "illumination optimization" point of view; in Chapter 6 we study some of the other features and ramifications of propagating true space-time codes. But one more question that comes to mind is – how do these algorithms actually arrive at their solutions, i.e. we know the broad mathematical steps, but what does the exact path to the final solution look like? In other words a question more about how they work, rather than just knowing whether they work or not. To learn more about such issues and also the intrinsic nature of our algorithms, several more tests were performed. These tests along with some other interesting finds have been reported in our next chapter – Maxi-min Analysis.

Chapter 5

Maxi-min Analysis

5.1 The Objective

In the last chapter we saw the performance of the different maxi-min algorithms. Although for most cases the results are promising, we also observe that qualitatively the solutions vary over a great range – many times they are great, most times good and sometimes even average or bad. Moreover we do not have any concrete or justifiable reason to explain such a behavior, except for the obvious fact that the whole process has an element of uncertainty or unpredictability attached to it. This condition kind of implies that we know something about the functioning of our algorithms, but not their exact functioning. To ameliorate this situation, it was decided to carry out a more rigorous investigation so as to understand the true nature, or the true personalities of our algorithms. Although these extra investigations do not provide us with all the answers, they do present us with some useful insights on how things work, and also help us draw some important conclusions about the maxi-min behavior.

5.2 The Process – 2 tests and 2 new algorithms

The focus of this extra analysis was mainly on the "Heuristic SCR convergence", as it had already emerged as the unanimous champion amongst all our maxi-mins. We have already seen that it is the upper bound on our worst SCR or

SCR$_{min}$, that sets the limit on how good our final solution can be (how much our lower bound can rise). And since this upper bound from (4.9) is given as the smallest of all individual maximum eigen values, we thought it would be a good idea to monitor this maximum eigen value for each individual target. The idea was to see how this bound shifts from one target to another, and thus make any predictions if possible, about the iteration pattern. This procedure comprised our *Test 1*.

However this whole line of thought leads us to another interesting examination. Recall from our earlier discussion that each individual $\mathbf{A}_i$ or $\mathbf{C}_i$ matrix has *P* times *Q* (or *R*) non-zero eigen values. We call these values as the significant eigen values, as the corresponding eigen vectors are the only vectors containing significant information about the matrix. The largest of the significant values, or the *maximum significant eigen value* is also the maximum value for the whole matrix (λ_i^{max}), and it is the one we consider while selecting our weakest target for the "Heuristic" algorithms. However the smallest of these significant values, or the *minimum significant eigen value* can likewise be utilized to decide our weakest target. It is because by definition, the largest eigen value (λ_i^{max}) needs to be greater than this value, and thus keeping the minimum significant eigen value high will automatically ensure that the largest eigen value or the upper bound on our *SCR*$_{min}$ also remains high. This leads us to a new class of "Heuristic" algorithms which we call the *"Heuristic SCR convergence MIN"* and *"Heuristic energy convergence MIN"*, as they are based on the idea of preserving the minimum significant eigen values (and also because we were running out of names).

Also note that the minimum significant eigen value is different from the minimum eigen value for the whole matrix (λ_i^{min}). All the concepts of maximum eigen value, maximum significant eigen value, minimum significant eigen value and the minimum eigen value for a target matrix are clearly depicted in Figure 5.1.
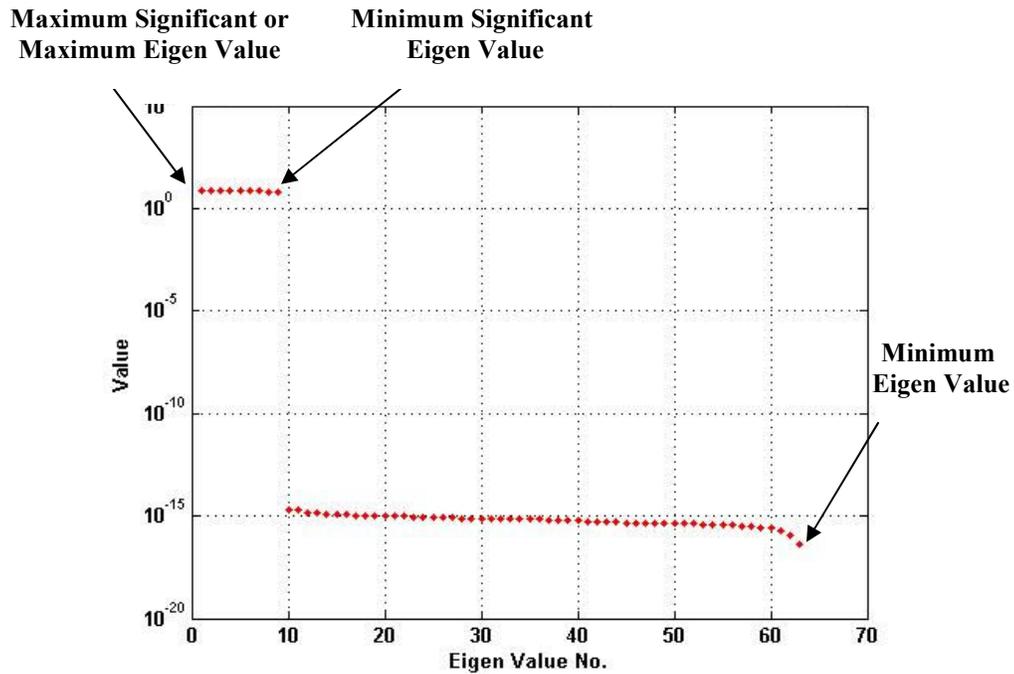
Figure 5:1 Eigen spectrum of individual matrix C$_i$, illustrating concepts of maximum and minimum significant eigen values

Since we had already caught on this new algorithm based on the minimum significant eigen values, we decided to monitor the minimum significant value with each iteration for all individual targets as well. This comprised our *Test 2*, where we were hoping to gain similar kind of insights as in case of *Test 1*. An obvious point of interest was also to compare the performances of the two kinds of "Heuristic"

algorithms – the normal ones based on the maximum significant eigen values, and the new ones based on the minimum significant eigen values. Note that the only single difference between the new algorithms and the old ones is that the new algorithms: *"Heuristic SCR convergence MIN"* and *"Heuristic energy convergence MIN"* select the weakest target based on the minimum significant eigen value, and not the maximum significant value. The results of our tests and also for the actual algorithms have been described next.

5.3 Test and Algorithm Results

A sample target-clutter pattern was selected and the maximum and minimum significant eigen value for all targets after every iteration was plotted for different algorithms. The idea was to look for trends in the iteration pattern that could help us make any definite conclusions about the functioning of our algorithms. Initially this was done for 9 basis functions for all four "heuristic" algorithms, but later with higher number of basis functions the focus was shifted on only the SCR convergence algorithms. It is because the SCR convergence algorithms - *"Heuristic SCR convergence"* and *"Heuristic SCR convergence MIN"* once again turn out to be more promising than the energy convergence algorithms. Also, since similar results were obtained for almost all cases, only the most relevant ones have been included here. The sample target-clutter geometry used for these tests and the new heuristic algorithms has been shown in Figure 5.2.
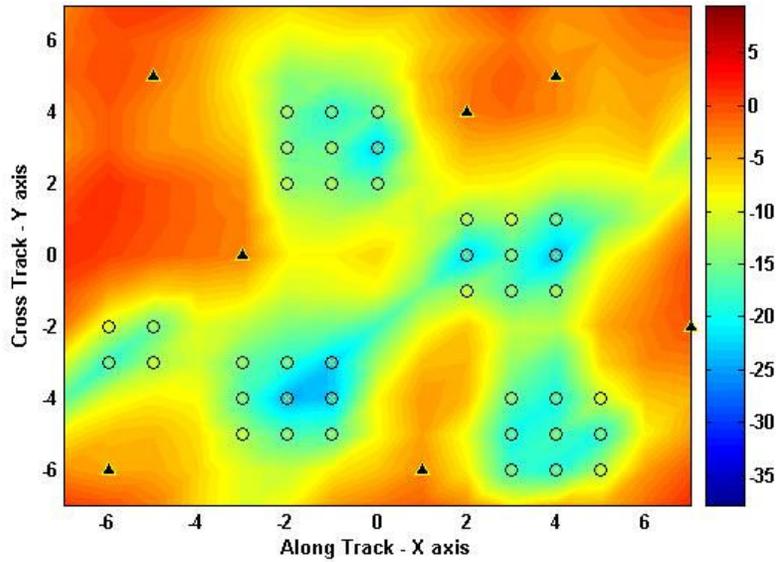
Figure 5:2 Sample target-clutter geometry used for all the Maxi-min Tests

Note that since there are just 7 targets, it was easy to show the maximum or minimum significant eigen values for all of them in just one plot. The above illumination pattern is for 14 antennas and 9 time-frequency basis functions.

The maximum and minimum significant eigen value plots for the "Heuristic SCR convergence" algorithm has been shown next. Note that for 14 transmitters and 9 basis functions the transmit signal dimension comes out to be 126, and therefore the number of iterations is just one less than this value.

Heuristic SCR Convergence

Max significant eigen value   Min significant eigen value
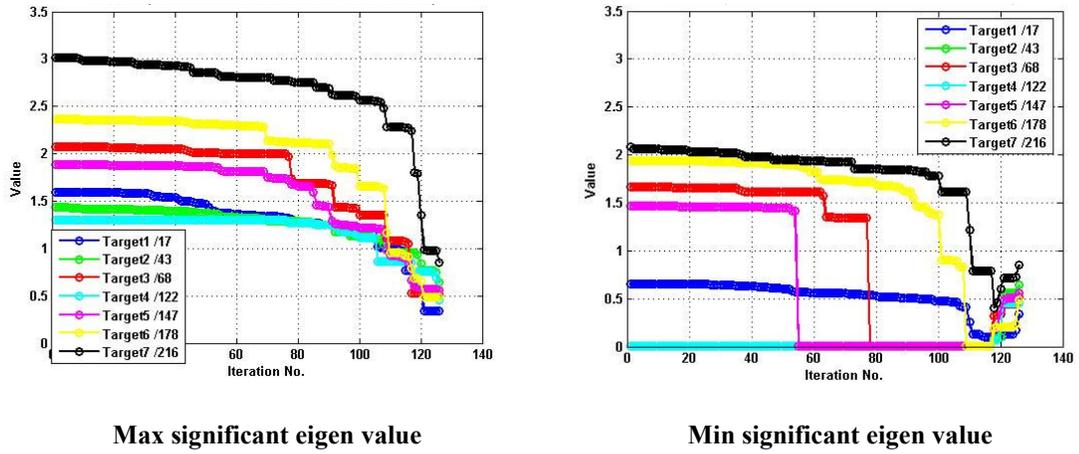
Figure 5:3 Maximum and minimum significant eigen value drop with iteration number for the Heuristic SCR Convergence and 9 basis functions

The same plots with a log scale for the *Y* axis have been shown in Figure 5.4. The log scale helps us see the drop in the minimum significant eigen value more clearly.

Heuristic SCR Convergence

Max significant eigen value   Min significant eigen value

Figure 5:4 Maximum and minimum significant eigen value drop with iteration number for the Heuristic SCR Convergence and 9 basis functions - Log scale for Y axis

128

Two important points can be noted from the above plots. First the iteration pattern for the maxi-min algorithm is totally unpredictable. It is not that the algorithm works on only the worst n targets or goes from one target to another in a foreseeable manner. During the process the maximum value for any target can drop the lowest, and then it becomes our weakest t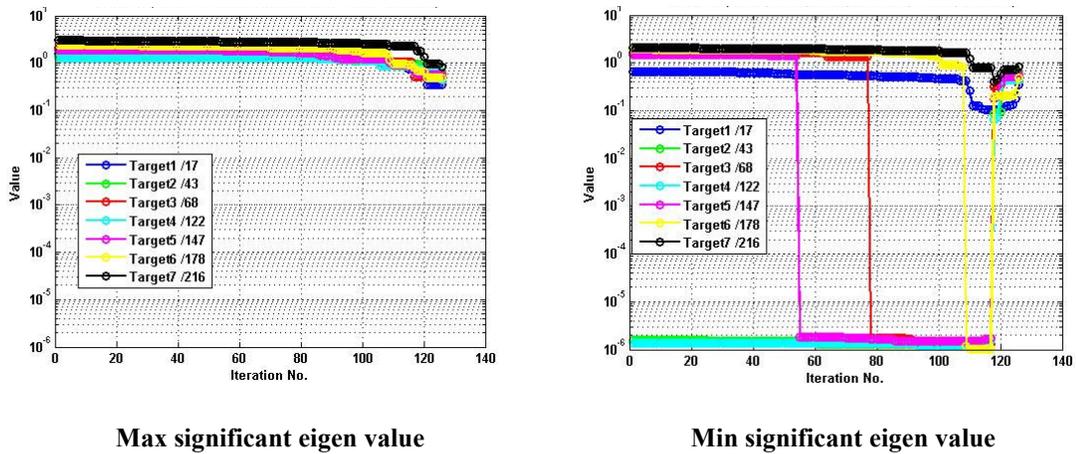arget or the target of special attention. As can be seen from the "maximum significant eigen value" plot of Figure 5.3, at some point during the iterative process the algorithm has worked on targets 1 (blue curve) and 3 (red curve) which are the initial 3rd and 5th worst targets respectively. But it didn't work on targets 2 (green) and 5 (pink) which are initially 2nd and 4th worst (these curves at any point are never the lowest). Thus we cannot make a conclusion that the maxi-min always works on the worst n, or some small percentage of the targets. In fact for some of the other cases tried, the algorithm even worked on the target which were initially the best (targets 6 & 7 here – yellow and black curves). Hence the only thing that can be concluded is that the iteration pattern is very unpredictable, so much so that during the course even the initial best targets can have major components thrown out from their best dimensions and end up as our worst targets. Note when we use of the term "work" in the above description, it means that the algorithm is throwing out worst solutions for that target or projecting out the worst vectors from the corresponding spectrum.

The second important point to be noticed is regarding the minimum significant eigen value. Note that this value drops monotonically for each target till about the 117th iteration, and then again rises to meet its corresponding maximum

eigen value at the last iteration (finally only one non-zero value has to remain in the spectrum). On first impression the subsequent rise after the initial drop appears to be confusing; how can the value get better when we are projecting more dimensions out of a finite dimensional search space? But it turns out that the behavior is explainable.

Recall once more what we discussed about the number of non-zero or significant eigen values for an individual target matrix. It is equal to the number of time-frequency basis functions, which are 9 in this case. Thus after 117 iterations or after 117 worst dimensions have been projected out, the only dimensions that survive correspond to these significant eigen values. The next projection now, does not correspond to a zero valued eigen value, but to one of these non-zero eigen values. Hence the projection causes one of these significant eigen values to go to zero, and only 8 non-zero eigen values remain in the spectrum after that. And therefore, there's a possibility that the minimum significant eigen value in this iteration (8th worst) is better than the minimum significant eigen value of the last iteration (9th worst). That's exactly what happens, and this value increases monotonically after that till it meets the maximum significant eigen value in the last iteration.

This behavior is thus justifiable, but the more important point here is about the actual significance of the maximum and minimum significant eigen values. As was the case with the lower bound on SCR_{min} trying to rise and meet the upper bound, the same is observed here for the minimum significant eigen value. The plots on the right in Figures 5.3-5.4 show that this value can drop to abysmally low levels during the iterative process, but it's the maximum significant eigen value that pulls it up in the

end. Hence for scenarios like these, it does not make much sense to try and preserve our minimum significant eigen values; a fact reinforced by the illumination results for the two kinds of codes shown below.

$SCR_{min} = 11.38$ dB $SCR_{min} = 8.38$ dB
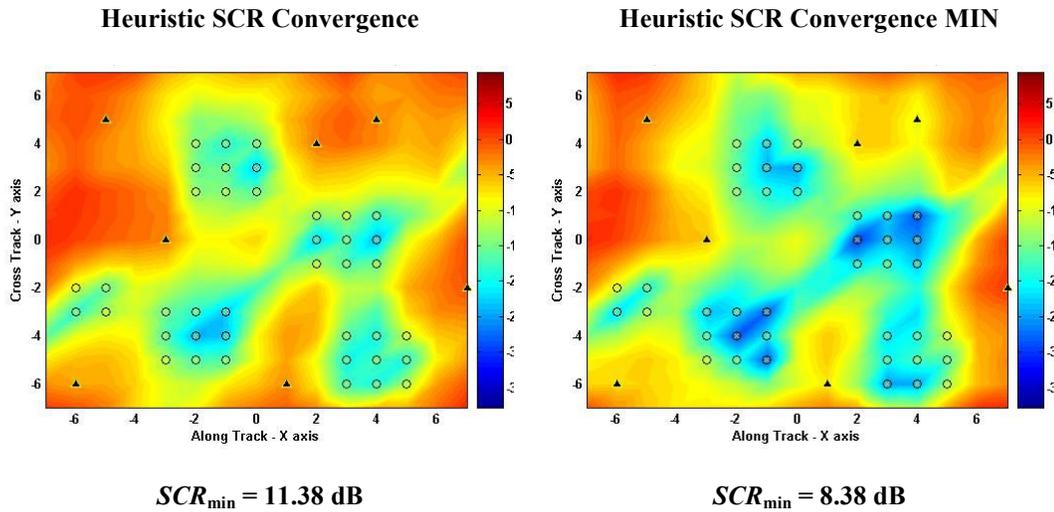
Figure 5:5 Comparison of the two Heuristic SCR algorithms

Although *"Heuristic SCR convergence MIN"* performs pretty decently itself, it can be seen that the performance of *"Heuristic SCR convergence"* is still better by around 3 dB. Thus it happily stays as our champion code. Similar behavior was observed for several other target-clutter geometries and more number of basis functions. In fact all analysis presented here was done for all four heuristic algorithms, for a number of target-clutter patterns and different number of basis functions. However comparable results were observed in each case: *maximum significant eigen value algorithms* perform better than the *minimum significant eigen value* and *SCR convergence* better than *energy convergence* (just like before), and thus all those results have not been included here. Only the ones that are most

131

representative and convey the most conclusive points have been shown in subsequent pages. The bottom line however remains that same – *no algorithm is as potent as the "Heuristic SCR convergence", and its operation remains highly unpredictable.*

Let us also look at the maximum and minimum significant eigen value plots for the "Heuristic SCR convergence MIN" algorithm, which have been shown below.

Heuristic SCR Convergence MIN

| Max significant eigen value | Min significant eigen value |
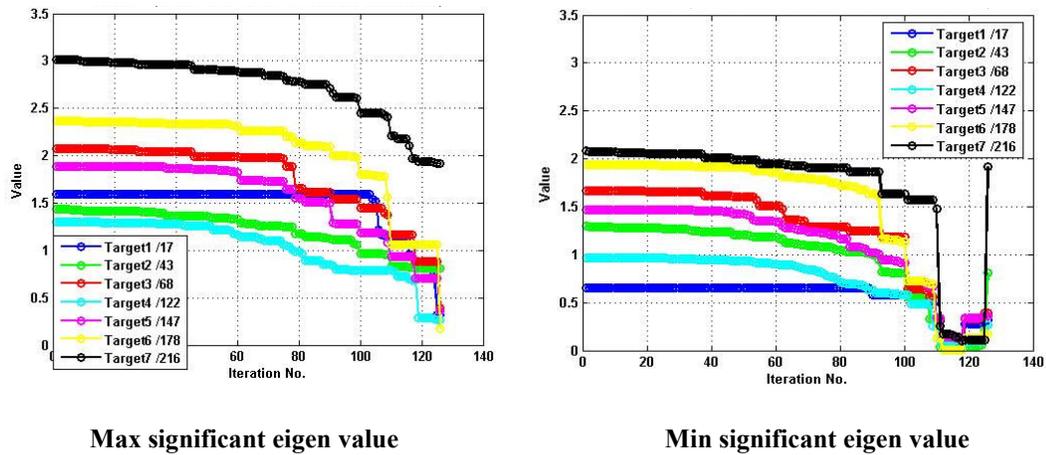
Figure 5:6 Maximum and minimum significant eigen value drop with iteration number for Heuristic SCR Convergence MIN and 9 basis functions

The maximum significant eigen value plot looks very similar to the one for "Heuristic SCR convergence" but for the minimum significant eigen value, the traces are much flatter. That seems natural as the algorithm is working on trying to preserve this value, and therefore it's expected that the minimum significant eigen values will fall much more slowly. However these values eventually do fall to very low levels like in the case of last algorithm, and get pulled up only in the last 9 iterations. This aspect is

better seen in the logarithmic scale plots. The complex nature of the iterative pattern can also be seen once again.

Heuristic SCR Convergence MIN
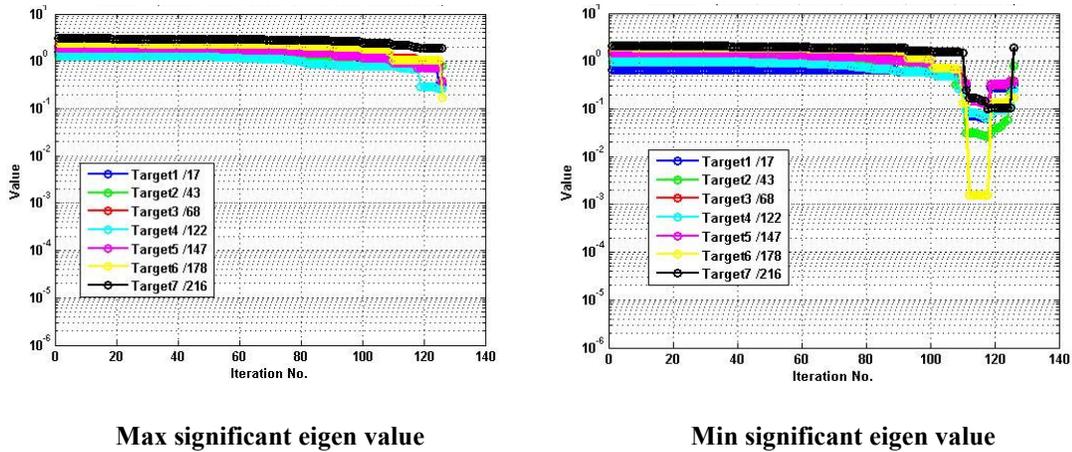

| Max significant eigen value | Min significant eigen value |

Figure 5:7 Maximum and minimum significant eigen value drop with iteration number for Heuristic SCR Convergence MIN and 9 basis functions - Log scale for Y axis

Note that the fall for the minimum significant eigen values is not as steep as in the earlier case. But just like the last algorithm, the targets which were very good to begin with – e.g. target 6 (yellow), can end up as our worse target somewhere down the iteration process.

5.4 A New Suboptimal Approach based on the Analysis

Based on the above plots for the maximum and minimum significant eigen values, a new approach proposed itself. From the linear plots we see that just near the 117th – 118th iteration mark (or in general after $W–P \times Q$ iterations) there is a sharp drop in the maximum significant value of most targets - or it seems that proceeding

133

further down just hurts rather than helps. A possible explanation is that by this stage we generally throw out most of the bad dimensions, and thus going further down just results in the expulsion of the surviving good ones. Therefore assuming that the remaining subspace is rich in good solutions (we have already projected out a lot of bad ones), why not stop here and make a guess in this smaller subspace? Hopefully we will end up with a solution that is pretty good, and maybe even better than the final one.

The resulting algorithm is thus called the *"Heuristic SCR convergence GUESS"*, because of its unusual idea of stopping and guessing (once again excuse our creativity, or the lack of it for not coming up with a better name). This idea is demonstrated in Figure 5.8 below.
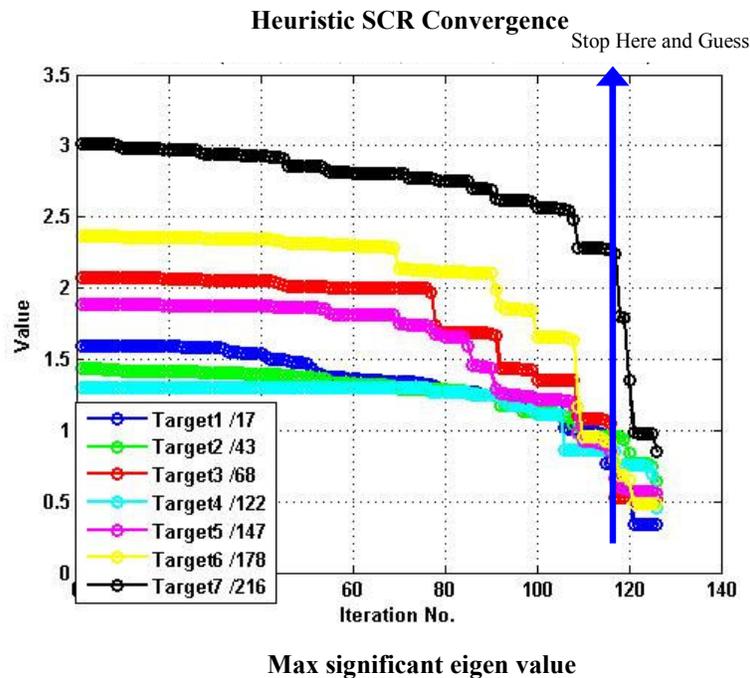
Figure 5:8 The suboptimal "guessing" approach idea

With this idea we were banking on the fact that since by this stage the upper bound (on SCR_{min}) has not fallen enough, there are more possibilities for good answers. But it turns out that likewise the lower bound has also not risen enough, and hence there are high possibilities of bad answers as well (as seen in Figure 4.2 - the lower bound generally rises the most towards the last few iterations). We therefore cannot look at any one bound independently. Both of them have to converge simultaneously to give the best solution. Hence even though this approach gave us some good solutions, due to its inherent indirect limitation of focusing on only one bound, it wasn't able to better our best code – still the *"Heuristic SCR convergence"*. Results for this new guessing algorithm have been shown below.

Heuristic SCR Convergence   **Heuristic SCR Convergence GUESS**

SCR_{min} = 11.38 dB SCR_{min} = 4.53 dB
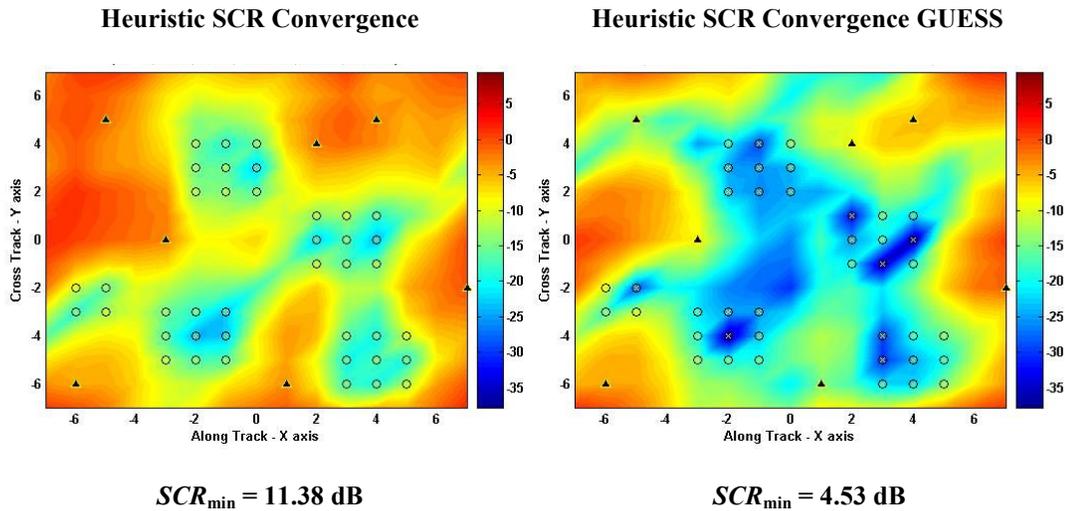
Figure 5:9 Illumination pattern for the new suboptimal guessing approach – Heuristic SCR

One noteworthy observation that came out of this whole exercise was regarding the optimality of our maxi-mins. The guessing approach was tried for all four maxi-mins: the "true" and "heuristic" "SCR convergence" and also the "energy

convergence". And although results have not been presented for all cases, it turns out that some of the algorithms actually get better with guessing. This somewhat confirms the inferiority of these algorithms as even by employing a suboptimal mechanism we are able to outperform our main algorithms. However, since for the *"Heuristic SCR convergence"* any form of sub-optimality results in a poorer solution, it reaffirms its position as our best code. Results for the guessing algorithm with respect to the *"Heuristic Energy convergence"* has been shown below:

Heuristic Energy Convergence **Heuristic Energy Convergence GUESS**

SCR_{min} = -11.44 dB SCR_{min} = 0.19 dB
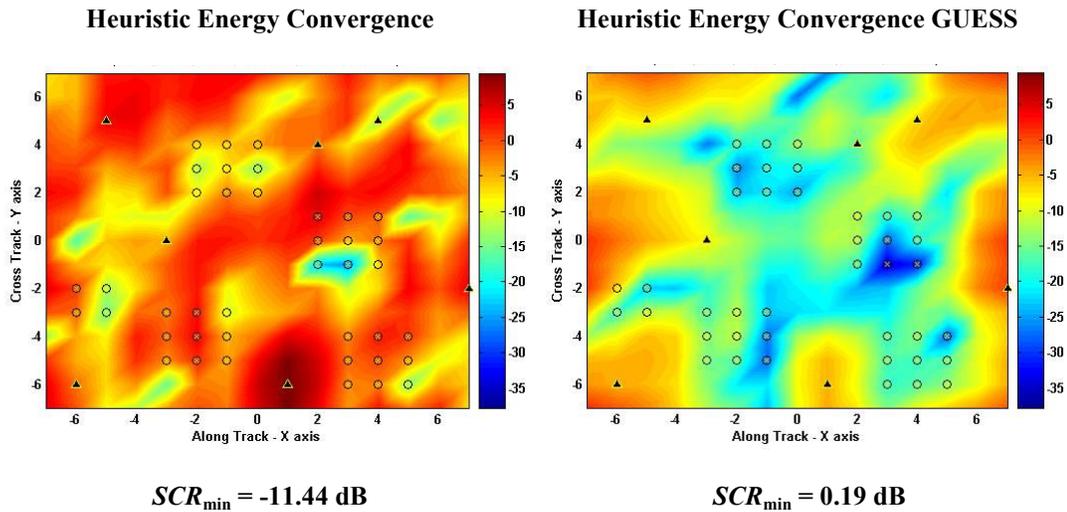
Figure 5:10 Illumination pattern for the new suboptimal guessing approach –

Heuristic Energy Convergence

But even after all these tests we were not convinced completely. The plots for the maximum significant eigen value are so flat towards the start (before they drop), that an inkling of doubt remained. To be absolutely sure that we are not missing out on any good solutions while the upper bound is still high, we decided to carry out one last test. The resulting SCR on all targets, due to the best solution (after every iteration) for each individual target was plotted. This way, if at any stage we found

136

that any of the individual best codes gave an acceptable SCR on all targets (or a SCR_{min} value better than the final value), we could have stopped and used that code as our final solution. This test was performed on the *"Heuristic SCR convergence"*, as right now we were just looking at methods to better our already best code. The results for this test, or the resulting SCR on all other targets by the best code for individual targets after every iteration have been shown below. However none of the best codes give a better SCR_{min} value at any point during the iterative process as compared to final value.
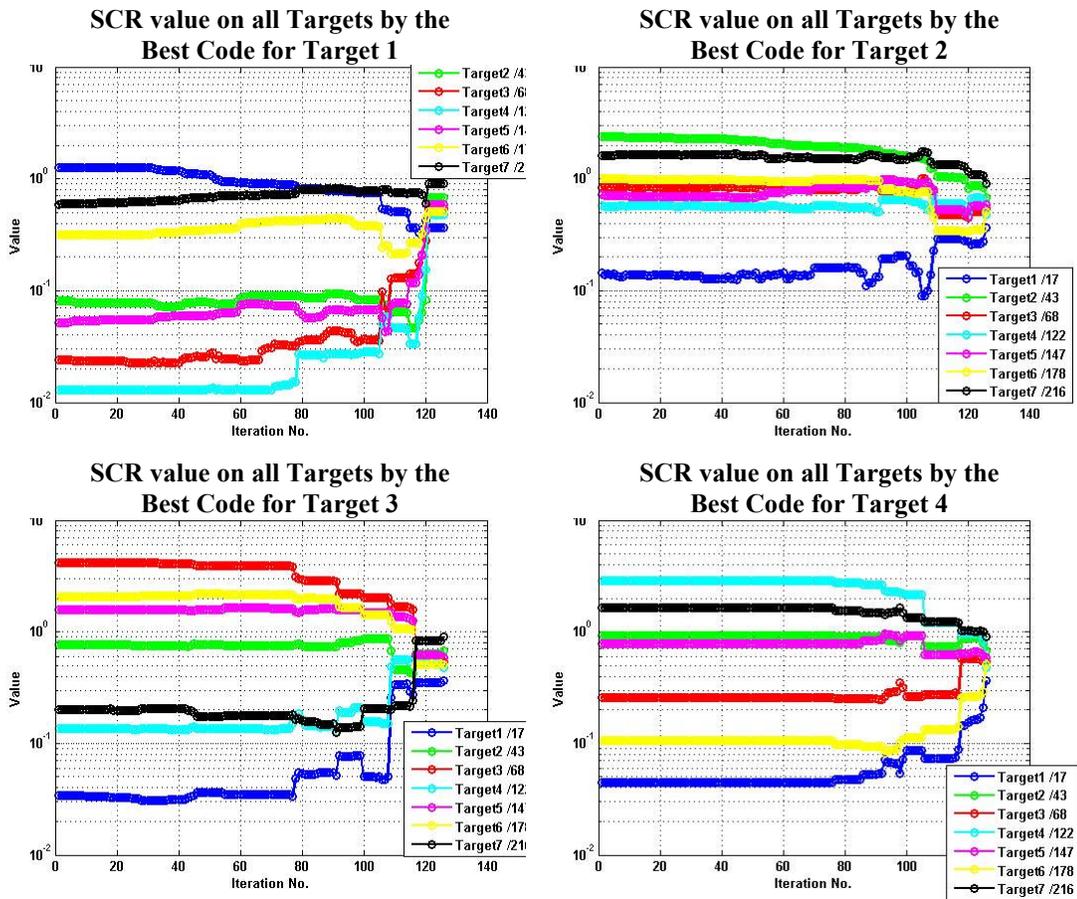
Figure 5:11 Resulting SCR values on all targets, by the best codes for individual targets I

137
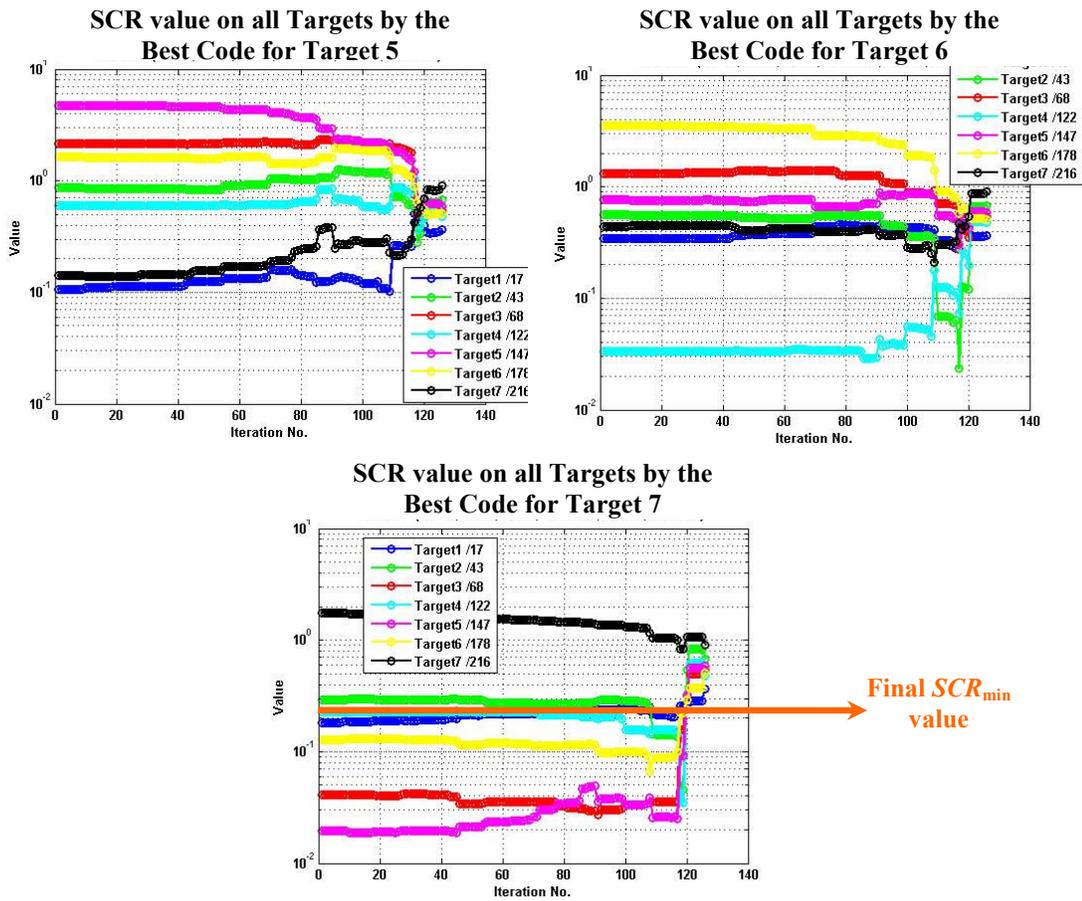
Figure 5:12 Resulting SCR values on all targets, by the best codes for individual targets I

As can be seen, all the 7 best codes converge to the same set of SCR values at the end. Actually they have to as towards the end only one vector remains in the eigen spectrum of all individual $\mathbf{C}_i$ matrices, and that vector solution results in this set of SCR values. Also at no point during the iterative process does any code give a better SCR_{min} value than the final solution (indicated by the orange arrow in the last plot). Thus we can conclude that the best code or the *"Heuristic SCR convergence"* can provide us with the best solution, only by iterating till the end. No form of suboptimal

approach or shortcut can result in an answer that is better than the final optimal solution.

5.5 A point about Basis Functions

In this chapter, we came across a lot of interesting finds through various tests and some new algorithms. But before winding up this piece on the maxi-min analysis, one vital point needs to be mentioned about the basis functions. We observe that for our sample geometry of Figure 5.2, we don't get a huge difference in the final solutions for 9 and 49 basis functions. This point is illustrated in Figure 5.13.

Heuristic SCR Convergence

9 Basis Functions	49 Basis Functions
SCR_{min} = 11.38 dB	SCR_{min} = 12.47 dB
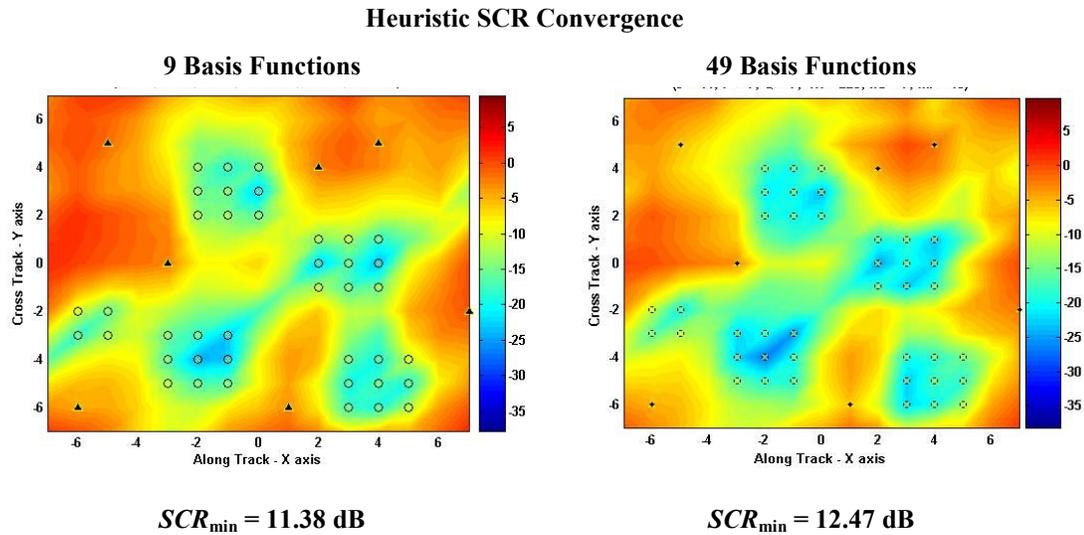
Figure 5:13 Heuristic SCR convergence performance for 9 and 49 basis functions

This pattern is kind of surprising. For the second case we have 40 more temporal dimensions or in all a total of $40 \times 14 = 560$ more space-time dimensions, but we still manage a meager improvement of only 1.09 dB in the SCR_{min}. With so many more time-frequency dimensions, don't we have a much greater flexibility and thus a

higher possibility of coming up with a better transmit solutions? The answer is yes; the number of good solutions do increase as we increase the dimension of our transmit signal, but then so do the number of bad solutions. And thus the likelihood of coming up with better or worse solutions both increase. Most of the time our algorithms exploit the optimistic side of this proposition and come up with better solutions, but the possibility of coming up with marginally better or even worse solutions is also present. This is a very important point and can be better inferred from Figure 5.14, where we show the fall of the maximum significant eigen value for different number of basis functions for the *"Heuristic SCR convergence".*
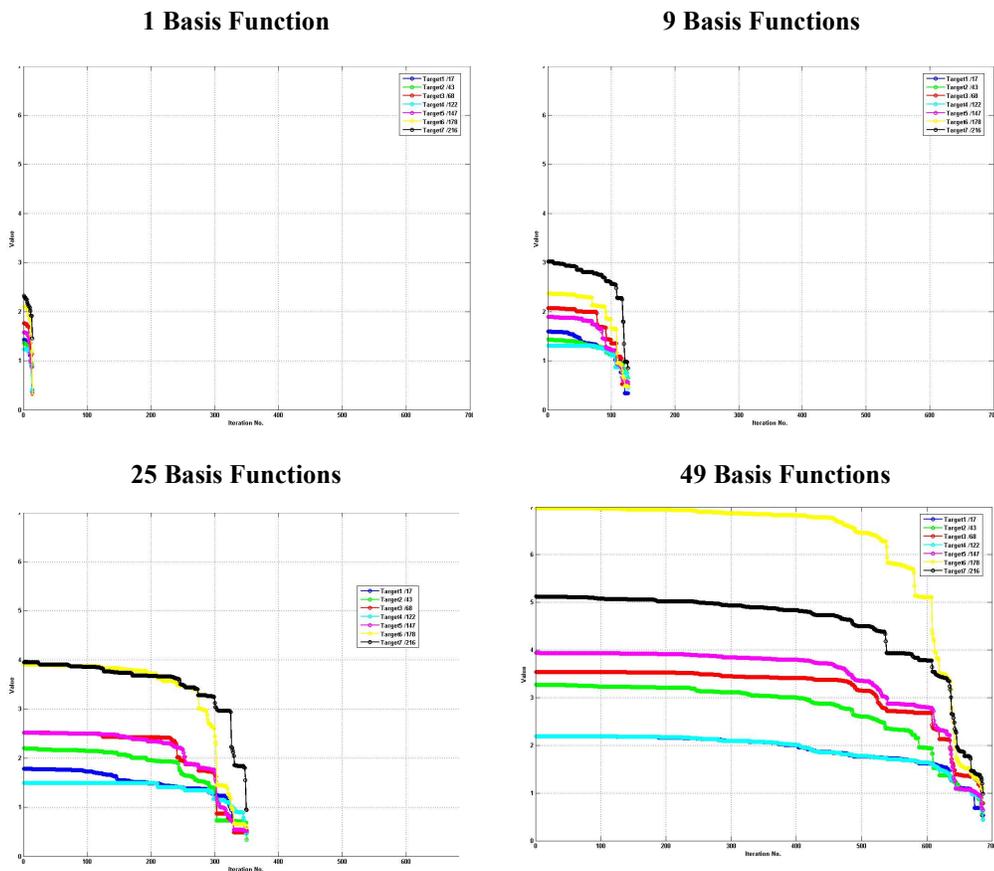
Figure 5:14 Fall of the maximum significant eigen value for different number of basis functions

These plots clearly show that as the number of dimensions increases, our starting point or upper bound gets higher (more good solutions in the bigger subspace). But at the same time the number of iterations or number of projections required to get rid of the larger number of bad solutions also increases, and hence we end up almost at the same final spot in all four cases. Thus more number of basis functions does not necessarily guarantee a better final answer.

One other significant point is about the type of basis functions. It's not that our algorithms will converge to the same good solutions irrespective of what basis functions are provided to them; i.e. the solutions are not independent of the form of the basis functions. As mentioned before, the choice of the basis functions plays an important role in eliciting good answers from our algorithms. We switched from the initial narrow timewidth / narrow bandwidth basis functions (pulses) to our present wide timewidth / wide bandwidth basis functions for the same reason; but further scope for improvement is always there. There might be better basis functions out there which may improve the performance of our algorithms even further. Determination of such functions and evaluation of their performance has been left as one of the future ideas in this study.

Now we are really at the end of this chapter. After having seen the different algorithms, evaluating their performance and even analyzing them thoroughly, what next? It turns out that the most vital attribute of these algorithms is their ability to come up with true space-time solutions. A small reference to this regard was made in Chapter 4, but in actuality, true space-time codes open up whole new vistas of

possibilities. Some of these properties of space-time codes, along with their potential

applications for radars have been described in our next chapter.

Chapter 6

True Space-Time Codes – *Attributes and Abilities*

6.1 Form of Space-Time Signals

We start this chapter by revisiting the form of space-time signal results. In Chapter 4 we got little flavor of this topic, when we saw that for a true space-time code different temporal signals propagate on different transmit elements. But there's a lot more to this observation. Firstly, we notice that space-time signals typically result in better illumination solutions than purely spatial signals; a fact confirmed by the numerous maxi-min results of Chapter 4. Secondly, we suspect that for most cases it happens because any other means to synthesize an identical illumination pattern (except by transmitting dissimilar transmit signals on different antennas) is physically impossible. One important point however, is that even though space-time solutions turn out to be better in most cases, there's nothing in the algorithm which says that it has to converge to such non-separable solutions. The basis function structure that exists can be used for synthesizing both spatial and space-time solutions. All algorithms just try to find the most optimal solution for their respective criterion, and in the process can converge to either spatial or a space-time solutions. As it turns out, that the standard codes typically result in pure spatial, while the maxi-mins in true space-time solutions. It's probably because the standard criteria are simple enough to be realized by conventional beamforming, whereas the maxi-mins are more intricate and thus require both the spatial and the temporal dimensions (also indicating that the

optimality of space-time solutions for these criteria). Supporting results for the above discussion are provided in Figures 6.1 - 6.6.

Note that in the first case there's only one target, and hence the best way to maximize the minimum SCR is to focus the main beam on the center of the illumination area. To achieve this, the same temporal signal needs to propagate on each spatial element (the array acts as one big aperture), and that's exactly what our maxi-min comes up with as its final solution. Equal energy, perfectly correlated time-frequency signals result on each antenna as can be seen by the correlation matrix plot on the right.
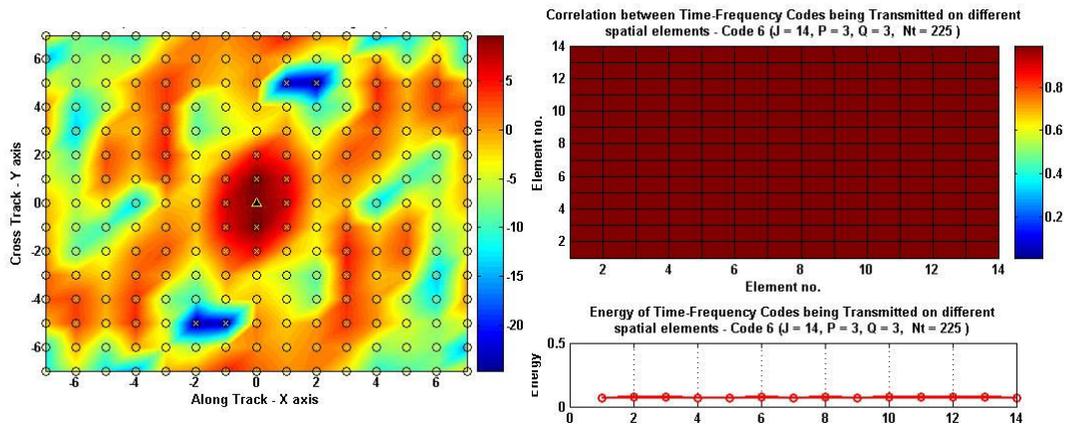
Figure 6:1 Transmit Signal Form: One Target (Heuristic SCR Convergence) - Predictable

For the single target case we know what the answer should be, and the algorithm does converge to the exact same predictable best solution. No information is provided to the algorithm hinting that the best solution is a beam-focusing one (purely spatial) for this case, yet it comes up with the right solution on its own. This

behavior also acts as a good sanity check for our procedure, and credibly confirms that things are working right for this algorithm.

Next we decided to try another case for which we knew what the answer should be. Instead of a single target, we now have an all target case of Figure 6.3. In such situations, the best approach to maximize the illumination area is to have perfectly orthogonal signals on each of the transmit element; the illuminated area then gets decided by the spatial extent of a single transmit aperture. We constructed one such vector for 9 transmit elements and 9 basis functions, by turning on only one (dissimilar) basis function on each of the 9 elements. Thus the temporal codes on the 9 different elements looked something like:

$$
\begin{bmatrix} 1/3 \\ 0 \\ 0 \\ 0 \\ 0 \\ 0 \\ 0 \\ 0 \\ 0 \end{bmatrix}
\begin{bmatrix} 0 \\ 1/3 \\ 0 \\ 0 \\ 0 \\ 0 \\ 0 \\ 0 \\ 0 \end{bmatrix}
\begin{bmatrix} 0 \\ 0 \\ 1/3 \\ 0 \\ 0 \\ 0 \\ 0 \\ 0 \\ 0 \end{bmatrix}
\begin{bmatrix} 0 \\ 0 \\ 0 \\ 1/3 \\ 0 \\ 0 \\ 0 \\ 0 \\ 0 \end{bmatrix}
\begin{bmatrix} 0 \\ 0 \\ 0 \\ 0 \\ 1/3 \\ 0 \\ 0 \\ 0 \\ 0 \end{bmatrix}
\begin{bmatrix} 0 \\ 0 \\ 0 \\ 0 \\ 0 \\ 1/3 \\ 0 \\ 0 \\ 0 \end{bmatrix}
\begin{bmatrix} 0 \\ 0 \\ 0 \\ 0 \\ 0 \\ 0 \\ 1/3 \\ 0 \\ 0 \end{bmatrix}
\begin{bmatrix} 0 \\ 0 \\ 0 \\ 0 \\ 0 \\ 0 \\ 0 \\ 1/3 \\ 0 \end{bmatrix}
\begin{bmatrix} 0 \\ 0 \\ 0 \\ 0 \\ 0 \\ 0 \\ 0 \\ 0 \\ 1/3 \end{bmatrix}
$$

Figure 6:2 Orthogonal temporal codes on 9 spatial transmit elements

The scaling of 1/3 is to normalize the space-time vector (so that it has unit magnitude). As is evident, the individual transmit signals on all antennas are perfectly orthogonal, and thus the illumination area was maximized. The illumination pattern and the correlation matrix for this case are shown in Figure 6.3.

Self Constructed - Perfect Space-Time Signal
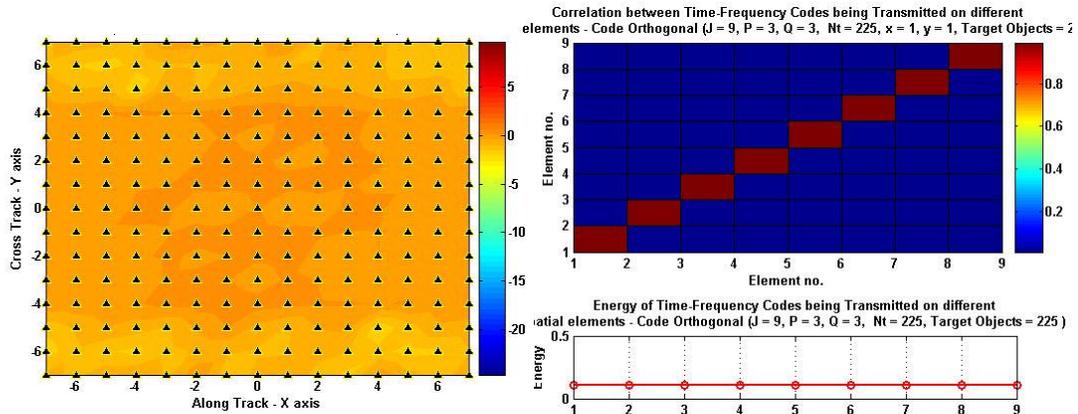
Figure 6:3 Transmit Signal Form: All Targets

(Perfectly orthogonal signal on each transmit element)

The next step was obviously to check what solution does our maxi-min comes up with for the same scenario. Results for the maxi-min are shown below in Figure 6.6.

Heuristic Maxi-min based on only the Target Energy
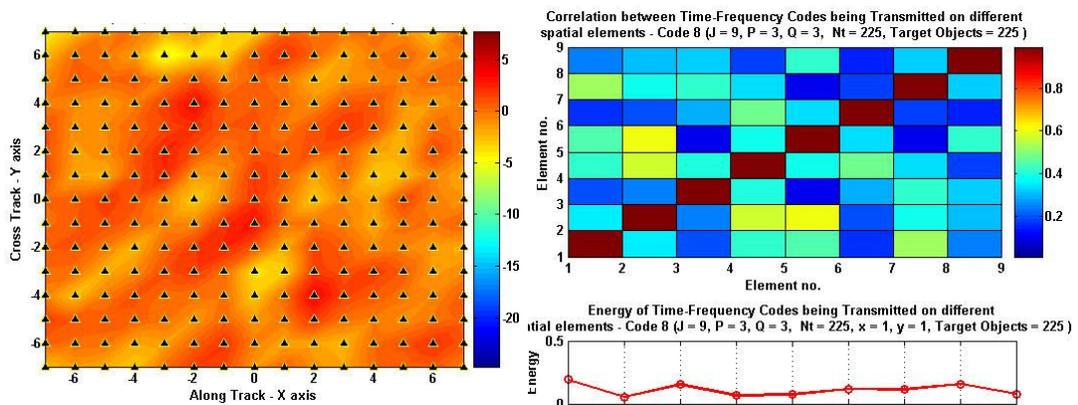
Figure 6:4 Transmit Signal Form: All Targets (Heuristic SCR Convergence) - Predictable

As can be seen, the pattern matches closely with that of Figure 6.3. The algorithm tries to illuminate all targets equally by coming up with highly uncorrelated, equal

146

energy signals on each transmit element. Contrast this with Figure 6.5 where the illumination pattern and correlation matrix for "Maximum Energy" code have been shown for the same case.

Maximum Energy
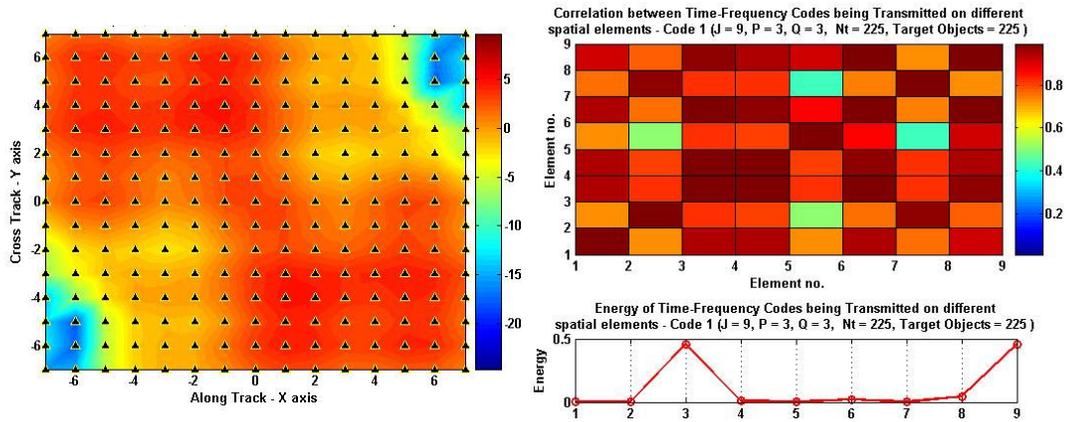
Figure 6:5 Transmit Signal Form: All Targets (Maximum Energy)

Note the high degree of correlation between temporal signals of different transmit elements. Also note the grossly unequal distribution of energy on spatial elements; effectively just 2 out of the 9 elements – 'Antenna 3' and 'Antenna 9' are energized for this case. This solution tries to maximize the total illumination energy on all targets, but sacrifices a few corner targets in the bargain – the familiar orphan problem of Chapter 3.

Also note that here we are comparing the "Maximum Energy" instead of the usual "Maximum SCR" with our maxi-min. The reason should be obvious, since there are no clutter objects in the scenario, there is no notion of SCR here. Even the maxi-min algorithm had to be altered slightly for this case. The algorithm of Figure

6.4 just aims at maximizing the minimum energy received by any target; hence it works on the $\mathbf{A}_i$ instead of $\mathbf{C}_i$ matrices. Also there is no concept of SCR and energy convergences (as there are no projections into and out of the squiggle domain), and thus we have only one type of "heuristic" and "true" algorithm each. The results shown in Figure 6.4 are for the heuristic algorithm, which is understandably called the "*Heuristic Maxi-min based on only the target energy*".

Thus we see that for both the simple and predictable scenarios our maxi-min comes up with fairly accurate answers, but what about the cases where the scenarios are not so easy to predict? One such case is shown in Figure 6.6 below.

Heuristic SCR Convergence
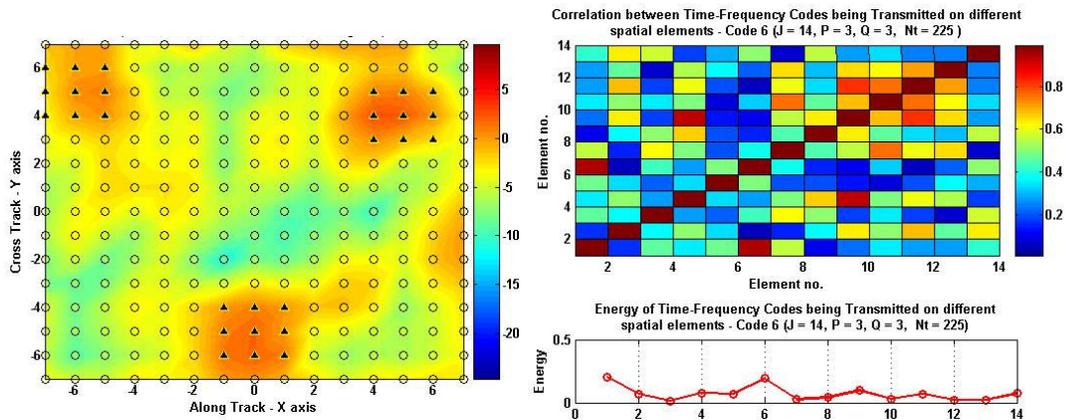
Figure 6:6 Transmit Signal Form: Typical (Heuristic SCR Convergence) – Non-predictable

We see that for such in-between cases, the transmit signal form is difficult to predict. Typically the individual temporal signals are partially correlated and have unequal energies, as can be seen from the figure above. It is hard to come up with any sort of rule or pattern regarding such signals, but the good news is then these transmit signals also become unique to our algorithms. There is no other way (except by using our

algorithms) by which we could have arrived at these solutions. And as already seen, these solutions are indeed good solutions not achievable by simple beamforming techniques. Thus to summarize, for most cases each array element truly needs to transmit a dissimilar time-frequency signal to result in a desirable illumination pattern; but the form of this absolute space-time signal is not trivial to predict and can only be determined through an intelligent and logical mathematical process, like our Maxi-min algorithms.

6.2 The target time-frequency response

Perhaps even more interesting than the form of these space-time signals at the transmitter, is the form of the resulting incident signal on each target. The transmit signal has energy spread across some bandwidth B and timewidth T, which gives us the necessary range and doppler resolution. But the spectrum of this signal as a function of time and frequency, is very different at the targets for the spatial and space-time signals.

For a multi-aperture radar, the resulting signal at any target is due to the coherent summation of all the individual temporal signals of different transmitter elements. The way these different temporal signals combine depends on the location of that particular target. Since for a spatial or separable space-time signal, the temporal signals on all antennas are identical, their coherent addition is also constant with position except for a phase change due to the delay and doppler shifts. It is this phase change over the timewidth and bandwidth of the radar, which results in the

required doppler and range resolution. The time-frequency magnitude and phase spectrums, resulting from a spatial "Maximum Energy" solution on two different targets separated by just one resolution cell have been shown in Figures 6.8 – 6.9. Note that by "time-frequency" spectrum or "time-frequency" response, we mean the magnitude and phase of each of the individual time-frequency samples at the target. But first let's take a look at the relative locations of these targets and the target-clutter geometry assumed, which have been shown in Figure 6.7.
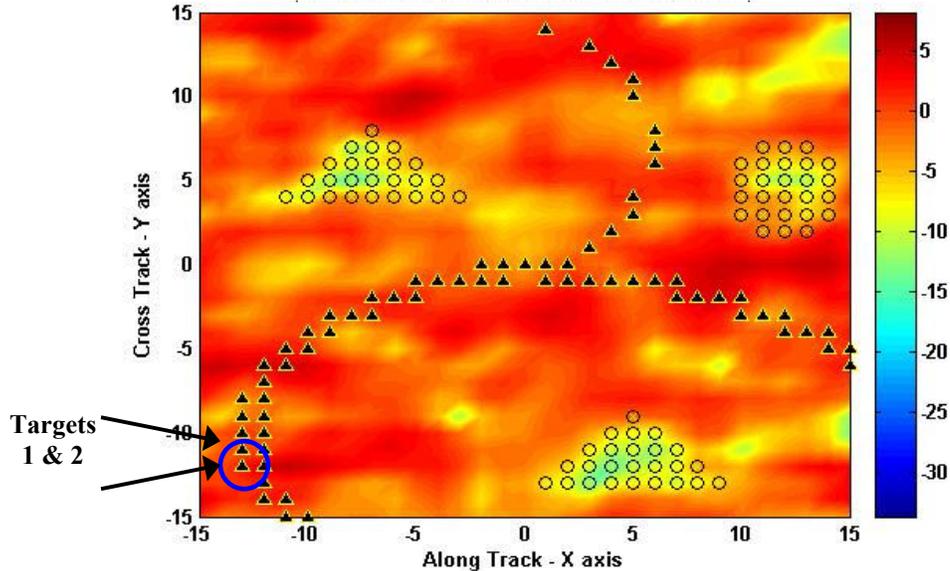
Figure 6:7 Location of two targets separated by just one resolution cell in range

As can be seen the targets are separated by just one resolution cell in range. The resulting magnitude and phase spectrums (over the radar time and bandwidth), on these targets by the "Maximum Energy" transmit solution are shown next.

150

Target 1

Magnitude Response   Phase Response
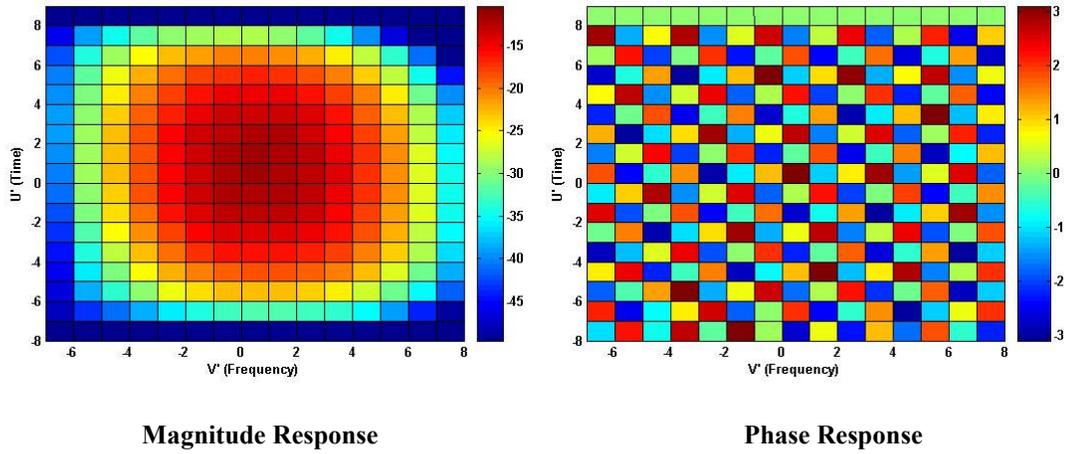
Figure 6:8 Magnitude and Phase response on Target 1 due to the "Maximum Energy" solution

Target 2

Magnitude Response   Phase Response
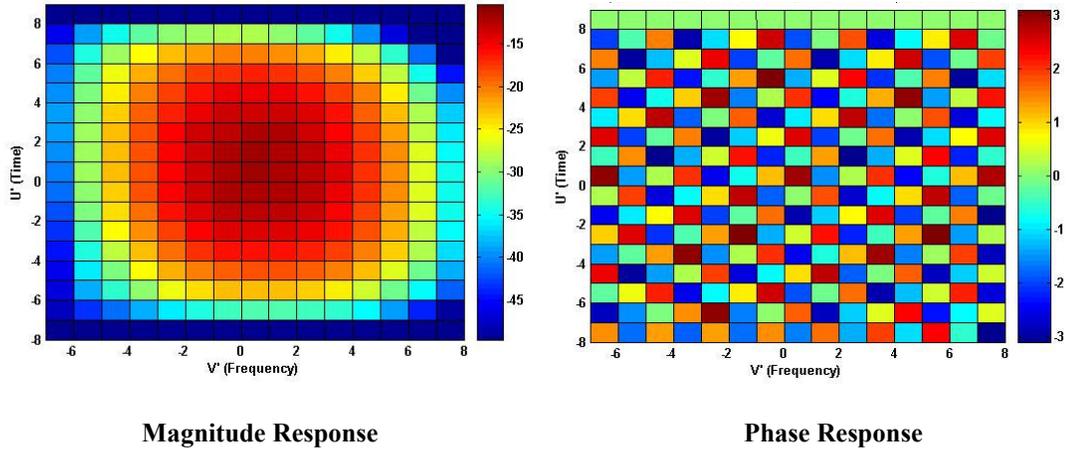
Figure 6:9 Magnitude and Phase response on Target 2 due to the "Maximum Energy" solution

It is evident that the magnitude spectrum is exactly the same for both cases. However the phase slope is different along the frequency axis, and thus the response from one target is just a phase shifted version of the other. We need this phase shift to last over a large time and/or bandwidth in order to be able to sufficiently decorrelate our target

responses, and thus resolve our targets. The difference in the two phase slopes can be better seen in the next plot, where it has been plotted as a function of time and frequency.

Difference in the Phase Response of Targets 1 & 2
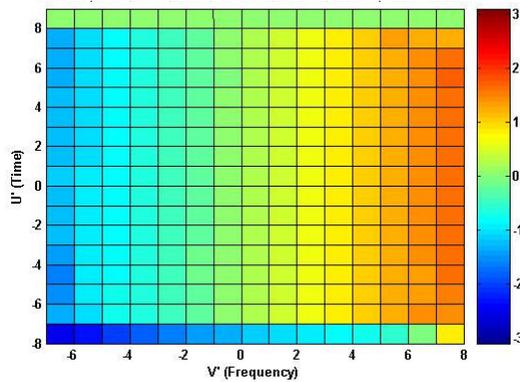
Figure 6:10 Difference in phase slopes – Targets 1 and 2

Note the phase difference does not change with time, as both targets belong to the same doppler bin. However this difference can be seen to change by a factor of about π radians over the bandwidth of the signal. Actually for absolute resolution, this change should be near to 2π radians. The reason we get half the phase change is because the propagation model was designed for the complete case of both transmit and receive; over which the change would indeed be 2π radians. But for the illumination optimization problem, we just consider the propagation from transmitter to the targets, and hence the phase change is half of what it normally would be. Thus in reality targets 1 and 2 would be non-resolvable, and the two corresponding responses highly correlated. But that doesn't affect the point we are trying to make

here even slightly; namely the magnitude responses at any two targets, for a pure spatial code, are identical and all the achievable resolution is solely due to the phase.

This behavior is however completely different for true space-time codes. Since the resulting time-frequency response at the targets is now due to the coherent summation of *dissimilar* temporal signals of different antenna elements, this time-frequency spectrum can be completely different at different target locations. Figure 6.11 shows the time-frequency magnitude response at the same two targets of Figure 6.7, now due to a true space-time solution ("Heuristic SCR convergence").

Target 1   Target 2
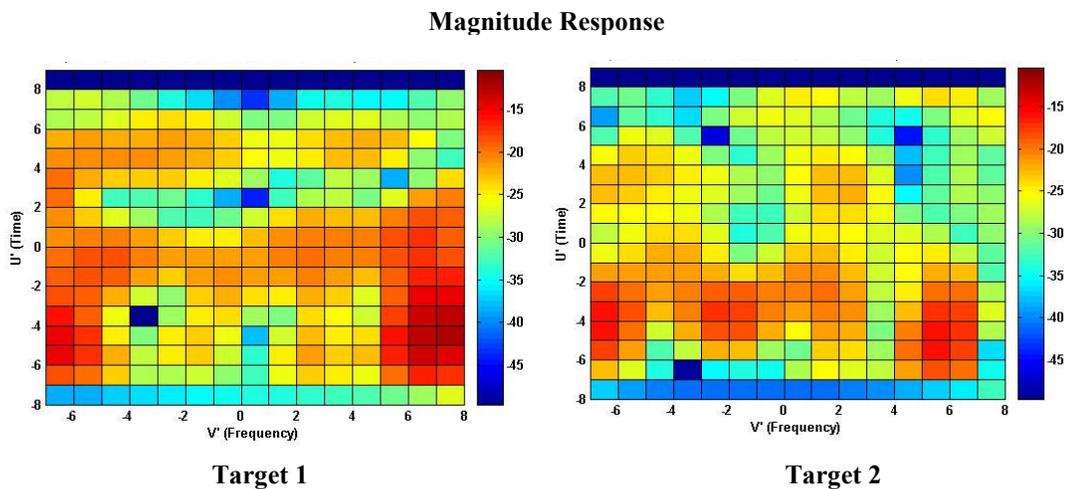
Figure 6:11 Magnitude Response at the two targets due to a true space-time solution

As can be seen, both the magnitude spectrums are quite different. The result has significant consequences for radar applications, as it implies that targets can also be resolved based on magnitude now in addition to the phase. Notice that the energy on the two targets is distributed differently as a function of time and frequency; essentially giving the impression that the two targets get illuminated by two different

transmitters. On the receive side it translates to having a different time-frequency transmitter present at each target location (which propagates its own signal back to the radar). Compared to the case where phase shifted versions of the same time-frequency signal are received from each target, this scenario definitely offers much greater potential for target resolution. Therefore if space-time signals can be constructed which result in dissimilar magnitude spectrums at the different target locations, then the cross-correlation between the various responses can be greatly reduced, and better radar resolution achieved.

Note however that the usage of space-time codes for improving radar resolution is also a kind of double edged sword. It's because due to the inherent structure of these non-separable codes (coherent addition of dissimilar temporal signals etc), we typically loose out on a part of the radar time and/or bandwidth. This can also be seen in Figure 6.11 where the relatively lighter resolution cells indicate the phenomenon (zero magnitude at those times and frequencies). This loss of time and bandwidth would ordinarily hurt our ability to resolve in doppler and range respectively, but as now we can resolve based on magnitude also, the lack of energy on some time-frequency cells can actually work to our advantage and helps us resolve better. But there is also an important clause to this aspect - *the magnitude responses on different targets due to a true space-time transmit code, can improve radar resolution only if they are significantly different*. In other words, only if the two magnitude responses are energized at different time-frequency locations (cells), will the cross-correlation between the responses reduce. Otherwise it would remain nearly

the same or may even reduce as we just end up loosing out on our timewidth and bandwidth (eventually resulting in poorer resolution).

Thus the potential for better resolution exists, but it can only be exploited if we come up with the right kind of space-time solutions. Determining optimal solutions for this criterion is a whole new area of study – "*Space-Time Ambiguity Optimization*", which has partly been dealt with in [8]. To wind up this section, we show the time-frequency magnitude responses on some of the other targets as well. Notice that each is different from the other.

Target 1

Target 2
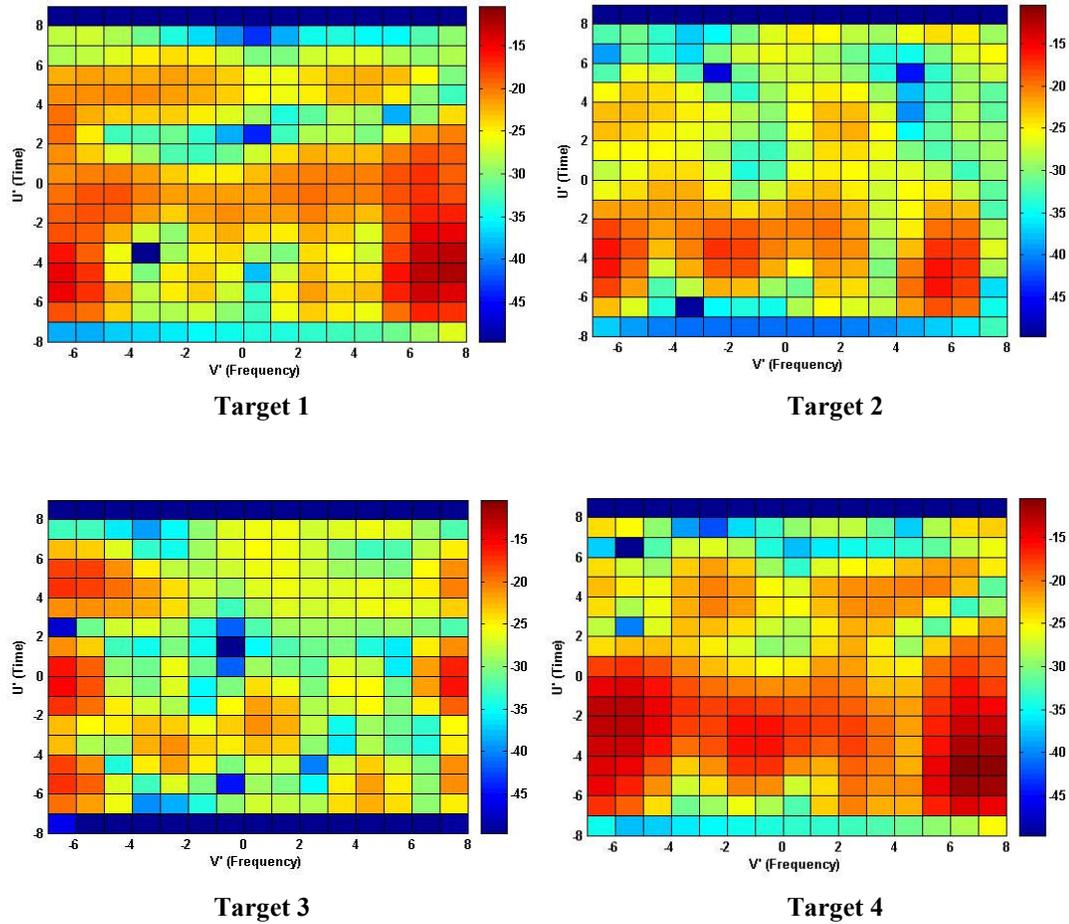
Target 3

Target 4

Figure 6:12 Magnitude Responses at different target locations due to a true space-time code

6.3 Space-time codes – one more prospect

In the long list of space-time code abilities, there's one more aspect which we discovered during our work on the target magnitude and phase responses (last section). Recall that the two targets 1 & 2 are separated by just one range bin, and are not resolvable ordinarily for the propagation from transmitter to ground. In other

words, both of them are so close to each other that they would lie within the main lobe of the range *time-frequency ambiguity function*. Note that the main lobe width of this temporal ambiguity function also turns out to be the width for the overall space-time ambiguity function, as for our case, the spatial resolution is not as fine as the temporal resolution (2.82). Until now the presumption has been that the width of this main lobe for the range and doppler ambiguity functions, is purely decided by the bandwidth and timewidth of the radar respectively, and once these parameters have been fixed there's no way it can be altered. Once again this turns out to be indeed true for single aperture radars and even phased arrays, but the possibility of obtaining reduced main lobe widths has never been examined for true space-time codes. Obviously all targets lying within this ambiguity function main lobe imply highly correlated target responses, and thus non-resolvability. The location of two such targets – 1 & 2 is once again shown in Figure 6.13; along with the correlation value between these responses for a purely spatial transmit code (obtained using "Maximum energy" algorithm).
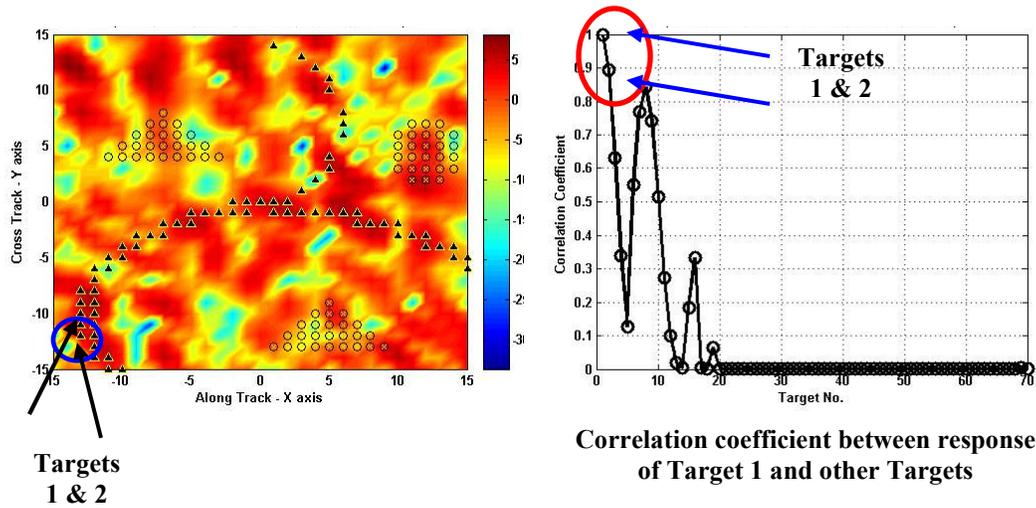
Figure 6:13 Correlation between responses of 2 targets within the main lobe of the space-time ambiguity function: Spatial code

The plot on the right actually shows the correlation between the response at target 1 and those at all other targets, and as can be seen the correlation coefficient value between the responses of targets 1 and 2 comes out to be very high – around 0.9. This was expected as the physical separation between the two targets is not large enough; and thus the difference between the two phase slopes cannot change by 2π radians over the available signal bandwidth. Furthermore, since the radar bandwidth is already specified, there seems to be no plausible way by which the two targets can be resolved or at least the cross-correlation between the responses is brought down.

Like mentioned before, the above statement is true only for conventional single aperture radars or spatial transmit signals. For space-time signals some very different and also interesting results are observed. Since for such signals we do not rely only on the phase change with respect to the timewidth or bandwidth for resolution, there is a possibility of improving resolution for even those targets which

158

would normally come under the main lobe of the ambiguity function. More simply, *the main lobe width for the ambiguity function can now be narrowed*; which can potentially be a very important result for radar applications. This point is also a kind of restatement of the earlier idea, that now we can better discriminate between two targets which are very close to each other by virtue of their dissimilar magnitude responses. The concept is illustrated in Figure 6.14, where we show the correlation between the target responses of the same two targets, this time for a true space-time code (generated using the "*Heuristic SCR convergence*" algorithm).
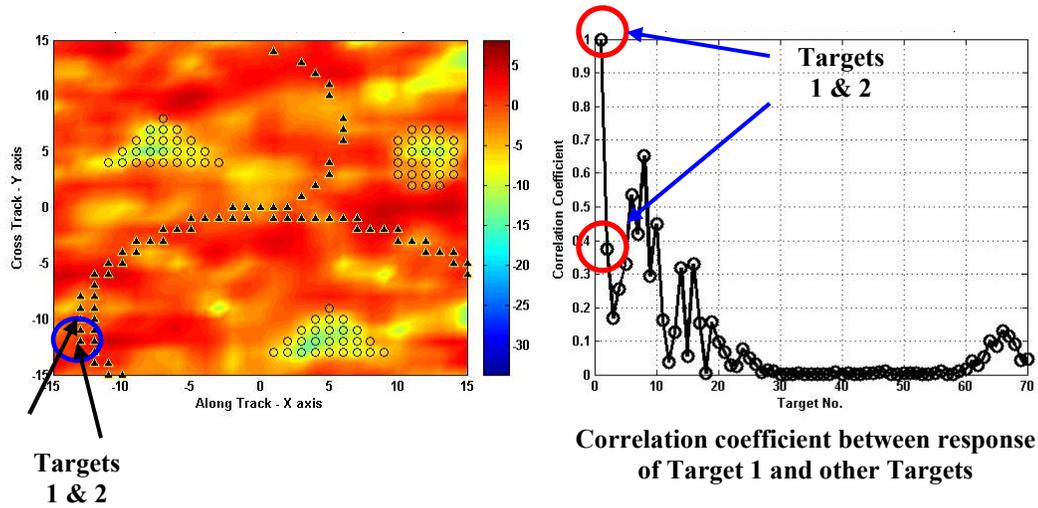

Figure 6:14 Correlation between responses of 2 targets within the main lobe of the space-time ambiguity function: True space-time code

The correlation-coefficient value between the same two targets is seen to drop to around 0.38, which though not great, is still a substantial improvement over the previous case (spatial code). This indicates that if appropriate space-signals are constructed which result in uncorrelated incident signals on the different targets, then the radar ambiguity function main lobe width can be reduced and there exists a

potential for reducing the cross-correlation between two very close targets. To illustrate this concept better, the actual range ambiguity function was plotted at 'target 1' for both a spatial and a space-time code. For better appearance of this plot, the target spacing has been reduced by half i.e. one additional target has been inserted between every two existing targets. The plots have been shown in Figure 6.15 and clearly show the narrowing of the main lobe width. Like stated previously, this is quite a significant discovery and can have profound ramifications on the radar system performance.
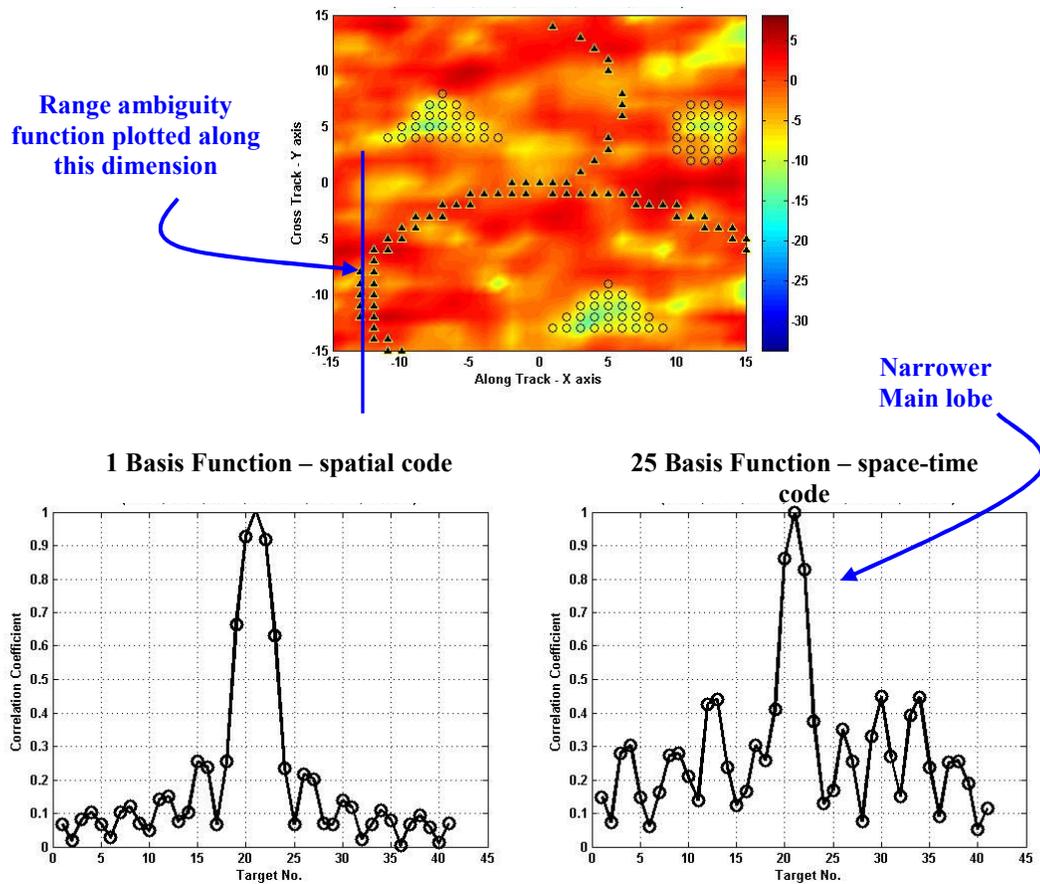

Figure 6:15 Potential for ambiguity function main lobe width reduction - space-time codes

160

6.4 True space-time nature – an alternate perspective

This is going to be the last section in this chapter where we again look at the space-time nature of our signals; but from a different viewpoint. We have already seen that the space-time signals perform considerably better than pure spatial signals with regard to the maxi-min criteria. And the reasons for this superior performance, we concluded, were the additional time-frequency dimensions available to the space-time codes. But what exactly do these additional temporal dimensions translate to? One simple way to think about it, is that the transmit signal now has multiple time pulses and frequency samples to take care of its targets. If a specific target cannot be energized by a particular pulse or frequency, then another pulse or frequency can be used to place energy on that target. In other words, the illumination pattern can vary from pulse to pulse or frequency to frequency.

This versatility is not available with pure spatial codes. Since all the antennas propagate the same temporal signal, their coherent summation on ground results in a constant illumination pattern with respect to time and frequency. At most, the pattern can vary in intensity due to the different energies of different pulses, but the energy distribution outline on the targets and clutter cannot change. However in case of true-space time codes, the different temporal signals of different antennas can interact coherently to result in a changing illumination pattern with time and/or frequency. And as mentioned before, this attribute enables the space-time codes to come up with better final integrated energy patterns on targets and clutter. The property also acts as a distinctive characteristic of space-time codes and can be used in addition to the form

of space-time signal results, to distinguish them from spatial codes. As an example the resulting illumination pattern by each of the pulses of a true space time code (generated using "*Heuristic Energy Convergence*"), for a particular target-clutter geometry has been shown in Figures 6.16 – 6.17.

Pulse 1

Pulse 2
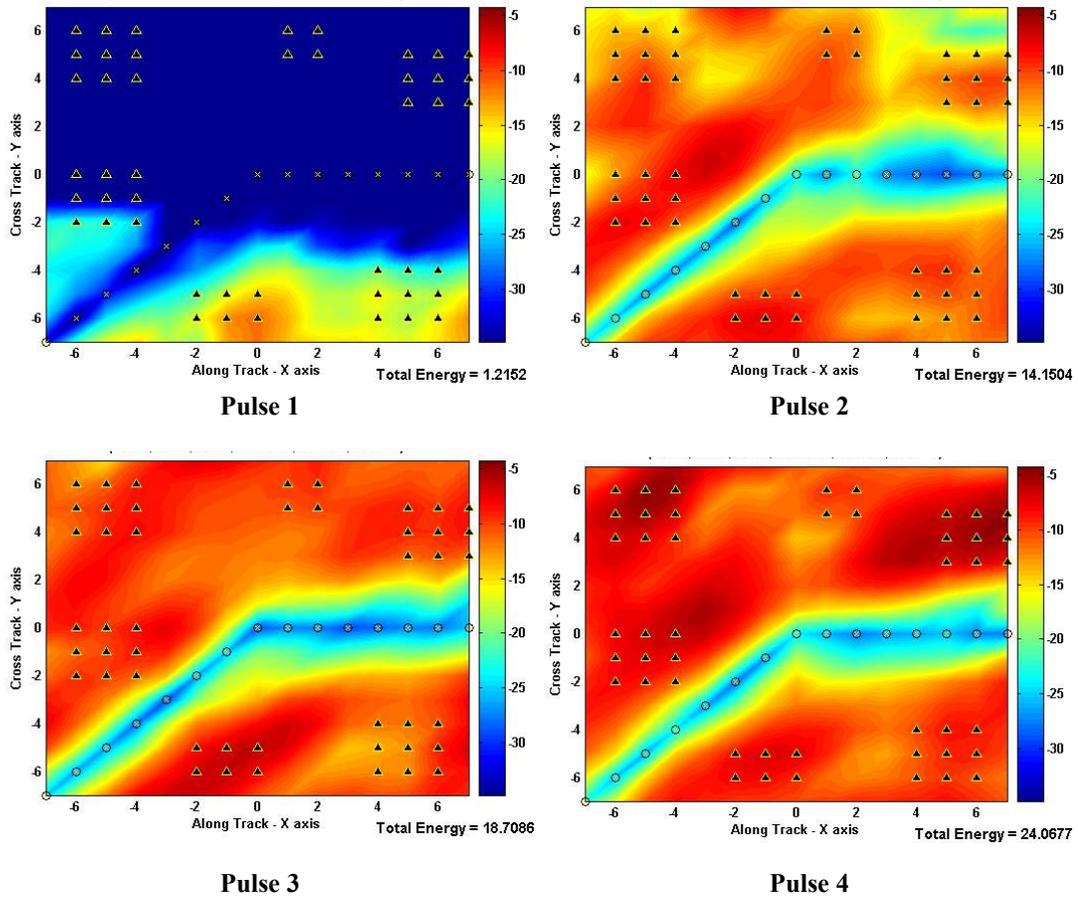
Pulse 3

Pulse 4

**Figure 6:16 Pulse to pulse illumination pattern for a true space-time code
(Pulses 1 to 4) – "Heuristic SCR Convergence"**

Pulse 5

Total Energy = 22.5788

Pulse 6

Total Energy = 15.6277

Pulse 7

Total Energy = 18.1118

Pulse 8

Total Energy = 17.5752

Pulse 9

Total Energy = 2.5194
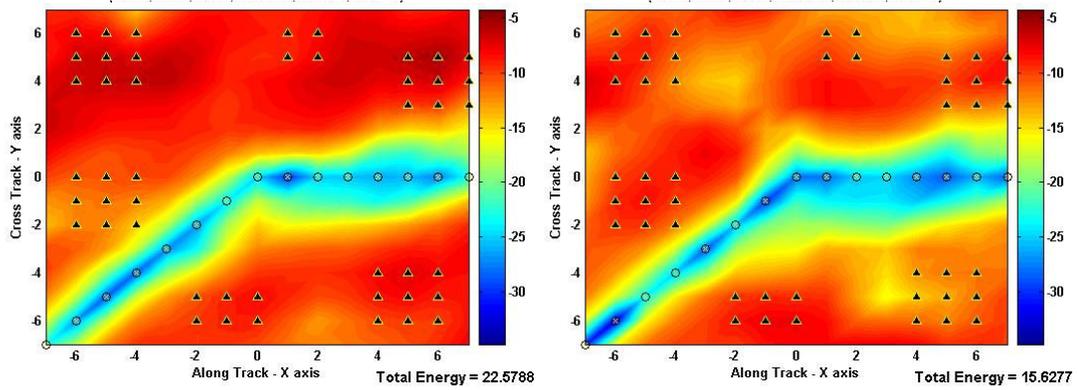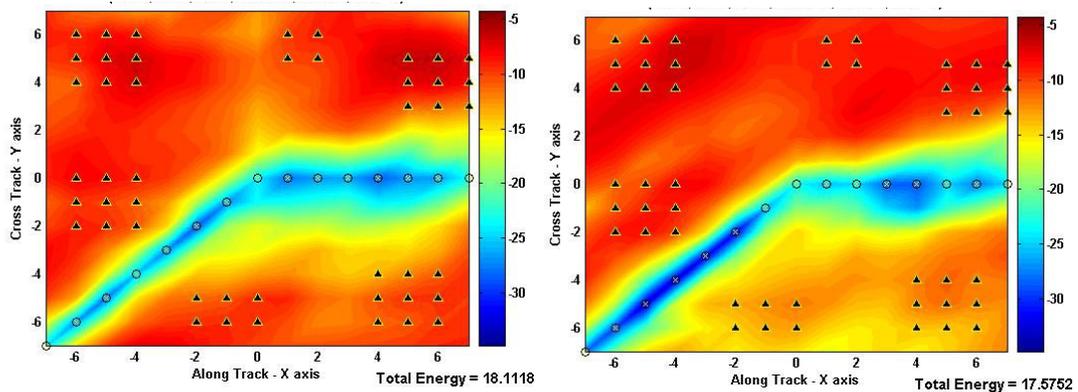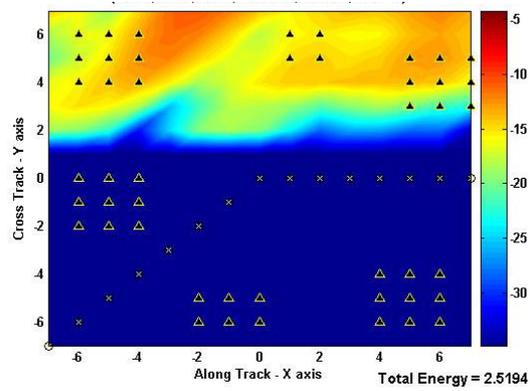
**Figure 6:17 Pulse to pulse illumination pattern for a true space-time code –
(Pulses 5 to 9) "Heuristic SCR Convergence"**

The above case is for 7 pulses sent by the transmitter ($U = 7$), and thus due to the interpolation reason of Chapter 2 we have 9 pulses or 9 time windows at the targets ($U' = 9$). The first and the last pulse at the targets ($u'=1$ and $u'=9$) just capture the leakage of the first and last transmitted pulses ($u=1$ and $u=7$), out of their respective observation windows, and hence for these pulses (*Pulses 1* and *9*) we see only part of the target area receiving energy. This is expected, as this is only the leakage out of a normal time window and hence does not constitute a full transmit pulse.

As can be seen from Figures 6.15 - 6.16, though the illumination pattern does not change greatly, it does vary a fair bit after every pulse. Each pulse is strong in some and weak for another portion of the illuminated region, but the cumulative effect of all pulses usually results in pretty effective illumination patterns integrated over the whole time. This property of non-separable space-time codes is indeed very efficacious, and is responsible for most of the impressive integrated energy patterns of earlier chapters. The total integrated energy pattern and the correlation matrix for this solution are shown in Figure 6.18.
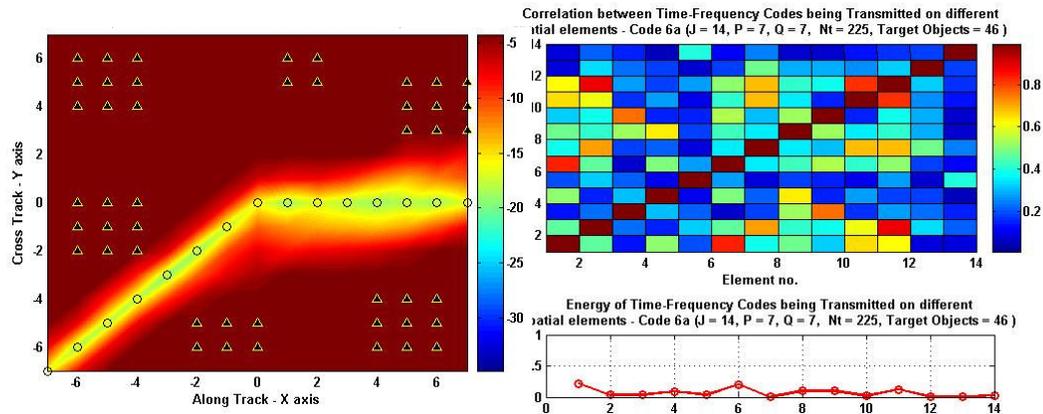
Figure 6:18 Integrated illumination pattern and correlation matrix for a space-time solution – "Heuristic SCR Convergence"

We have not included the pulse to pulse energy patterns for the standard spatial codes (which were pretty static), but for comparison purposes the integrated illumination pattern and the correlation matrix for each of the standard codes, along with that of *"Heuristic SCR convergence"* have been shown in Figures 6.19 and 6.20. Note that the color scale in Figure 6.18 has been changed to enable better observation of the finer variations in the pattern. Once again the superiority of "Heuristic SCR convergence" over the standard codes can be appreciated from these figures.
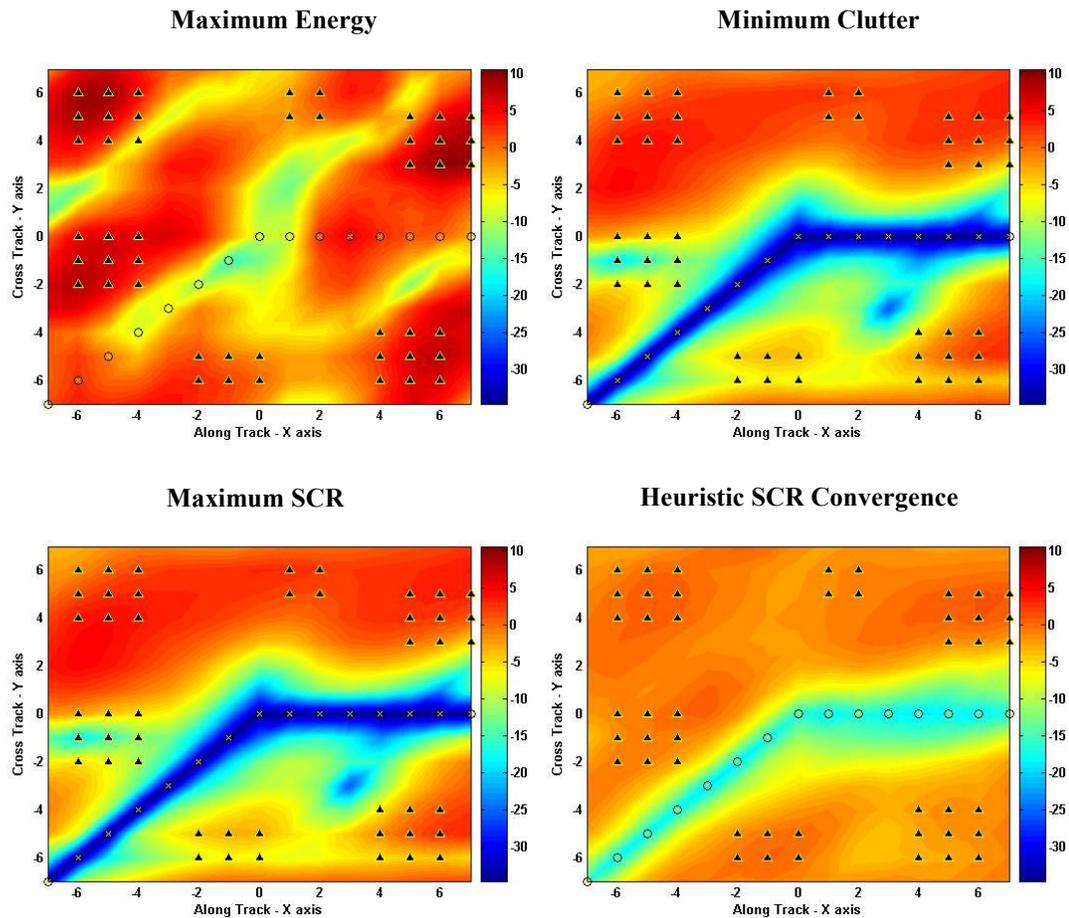
Figure 6:19 Integrated illumination pattern for all types of codes – standard and maxi-min

Note the similarity between "Minimum Clutter" and "Maximum SCR" solutions for this particular scenario. This type of resemblance is not surprising. For some of the target-clutter arrangements, the best way to maximize the average SCR on all targets is indeed by putting zero or minimum energy on the clutter objects. The affinity between the two solutions or vectors can also be seen in the correlation matrix plots below.
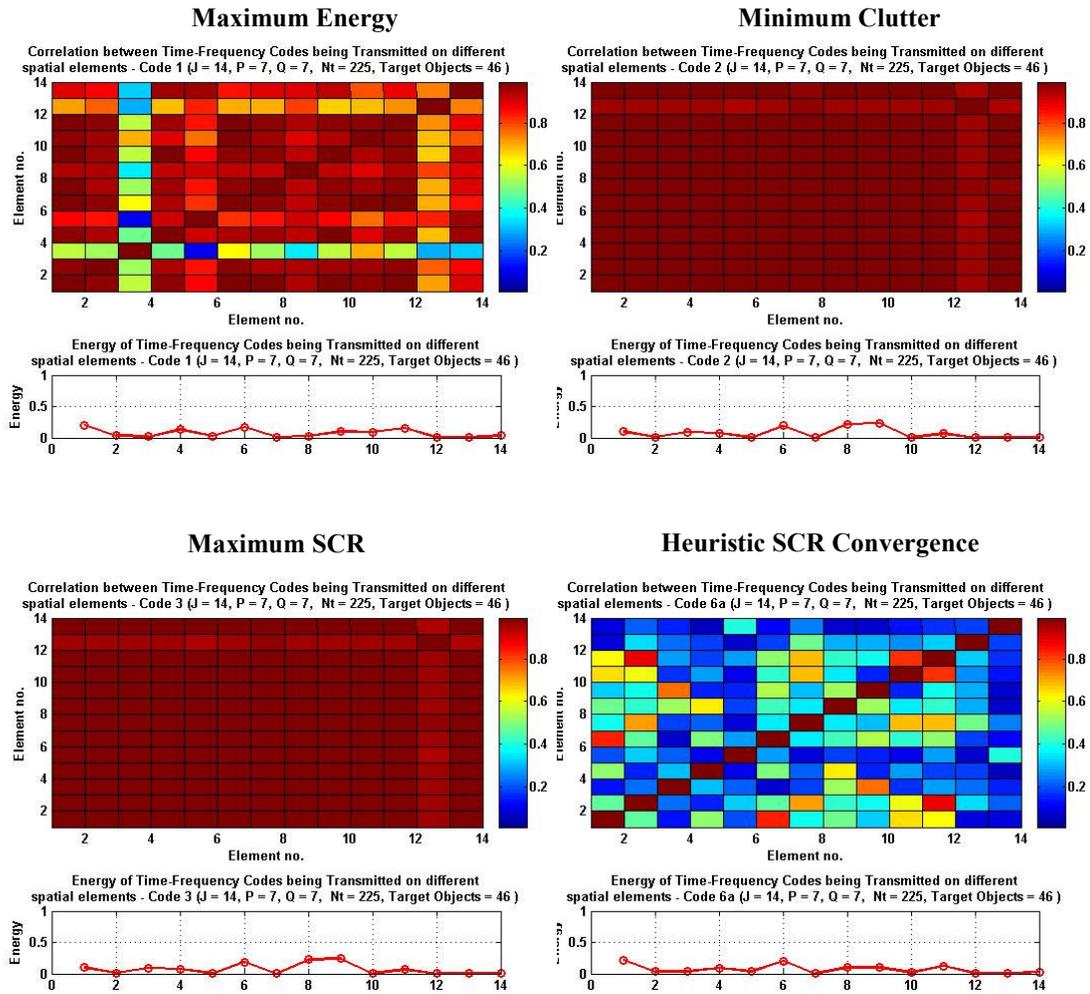
Figure 6:20 Correlation matrix for all types of codes – standard and maxi-min

Once again the spatial nature of the standard codes and the true space-time nature of the maxi-min can be inferred from these plots. This also brings us to the end of this chapter in which we saw few other features, and capabilities of true space-time codes. In fact with this topic, we also complete majority of the more significant stuff in this thesis. The next chapter which is last but one, describes some of the other tests/ algorithms which were tried keeping specific applications in mind. And therefore

these experiments although interesting in their own light, are somewhat limited in their scope and do not make for as big a news as the stuff seen up till now.

Chapter 7

A Few Last Experiments

As mentioned towards the end of the last chapter, by now we have already covered the most significant portions for this thesis. But that does not mean that those were the only ideas that were ever tried. In all, we worked on a lot of concepts; not all of which were successful. Many did well and have thus been recorded in the last six chapters, but some others also resulted in just partial successes, or even total failures. Nevertheless, few of them make up for some really readable material, and hence it was decided to include them at one place in this document. Please note that although some of these ideas themselves manifest in the form of algorithms, the others are just propositions to aid the existing algorithms under special circumstances.

7.1 Operations in subspace orthogonal to clutter

Recall the "Maximum SCR" algorithm of Chapter 3. On the whole it's an effective algorithm, and performs pretty well (typically) with respect to the goal it has been designed for - namely maximizing the average SCR on the targets. But there is one condition for which this algorithm will not work normally; the case when the number of clutter objects are less than the number of transmit antennas (a pretty rare scenario actually). From our discussion of Chapter 3, we know that for such a case the eigen spectrum of $\mathbf{B}$ will have some truly zero eigen values (number of non-zero eigen values $= n_b \times R < J \times R =$ the total number of eigen values in the spectrum) One

way to think about it is that since the number of clutter objects are so few, there are dimensions available to put zero or minimal energy on these objects. An example spectrum for the **B** matrix is shown in Figure 7.1. Note that for this case we have 4 clutter objects, 9 time-frequency basis functions and 14 transmit elements.

Eigen Spectrum of **B**
4 clutter objects, 9 temporal basis functions
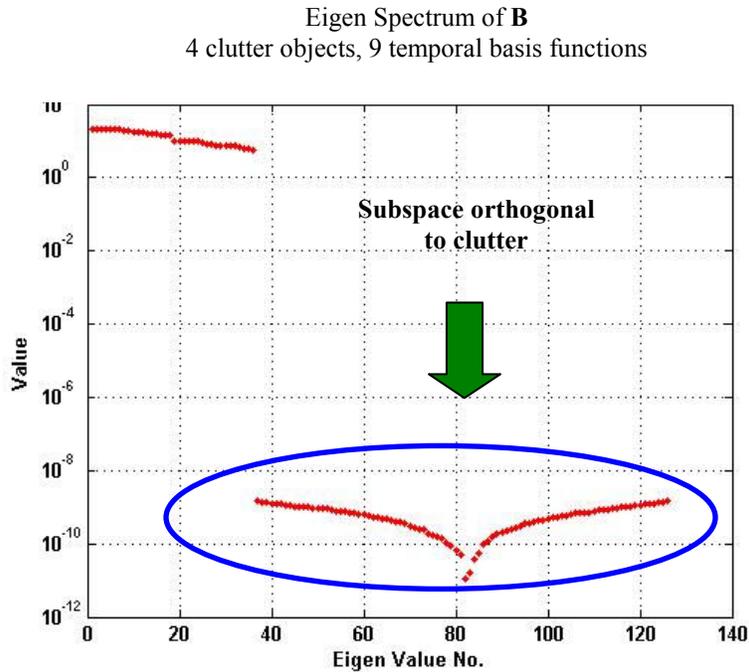
Figure 7:1 Concept of subspace orthogonal to clutter

Hence we have a total of 126 eigen values, out of which only $4 \times 9 = 36$ associated with the four clutter objects are non-zero. These are the only 36 dimensions which can result in any form of illuminated energy on our clutter objects. The eigen vectors corresponding to the remaining 90 values define a vector space orthogonal to the clutter; and any and every vector in this subspace results in zero total energy on the clutter objects.

This concept of orthogonal clutter subspace turns out to be very important for the case of very few clutter objects, as now the vector solution maximizing the total SCR, always lies within this orthogonal subspace. Each vector here results in zero or very little energy on the clutter objects, and hence potentially infinite SCR for our targets. But when the $\mathbf{B}^{-1/2}$ matrix is formed using (3.22), i.e. using only the non-zero values of $\mathbf{B}$, we essentially project out this subspace and thus eliminate all our possibilities of coming up with the right answer. An alternate method is therefore required for this special case. But before that, let's take another look at the above discussion which has been graphically depicted in Figure 7.2. Note that for this case we have 2 target objects, and hence the number of non-zero eigen values in the spectrum of $\mathbf{A}$ are $2 \times 9 = 18$.
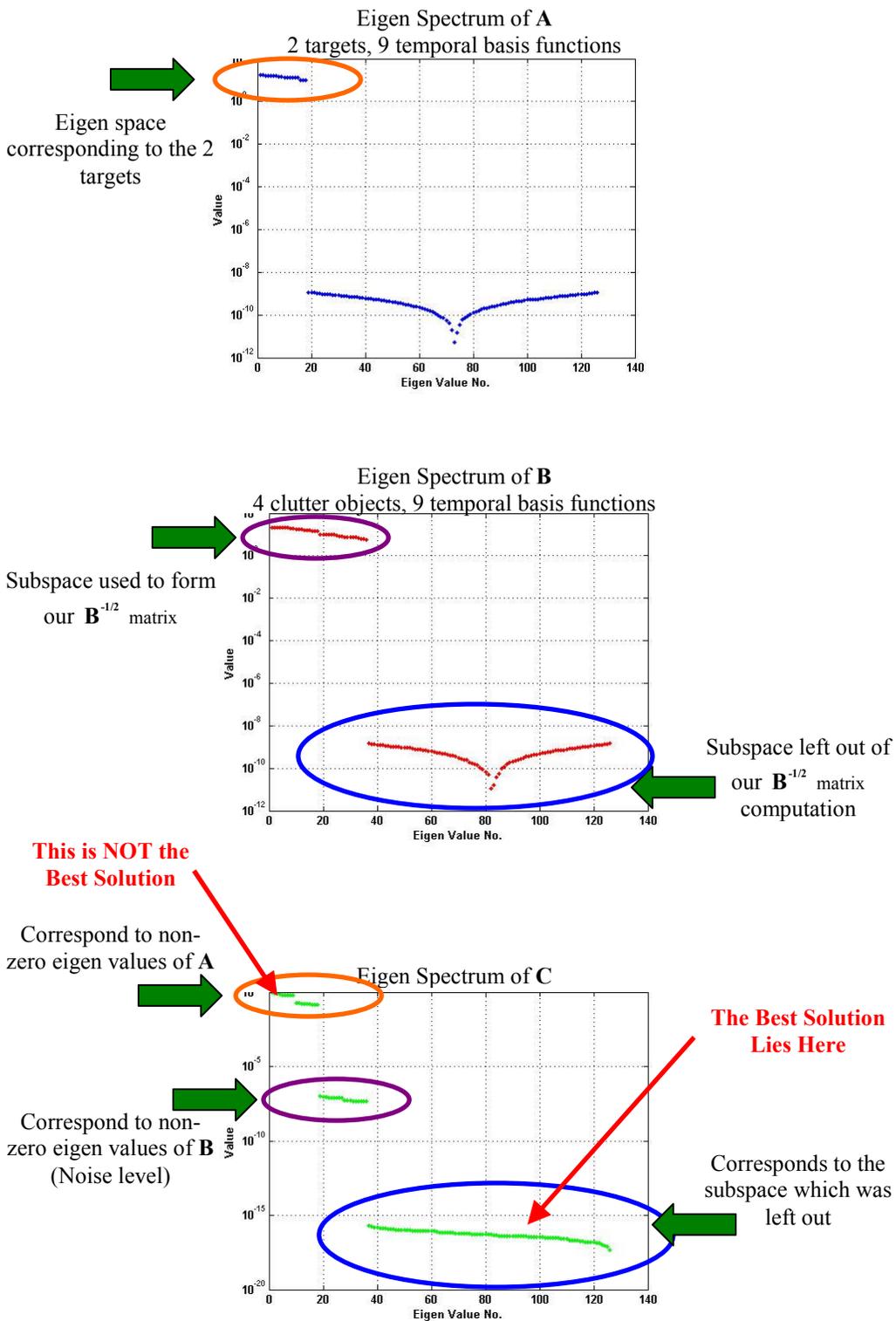
Figure 7:2 Limitation of the Maximum SCR algorithm

As can be seen, the algorithm will return the vector corresponding to the largest eigen value of $\mathbf{C}$ as our "Maximum SCR" solution. However the actual best solution was part of the initial subspace orthogonal to clutter, and was thus left out of the $\mathbf{C}$ matrix computation. Therefore in such cases we will arrive at the wrong answer using our algorithm. Moreover this issue is of concern not only to the "Maximum SCR", but to all our maxi-mins as well. It's because all the maxi-min criteria also involve the best or worst SCR for individual targets, and hence need the correct eigen values for the $\mathbf{C}_i$ matrices. The subspace which appears to be the zero subspace (worst) in the eigen spectrum of $\mathbf{C}$, is actually a very high value subspace (best), and thus cannot be ignored for any of the maxi-min algorithms.

As a remedy a newer version of the "Maximum SCR" was developed, which we call the *"Maximum Target Energy - in subspace orthogonal to clutter"*. In this method we project out the dimensions which put even a little energy on our clutter objects right at the start, and then search for the best solution in the remaining subspace. Since there are multiple solutions which can minimize or result in zero energy on the clutter, we find our best solution as the vector which also maximizes the total energy on the targets (hence the name for this algorithm). The whole idea is depicted graphically in Figure 7.3.

Eigen Spectrum of **B**
4 clutter objects, 9 temporal basis functions

Project out this subspace right at the start

Look for the Vector which maximizes the energy on the targets
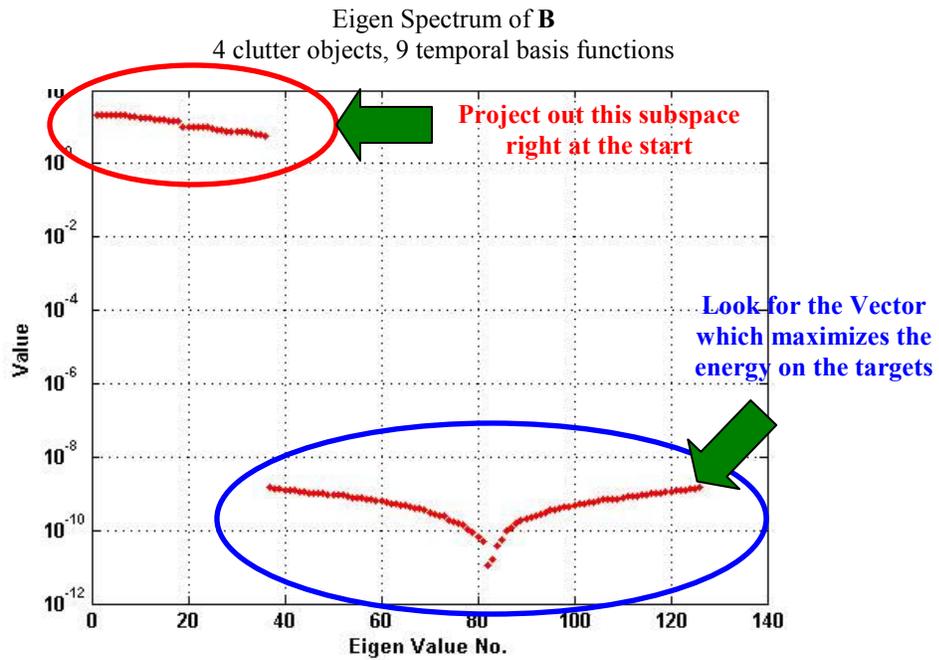
Figure 7:3 Idea behind the new version of the "Maximum SCR"

A mathematical step by step description for the same procedure is also presented below.

<u>Maximum Target Energy in subspace orthogonal to clutter</u>

1. First compute a new matrix $\mathbf{B}_\perp$ as:

$$\mathbf{B}_\perp = \sum_i \hat{e}_i^\perp \hat{e}_i^{\perp\prime}$$

Where $\hat{e}_i^\perp$ are the eigen vectors of **B** corresponding to the zero eigen values.

Therefore $\mathbf{B}_\perp$ is our projection matrix orthogonal to the clutter subspace.

2. Next, define a new matrix **D** as:

$$\mathbf{D} = \mathbf{B}_\perp{}' \mathbf{A} \mathbf{B}_\perp$$

174

Thus we project out the entire clutter subspace in one go. Note that for the maxi-mins each individual $\mathbf{D}_i$ matrix can be computed as $\mathbf{D}_i = \mathbf{B}_\perp{}' \mathbf{A}_i \mathbf{B}_\perp$

3. The problem now reduces to that of maximizing $\mathbf{S}' \mathbf{D} \mathbf{S}$. Writing $\mathbf{D}$ in terms of its eigen values and vectors:

$$\mathbf{D} = \sum_n \lambda_n^d \, \hat{e}_n^d \, \hat{e}_n^{d\prime}$$

We see that the vector $\mathbf{S}$ which maximizes the total energy on the targets, and at the same time results in zero energy on the clutter, is the eigen vector associated with the largest eigen value of $\mathbf{D}$.

4. $\therefore$ the optimal solution is given by:

$$\mathbf{S} = \hat{e}_n^d \text{ associated with } (\lambda_n^d)_{\max}$$

This algorithm was seen to perform comparably to the original "Maximum SCR", for the applicable cases of lesser number of clutter objects. The concept of projecting orthogonal to the clutter subspace and then searching for our best solution was also extended to the maxi-mins, by using the individual $\mathbf{D}_i$ instead of the $\mathbf{C}_i$ matrices. Another important point to be noted is that there is no concept of squiggle and non-squiggle domain here, just as it was for the maxi-min based on only the target energy (essentially this case reduces to the same idea). Hence for very few clutter objects, we just have two versions of the maxi-min – the "true" and the "heuristic", and the heuristic is once again seen to perform better than the true.

Even though this variation for the "Maximum SCR" has been described in sufficient detail here, for most cases we never had to resort to this algorithm. It's

because for almost all our tests we just have 14 transmit elements, and thus rarely are there fewer clutter objects in the target-clutter pattern. Even for most practical scenarios such an eventuality (of having lesser clutter regions than the number of antennas) seems highly unlikely, and thus this algorithm has not been given as much standing, as to the ones before. The idea was just to draw attention to this special case for which the existing algorithms may give erroneous results, and to suggest a possible remedy for the same.

7.2 Maxi-min Operations on reduced number of Targets

In the chapters before we have pointed out the huge processing costs associated with the maxi-mins. This sometimes turns out to be a big overhead and constraints our ability to run/ debug larger cases. Therefore we were always looking for methods which enabled us to cut down on this computational time. The next experiment that was tried deals with this precise problem, and aims at making our algorithms faster by giving them *'fewer but more pertinent'* targets to work on. The idea is - if we can predict the weakest targets, or the ones most worthy of our attention from the standard "Maximum SCR" code results, then we can make the maxi-mins work on only these targets and come up with our solutions quicker. It's because fewer targets for the maxi-mins directly translate to fewer projections, evaluations, eigen decompositions and thus much faster executions.

The exact scheme adopted was to consider only those targets for our maxi-mins, which had an SCR value less by a specified margin (say 10 dB) compared to

the maximum value for any target. And all the weak targets were selected based on the "Maximum SCR" results (which are much faster to attain). The hypothesis was that the targets with the best SCR values for this solution were anyway the easy targets, and thus did not warrant any special attention. Any solution that we come up with (for improving the SCR on the remaining weak targets) would automatically result in a good enough SCR for these targets. This theory did seem to work for the cases that were tried, and some interesting, even unexpected results were obtained.

Few of these results have been shown in Figures 7.4 – 7.5. Note that for these cases the weaker targets (to be given as input to our maxi-min algorithm) were short listed based on the same 10 dB criteria as mentioned before – i.e. if a target received an SCR less by 10 dB or more than the best SCR for any target (for the "Maximum SCR" solution), then it was marked as a weakling and given as input to the maxi-min algorithm to work upon.

Maximum SCR

SCR_{min} = -3.49 dB

Weaker Targets selected based on this criteria

Heuristic SCR Convergence

SCR_{min} = 2.51 dB

Heuristic SCR Convergence - Reduced

SCR_{min} = 2.51 dB
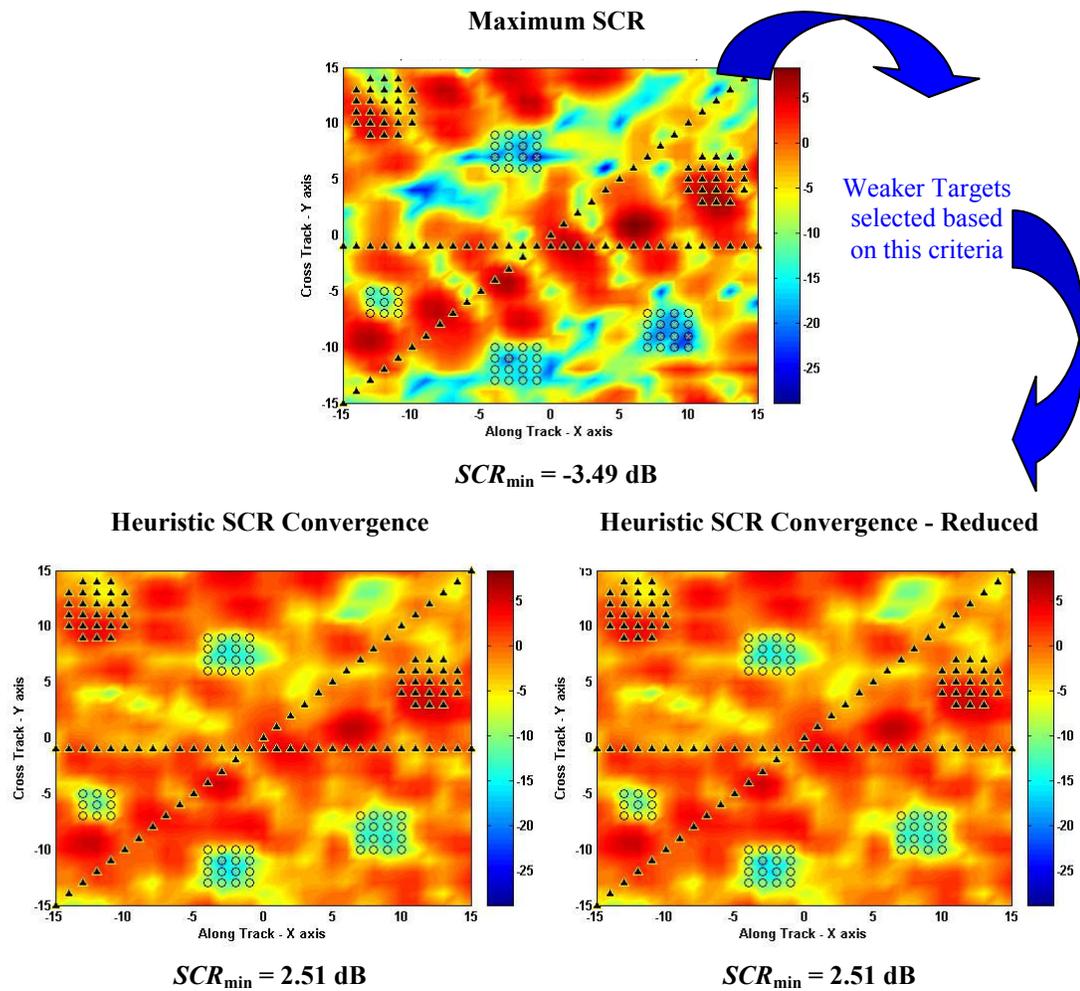
Figure 7:4 Effect of the reduced target algorithm – "Heuristic SCR Convergence"

Note that these results are for 25 time-frequency basis functions and 14 transmit antennas. Thus the transmit signal dimension is 350 in this case. As can be seen both the original *"Heuristic SCR convergence"* and the new *"Heuristic SCR convergence - Reduced"* result in exactly the same illumination pattern, and thus arrive at the same answer. However the *"Heuristic SCR convergence - Reduced"* arrived at its solution by operating on only 45 targets as compared to 108 for the *"Heuristic SCR convergence"*. The fewer targets were selected using the 10 dB criteria, and enabled

our algorithm to come up with its solution in less than half the time as the original version. To get a better idea, the original "Heuristic SCR convergence" took 36 hours for this simulation; where as the new reduced target algorithm arrived at its solution in just 17.5 hours. These results initially look promising and indicate a potential for arriving at our solution much faster, but there is more to this observation than what meets the eye. To understand this point, let's look at the same results for one of the other maxi-mins - the "Heuristic Energy convergence".
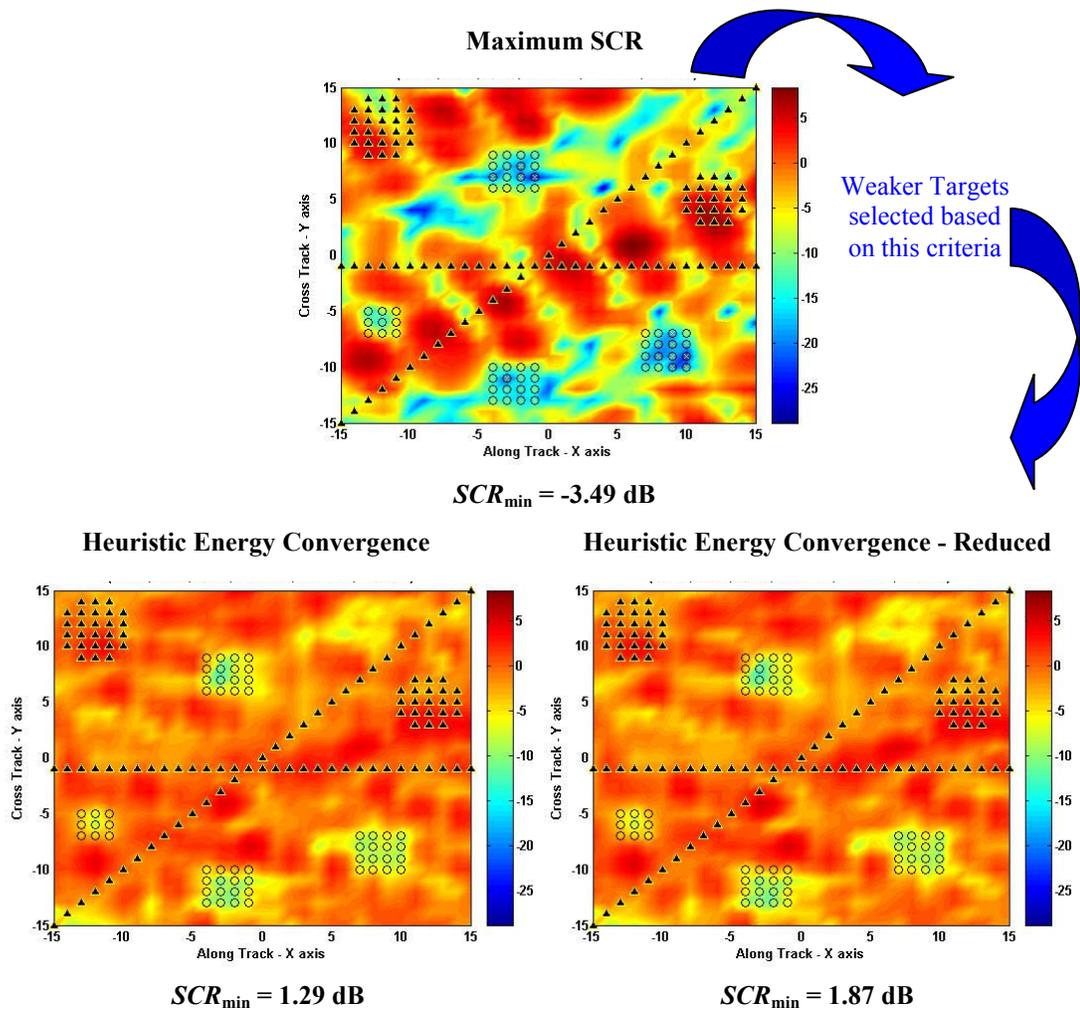

SCR_{min} = -3.49 dB

SCR_{min} = 1.29 dB

SCR_{min} = 1.87 dB

Figure 7:5 Effect of the reduced target algorithm – "Heuristic Energy Convergence"

Although hard to notice at first glance, the two illumination patterns are very slightly different for this case. The reduced target algorithm not only comes up with a different, but also finds a marginally better answer than the original algorithm. This phenomenon is rather surprising as even though the algorithm works on fewer targets or has lesser information to begin with, it still ends up with a better answer (*note that this better solution part did not apply to the "Heuristic SCR convergence"; once again reaffirming its position as the most optimal, or the champion code*). The discovery although startling, is not implausible. Note that due to the seeking nature of our algorithms, it's quite possible to go down completely different search paths and arrive at entirely dissimilar solutions, if the start points given to the algorithms are not same.

Thus even though satisfactory results are obtained for both the above cases, this small observation hints that the approach is not optimal and we always have the possibility of going down the wrong path or coming up with worse solutions (which did happen for some of the other cases attempted) . The behavior should not surprise us, as in a way it is the same conclusion that was reached in Chapter 5 - *predicting the algorithm iteration pattern, the targets which it operates on, or even the number of such targets is not viable*. The suboptimal nature of these algorithms acted as a dampener to the immediate plans of pursuing them further, and it was decided to put them on hold for some time. The idea was to revert to them only if a real constraint on time arrived at a later stage. However subsequently the focus shifted to other problems, and we never got a chance to visit these algorithms again. Nevertheless,

during the course of our work we discovered another kind of fast procedure, which is much speedier and also seems to have greater application. We call it the *"fast algorithm"*, and it has been described in the next section.

7.3 The Fast Algorithm

This is one of those other techniques which aims to find equally effective solutions, just a lot quicker. The idea behind is simple - try to find the best solution in a smaller dimensional subspace, which is rich in good solutions for all targets. And we come up with this smaller search space, by using the individual best solution for each target had it been present alone with the clutter. In other words form a projection matrix **P** using the largest eigen vector for each of the $\mathbf{C}_i$ matrices, and then use this matrix to make the first projection. The theory was that since the resulting subspace consists of the individual best solutions for each target, hopefully it would also contain a lot of combined good solutions for the targets together.

The only delicate part in the process was to form the initial projection matrix **P**, from the selected best vectors. Usually this is a pretty straightforward step if the vectors are orthogonal to each other, and our standard expression can be used -

$$\mathbf{P} = \sum_i v_i^{best} v_i^{best\prime}$$, where v_i^{best} are the individual best vectors for each target. However for this case, the individual best vectors for the targets may or may not be orthogonal to each other (in fact typically they are not). Therefore the correct procedure for forming our projection matrix **P**, from a set of non-orthogonal vectors was found from [35] and is given on the next page.

$$\mathbf{P} = \mathbf{U} \times (\mathbf{U'U})^{-1} \times \mathbf{U'}, \text{ where}$$

$$\mathbf{U} = \left[v_1^{best}, v_2^{best}, v_3^{best}, \cdots, v_{n_a}^{best} \right]$$

(7.1)

Like mentioned before v_i^{best} is the best vector for target i, assuming it's the only one present with the clutter. This matrix $\mathbf{P}$ is then used to make the initial projection into this smaller subspace, before the maxi-mins start looking for their best solution. The dimension of the new projected space is equal to the number of targets n_a which is typically less than the original dimension W. Hence there are fewer iterations, and the maxi-mins converge to their solutions quicker. The exact gain in terms of the computation time obviously depends on the number of temporal basis functions, as that is what ultimately decides the transmit signal dimension for a given number of spatial elements.

This approach is obviously suboptimal as it does not consider all the available transmit dimensions; but it still gives us pretty good results and also substantial savings in terms of processing time. The concept is also different from the earlier reduced target algorithms, as here we assign equal importance to all our targets not ignoring some of them completely. Few results for the heuristic and the true fast algorithms, along with the results for the corresponding slower maxi-mins are shown in Figures 7.6 and 7.7 respectively.

Heuristic SCR Convergence Fast

SCR_{min} = 10.74 dB

Searches in a 7 Dimensional space

Heuristic SCR Convergence

SCR_{min} = 11.38 dB

Searches in a 126 Dimensional space

Heuristic Energy Convergence Fast

SCR_{min} = 6.54 dB

Heuristic Energy Convergence

SCR_{min} = -11.44 dB
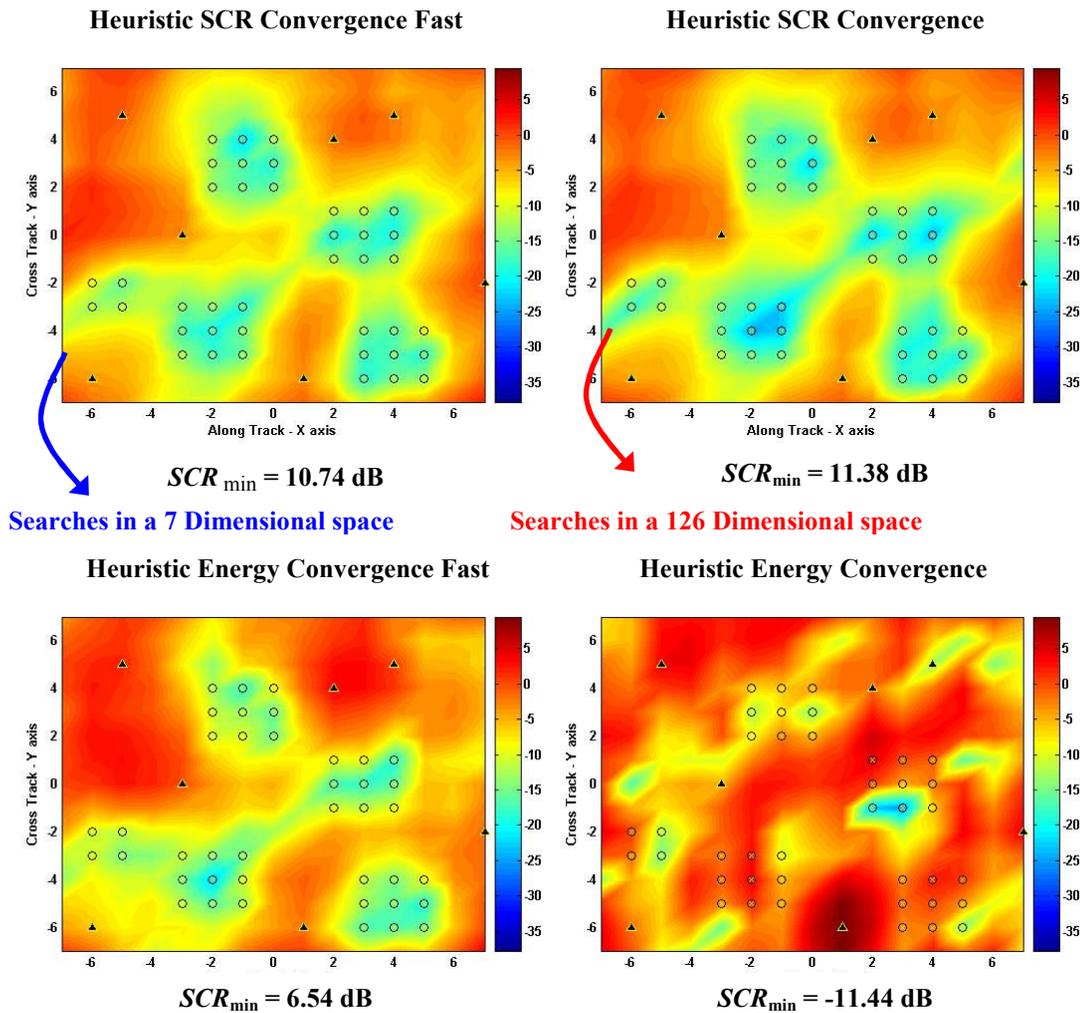
Figure 7:6 The Heuristic "Fast" Algorithms

Note that the fast algorithm performs impressively in both cases. For the SCR convergence it gives a comparable solution to the original "Heuristic SCR", where as for the energy convergence it even betters the original "Heuristic Energy convergence" – that also by a considerable margin of 18 dB. In fact the original "Heuristic Energy" gives an entirely unacceptable solution from a maxi-min point of view, but the faster version even while searching in a smaller subspace is able to

come up with a much superior end result. The results for the true algorithms have been shown next.

Figure 7:7 The True "Fast" Algorithms

Both fast answers are still pretty good. Note that these cases are for 9 time-frequency basis functions and 14 antennas, which again gives a transmit signal dimension of 126. Hence all original maxi-mins have to search for their best solutions in a 126 dimensional subspace. Contrast this for the fast algorithm, which explores only the 7
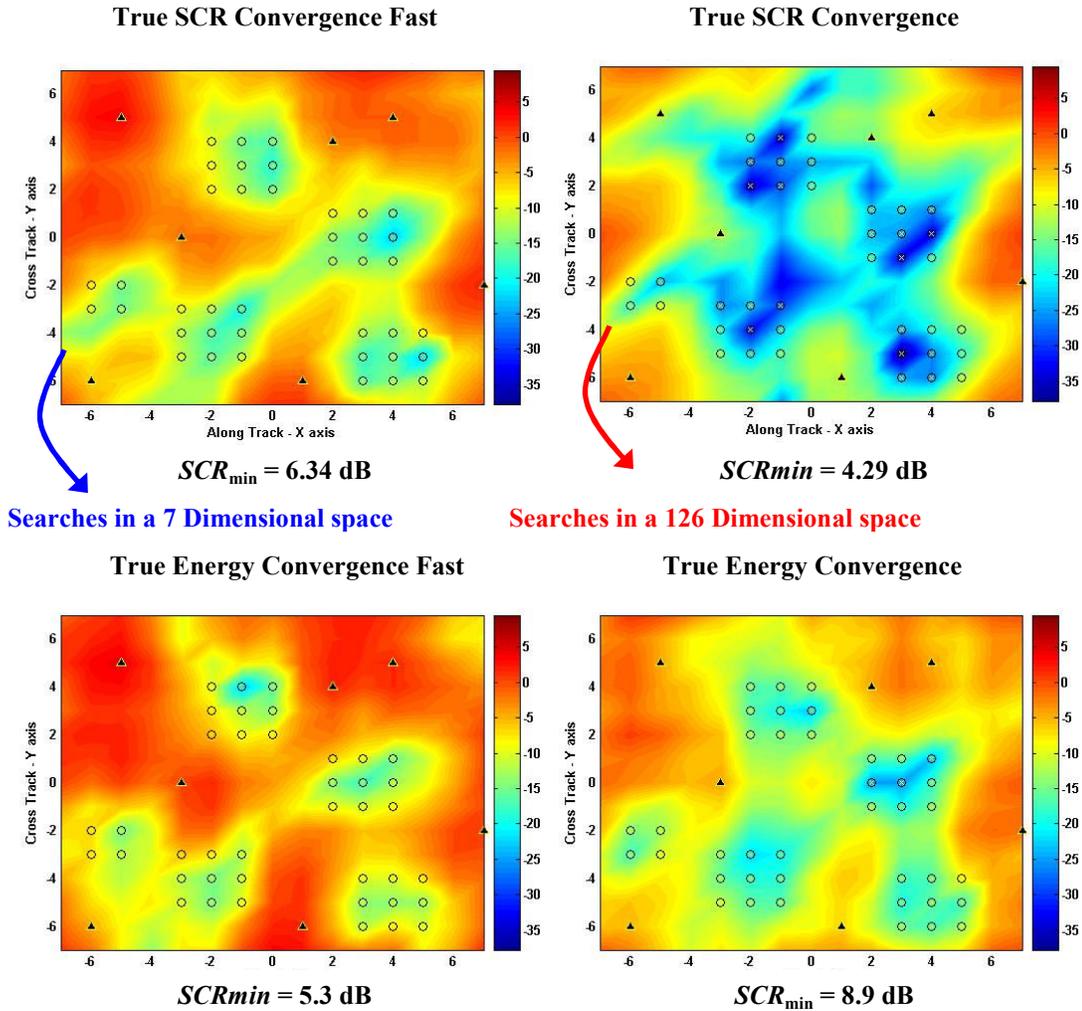
best dimensions associated with each target. Thus the improvements in speed are also phenomenal; the fast algorithms being quicker by a factor of almost 15 in this case. For larger number of basis functions the savings are even more substantial.

Also note that at times the fast algorithm seems to be a completely different algorithm, taking entirely different paths to converge to equally good but dissimilar answers. This is evident by the correlation between some of the final solution vectors (obtained from the original slower maxi-mins), and their component in the initial rich subspace defined by matrix $\mathbf{P}$. For each of the above algorithms this value was computed as $(\mathbf{P}\times\mathbf{S})'\times\mathbf{S}$, where $\mathbf{S}$ is the solution vector obtained from the slower maxi-min. This value comes out to be in the range of 0.02 to 0.6, indicating that many a times only a small component of our final solution lies in the initial subspace. In other words, the final vector obtained from the original maxi-mins can be lying completely out of this space, and it's not that the main algorithms just steer us into this solution rich subspace.

Let's now look at the performance of the three fast algorithms (which were perceived to be the best) for one of the more difficult scenarios. The target and clutter are more closely interspersed and all algorithms have a tough time in coming up with reasonably good answers. These results are shown in Figure 7.8 on the next page.

185

Heuristic SCR Convergence Fast

SCRmin = 1.25 dB

Heuristic SCR Convergence

SCRmin = 1.40dB

True SCR Convergence Fast

SCR_{min} = 0.55 dB

True SCR Convergence

SCRmin = -4.86 dB

True Energy Convergence Fast

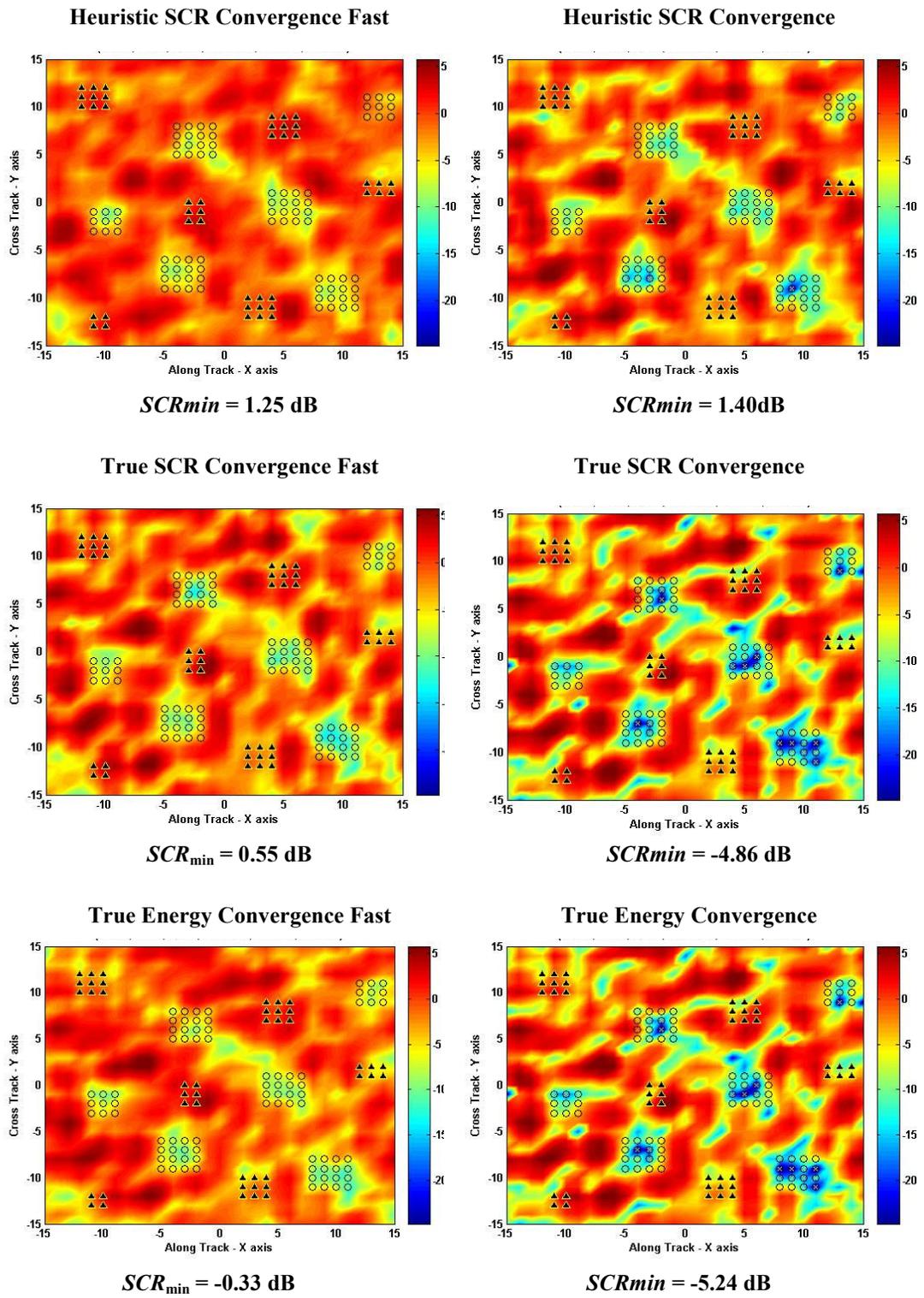SCR_{min} = -0.33 dB

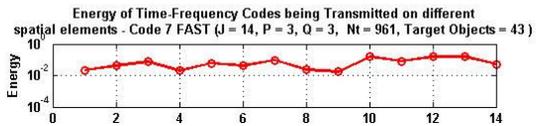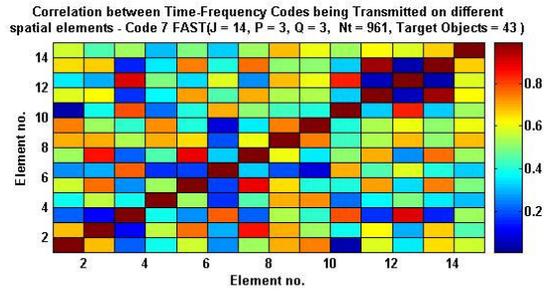**True Energy Convergence**

SCRmin = -5.24 dB

**Figure 7:8 The "Fast" Algorithms – another example**

Once again the fast codes can be seen to perform comparably if not better than the original slower algorithms. But one point which strikes out from this result and also from Figures 7.6 - 7.7 is that most of the fast algorithms can come up with better answers compared to their original slower counterparts, with the exception of only one algorithm - *"Heuristic SCR convergence Fast"*. For all cases tried it could at most come up with nearly as good solutions as the *"Heuristic SCR convergence"*, but never better. The other fast algorithms were also not able to (even once) outperform this champion code, again confirming the truly optimal nature of our champion. Over the course we have seen that any form of suboptimality – stopping with the iteration procedure and guessing in a potentially good space, working on the fewer weaker targets, or even searching in a smaller but qualitatively richer subspace - just seems to make the solution worse for this code. However the same techniques on occasions result in better solutions for the other maxi-mins. This behavior yet again confirms what we have already concluded, and makes us reiterate once more what we have stated many times before – *The "Heuristic SCR convergence" is our most optimal code and the unrivalled champion amongst maxi-mins, period!*

The correlation matrix plots for the above fast codes have been shown in Figure 7.9. As was expected, it turns out that all these codes are true space-time codes with fairly uncorrelated temporal signals on the different transmit elements. This once again entails that achieving desirable patterns for the maxi-min criteria, calls for the utilization of additional degrees of freedom available only with the non-separable space-time codes.

Heuristic SCR Convergence Fast

True SCR Convergence Fast
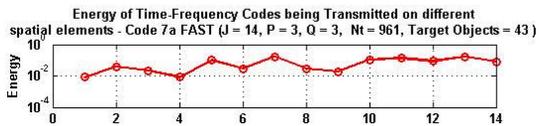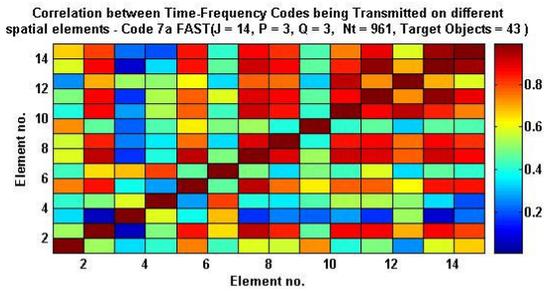
True Energy Convergence Fast
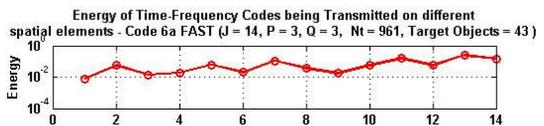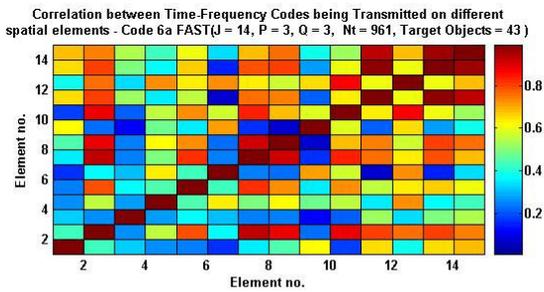
Figure 7:9 Correlation Matrix Plots – "Fast" Codes

The true non-separable nature of these codes, and their ability to produce effective results motivated us to delve a little more. Some questions that popped to mind were regarding the actual "richness" of the initial rich subspace. Is this subspace so abundant that any and every vector here would make a good solution? Do we even need our algorithms? What happens if we just select a vector at random in this initial space, does it make an acceptable solution? To find an answer to these questions, we did exactly the same thing, i.e. selected two vectors at random in this subspace and plotted the resulting illumination patterns. These patterns have been shown in Figure 7.10.

Random Code 1　　　　　　　　　　　　　　**Random Code 2**

SCR_{min} = -3 dB　　　　　　　　　　　　$SCRmin$ = -5.4 dB
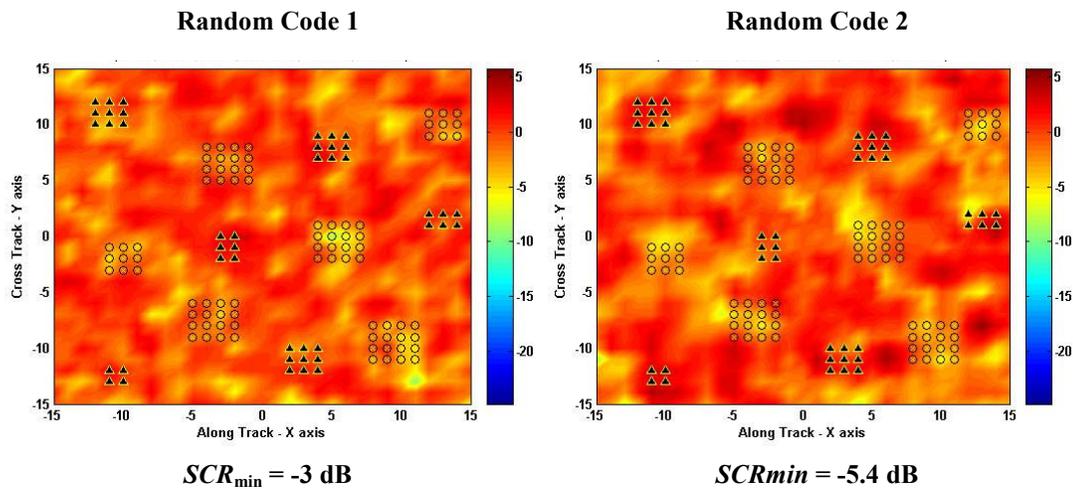
Figure 7:10 2 Random Codes in the initial projected subspace

As can be seen none of the codes give us an extraordinary result. Numerically the answers may not look that bad, but it's clear that no attempt has been made to maximize the SCR_{min}. The only reason they 'kind of' work, is probably because of the makeup of this algorithm. The projection into the initial subspace necessitates putting energy on all the targets and therefore we don't get any real orphans.

However most of the clutter objects also collect energy in the bargain, and the solution is a lot worse from just an average or total SCR point of view. Anyway, this small test allays our fears and proves that the algorithms are very much necessary to come up with the best solutions. Projecting into an initial rich subspace may narrow down the field for us, but we still need the maxi-mins to dig out the best answer.

This almost brings us to the end of this discussion on the fast algorithms, though one last point still needs to be mentioned regarding their potential applications. Although not optimal or guaranteed to give the best solution, these algorithms do give us pretty satisfactory answers and that too very quickly; therefore they visibly find relevance in huge time intensive scenarios. But another possible use is in applications which do not require the full radar timewidth and/or bandwidth - like the MTI.

Recall our $\mathbf{F}$ matrix from the chapter on radar models (2.61). This matrix is placed in front of the actual target matrix $\mathbf{H}_t$ and results in a new propagation matrix $\mathbf{H}'_t$ (for each target). As described before the matrix $\mathbf{F}$ actually contains the full space-time attributes of our transmit signal, and essentially projects us into a wide timewidth-wide bandwidth subspace. This wide timewidth and bandwidth enables us to have good resolution, which is critical for many radar applications like the wide area SAR. But there are also applications like the MTI which do not necessitate this constraint on the time and bandwidth of the radar, i.e. the moving targets are presumed to be sufficiently separated and hence do not need as fine a resolution to be discriminated. Thus observing over the full time and bandwidth may just mean an

additional computational load for these problems. In addition, restricting ourselves to this wide timewidth-wide bandwidth subspace (which is not required), may also diminish our chances of coming up the best possible code for such applications.

One interesting proposition that comes out of this effort on fast codes, is to replace our initial wide timewidth-wide bandwidth projection with the fast projection – i.e. pull out the $\mathbf{F}$ matrix from the target matrix computation, use the original $\mathbf{H}_t$'s instead of the $\mathbf{H}'_t$'s, and then employ the fast algorithms on this set of data. Basically with this concept we are saying that out of all the possible solutions, we prefer the ones which do the job better (like put energy only on the moving targets while nulling out the clutter), and not the ones which necessarily have a larger time and bandwidth (or give us better resolution). This appears to be an interesting idea, but could not be followed up due to the lack of time. However it can be included as one of the future goals and may result in exciting finds at a later stage.

With this, we finally arrive at the end of this section. Some other work was actually attempted for the MTI although it wasn't very successful. The MTI effort and another ambitious idea of generating a space-time *"target decorrelating code"* have been described next.

7.4 More ambitious ideas – Decorrelating Code and the MTI

This section describes two of the relatively grander ideas which were attempted, but were not entirely successful. The intent is just to make the reader aware of their presence and also provide some possible pointers towards future work.
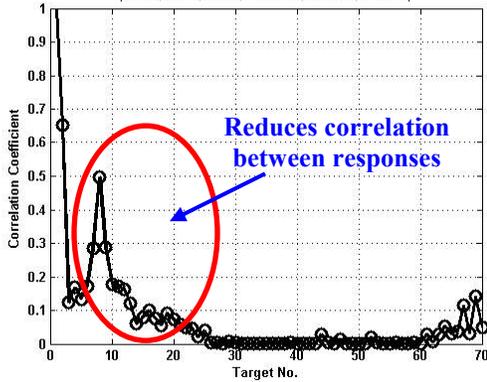
7.4.1 The Decorrelating Code

Since the maxi-min had been seen to have a potential for improving target resolution (by virtue of its true space-time nature), an attempt was made to exploit this aspect a little further. We decided to try out a *"target decorrelating"* algorithm which was aimed at minimizing the correlation between any two target responses, in addition to performing the standard maxi-min operation i.e. maximize the minimum SCR for all targets. The idea used was to regard even the other targets as clutter when considering the best solutions for a particular target individually, i.e. while computing the $\mathbf{C}_i$ matrix for one target the $\mathbf{B}$ matrix was formed using the $\mathbf{H}_i$ matrices of all the clutter objects, as well as the remaining targets. The maxi-min algorithm like the *"Heuristic SCR convergence"* was then executed normally on these matrices. Thus with this idea we hoped to get an overall best code, - a solution which would give us a reasonably good SCR_{min} (illumination optimization), along with a fairly less correlation value between the various target responses (ambiguity optimization).

The approach did seem to work for the initial cases that were tried (at least in terms of reducing the correlation), but it also sacrificed the illuminated energy on our targets and thus the solutions were not satisfactory from an illumination optimization point of view. Some of these energy and correlation results have been shown in Figures 7.11. Note that this is the same case where the maxi-min code - *"Heuristic SCR convergence"* gave us a reduction in the ambiguity function main lobe width. The *"target decorrelating code"* does not give us as much of a reduction, but it

significantly reduces the correlation between the primary response (of 'target 1') and

the other target responses.

**Correlation coefficient between response
of Target 1 and other Targets**

Target Decorrelating Code
(Based on Heuristic SCR
Convergence)
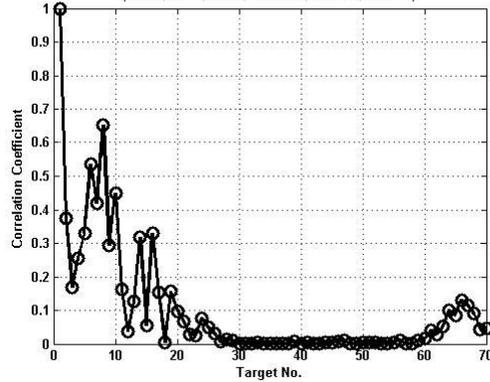
Heuristic SCR Convergence

Target Decorrelating Code
(Based on Heuristic SCR
Convergence)
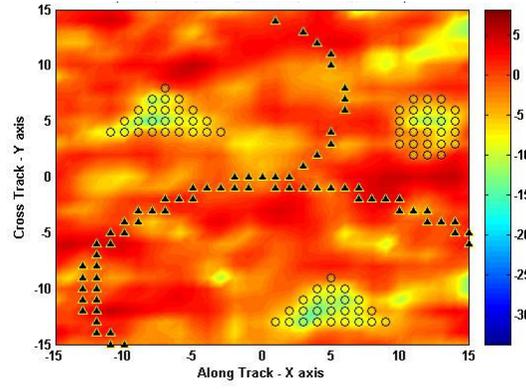
Heuristic SCR Convergence

Figure 7:11 Correlation and energy results for the new "Target Decorrelating Code"

193

Note that the only other target - 'target 8' besides 'target 2' with a high correlation value in Figure 7.11, is just separated by one resolution cell in along track form 'target 1' and is hence non-resolvable for our case (one way propagation from the transmitter to targets). Apart from that, the new decorrelating code performs quite well in terms of reduc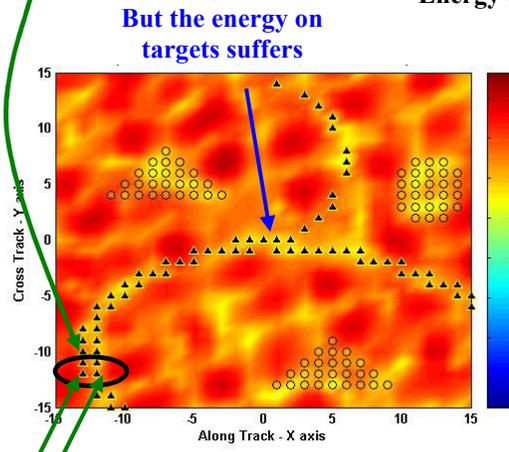ing the correlation between the target responses. However this solution can still not be called a good solution as it totally ignores the other important characteristic of a good transmit signal – improving the worst and average SCR for the targets. Notice that in this case the targets get almost the same energy as the clutter objects, and therefore we get a poor result in terms of both the worst as well as the average SCR. The reason for this behavior can perhaps be found in the design of the code. Since each target gets considered as clutter in turn by each other target, most likely the overall effect is to attribute these targets as clutter (for the sake of putting energy) and thus diminishing the resulting energy on all of them. Moreover for some of other cases, this code performed just as well as the original max-min even in terms of the correlation (and still worse in energy) making it an unimpressive candidate for our choice of transmit signal. The results for these cases are shown in Figures 7.12 – 7.13.

Energy on the Targets

Maximum Energy
(Spatial)

Maxi-min based on only the
targets

Target Decorrelating Code
(based on Heuristic SCR
Convergence)
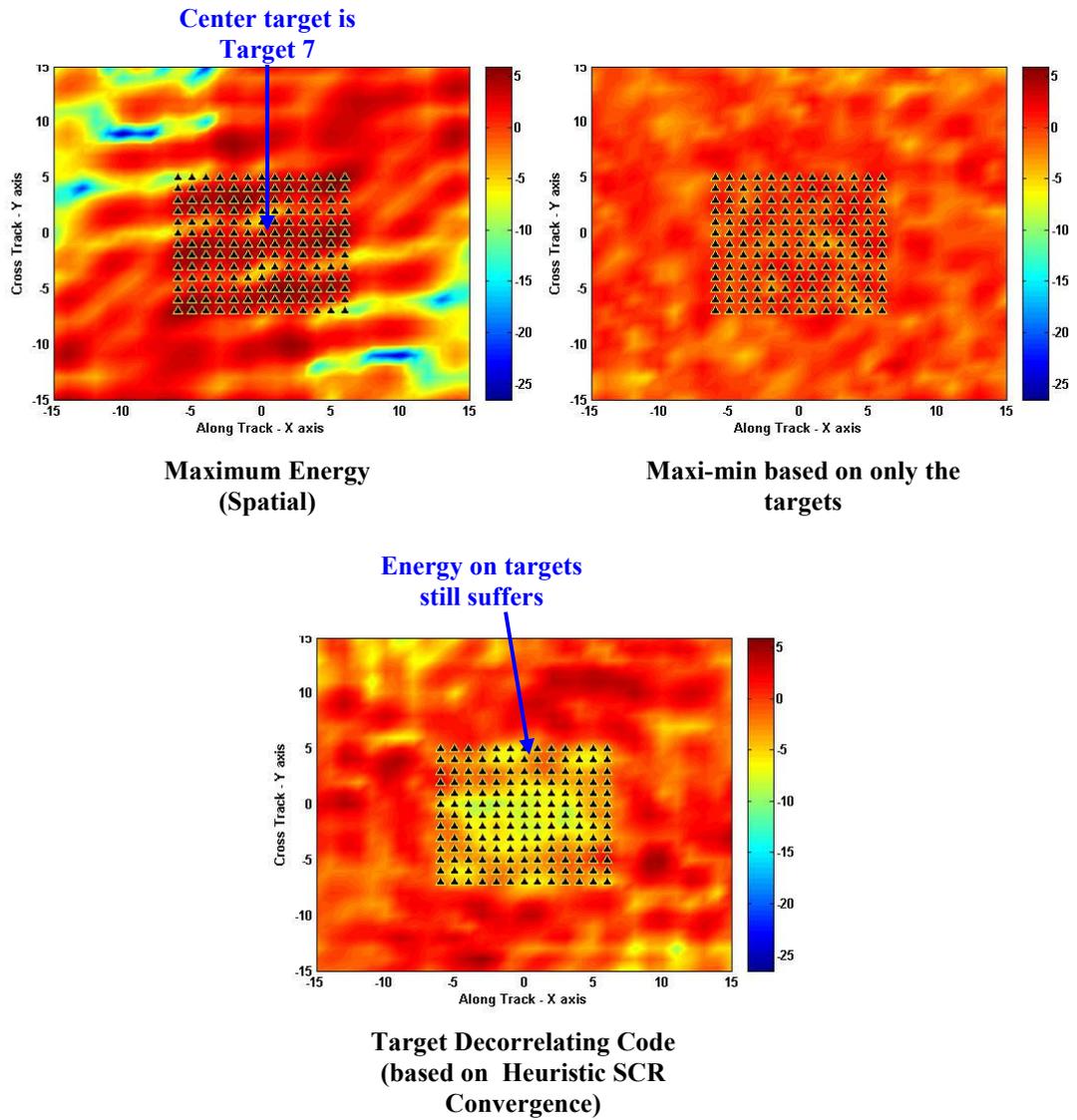
Figure 7:12 Illumination pattern for the new "Target Decorrelating Code" – another example

Since this is in all target case the maxi-min based on the target objects has been used. The correlation between the response at target 7 (the centermost target of the grid), and at the other targets in the along track direction has been shown in the next figure for all the three codes. We can perceive the reduction in the main lobe

width (even for the new code as compared to the spatial code), but no significant advantage can be seen in terms of reducing the correlation with the other targets vis-à-vis the original maxi-min.

Correlation coefficient between response of Target 7 and other Targets in Along Track

Maximum Energy (Spatial)

Maxi-min based on only the targets

Reduction in the main lobe width

and otherwise also very similar to the original maxi-min

Target Decorrelating Code (based on Heuristic SCR Convergence)
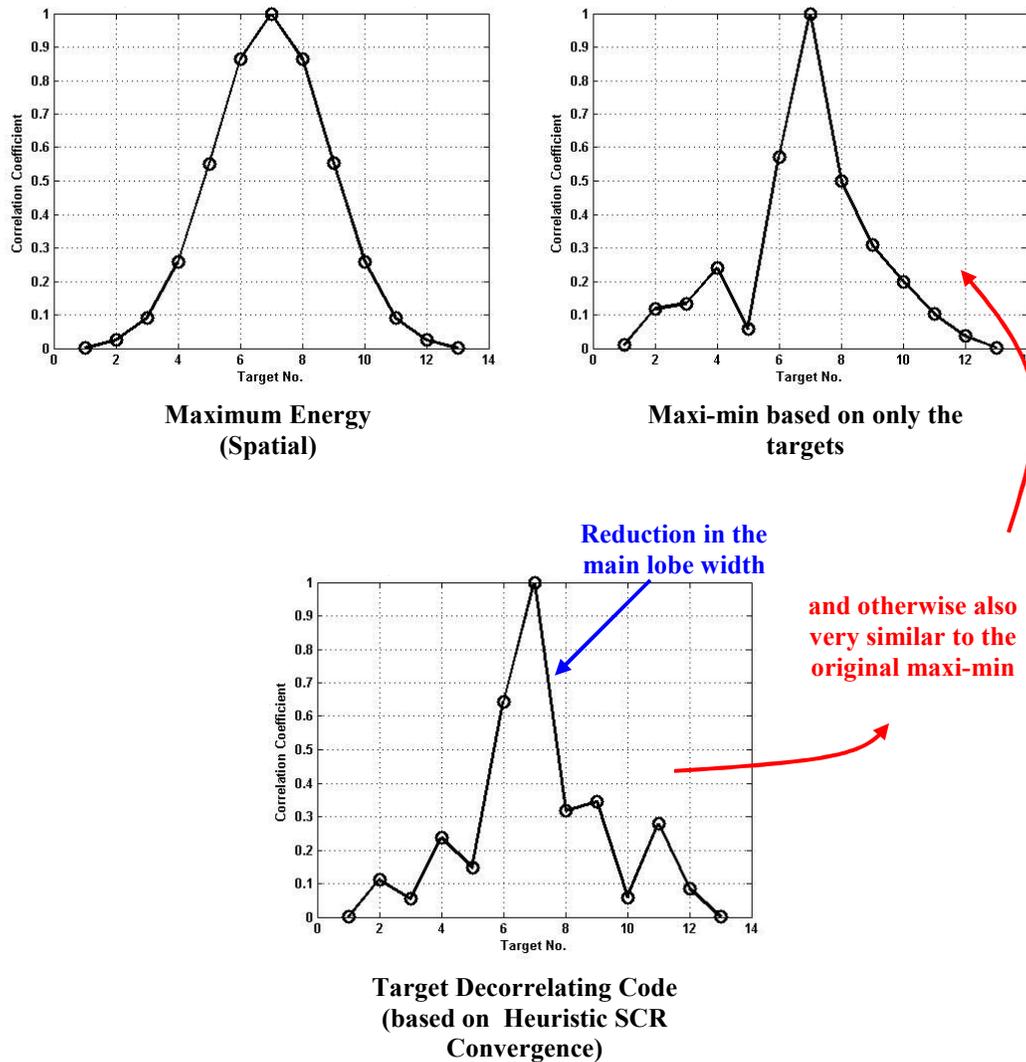
Figure 7:13 Correlation results for the new "Target Decorrelating Code" – another example

Thus most of the times the *"target decorrelating code"* just gives us similar correlation results along with worse energy distributions; and thus in its current form does not seem to be of any great utility. But the results shown here and also in Chapter 6, indicate that space-time codes if constructed intelligently do have the potential to reduce the cross-correlation between dissimilar target responses. Some work has been done independently on this problem of ambiguity optimization [8], but a real challenge is to combine both the criteria of *"illumination"* and *"ambiguity"* optimizations and come up with the most ideal codes for SAR applications.

7.4.2 The MTI problem

As a matter of fact, there's not much to report about this problem. This was the last trial that was conducted and completely implausible results were obtained. Once again we could not investigate into the problem further due to shortage of time, but it would still be a good idea to share the underlying concepts with the readers.

After the reasonable success of our maxi-mins, we wanted to find out whether the same theory can be extended to the moving target case - i.e. equal energy is distributed on the mobile targets while the stationary clutter is nulled out simultaneously. Thus instead of discriminating the targets in space, we now wished to resolve them in the dimension of their radial velocity. In the absolute sense, the idea can even be extended to resolving moving targets and stationery clutter objects that are co-located in physical space. It's because even though the objects may occupy the same point in the 3-D physical space, in the 4-D target space also involving the radial velocity they will be at different locations.

Our aim is to illuminate the different regions of this 4-D space depending upon our definitions of target and clutter (e.g. for MTI the moving objects become targets and hence we would like to throw energy on the non-zero velocity portion of this total space). What it actually means is that the radar has to track the moving target as it moves from one stationary resolution cell to another, and change the energy distribution pattern accordingly. However based on our results it appears as if that the present radar model is not capable for handling such cases yet; and necessary modifications will need to be made before this case can actually be experimented. Some of the incredible outcomes that resulted on attempting the MTI problem have been shown in Figures 7.14 – 7.15. Note that for each of these cases the illumination pattern has been shown as a function of one dimension of space (along track) and other of radial velocity.
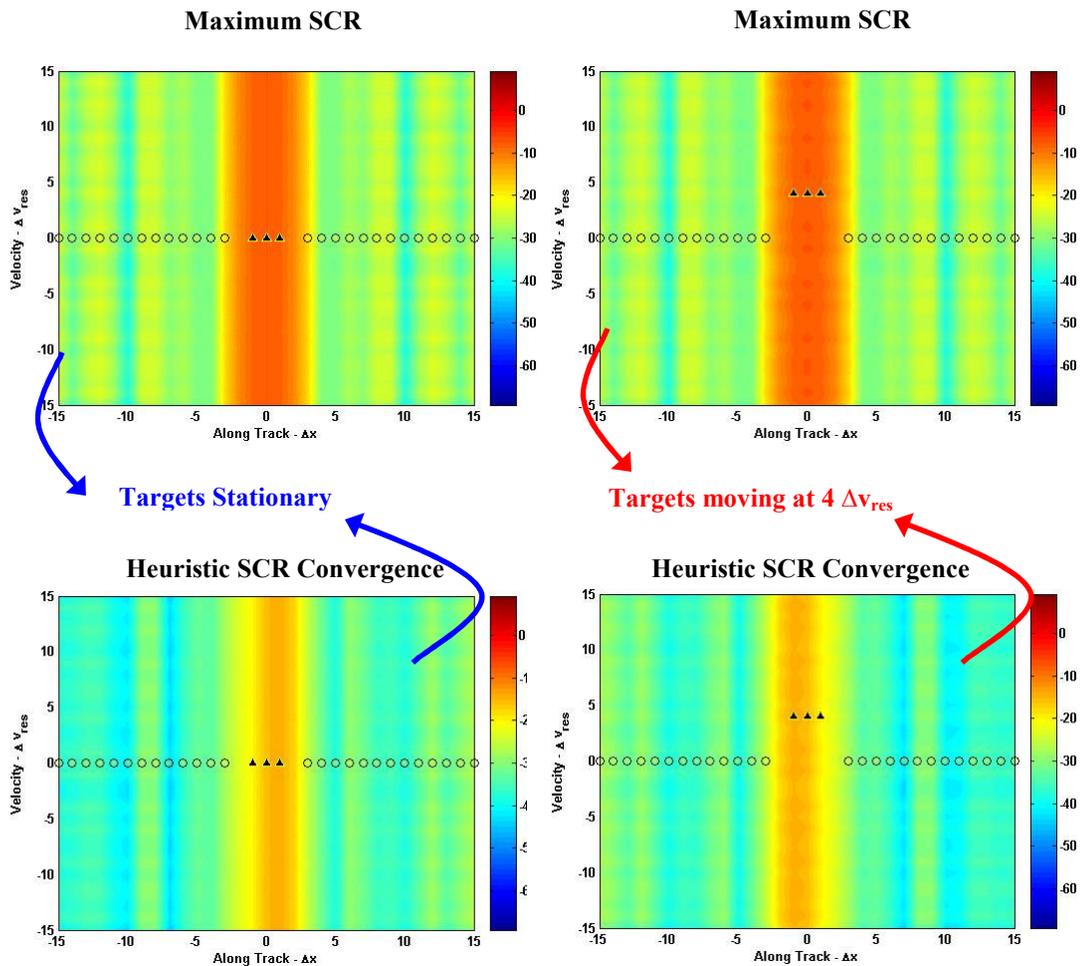
Figure 7:14 MTI problem for range bin one resolution cell away from the center

As can be seen from the caption here, all targets in this case belong to a range bin one resolution cell apart from the center of the illumination area. These patterns indicate that the radial velocity does not produce any effect on the resulting illumination pattern, i.e. the resulting illuminated energy cannot (or only very slightly) change as a function of velocity. Or once more in other words, the targets cannot be separated on the basis of their velocities at all. But before drawing any conclusions here, let's look at another case where all the stationary and moving

targets are from the range bin exactly at the center of the illumination area. These results have been shown in Figure 7.15.

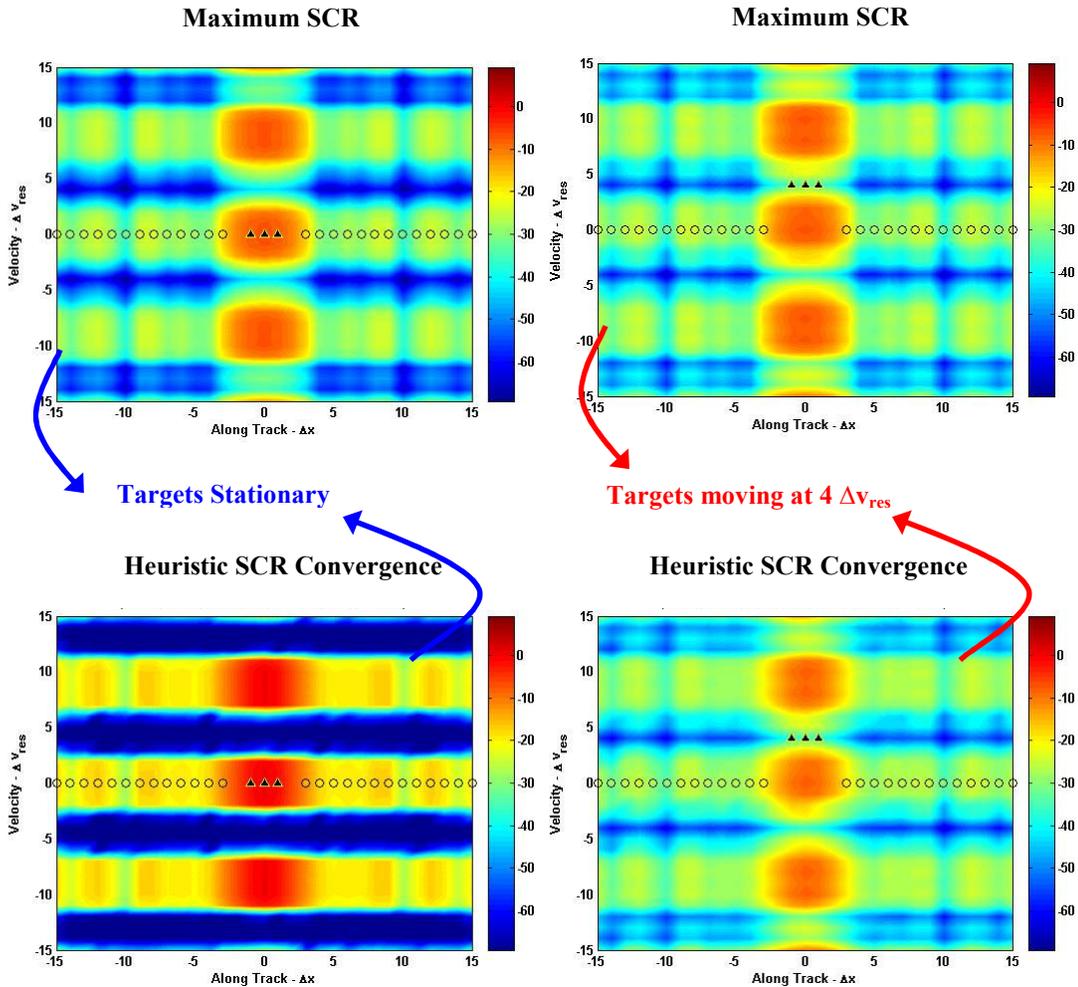**Figure 7:15 MTI problem for range bin exactly at the center**

These results are totally contradictory and thus suggest the reverse of what have seen before. In fact we see a heavy dependence of the illumination energy on the radial velocity, but this energy is kind of independent of the location of the targets themselves. As can been seen, the location of targets is moved from the zero velocity

bin to $4\Delta_{\mathbf{vres}}$ ($\Delta_{\mathbf{vres}}$ being the minimum resolvable velocity of the radar based on the signal timewidth) but the nulls and peaks in the illumination pattern change only in intensity, and not in location. More simply, the illumination pattern is rather constant in the dimension of the radial velocity (and doesn't seem to depend on the location of targets or clutter objects at all). This result does not make much sense either. Moreover this behavior was observed only for the range bin at the center of the illuminated area; for all other bins the conflicting illumination pattern of Figure 7.14 was obtained. Both these unusual results point to a definite shortcoming in the radar model with respect to the non-stationary target case; and the model needs to be rectified first before it can handle the MTI. Thus at this stage, drawing any conclusions regarding the applicability of our algorithms to the MTI problem would just be presumptuous. The field is still wide open and will potentially make an exciting study for future endeavors.

This brings us to the end of this penultimate chapter on the final trials and experiments. In here, we got to see a few more variations of our algorithms and were also able to appreciate some of the other potential applications of space-time codes. Besides these, several other algorithms were tried, like the maxi-min for the minimum target energy and even a mini-max for the maximum clutter energy. But these methods do not present anything strikingly noteworthy, and have thus been left out of this discussion. Thus we finally finish with all the work that was done on space-time codes for radars. A brief summary of the vital points, along with possible opportunities for future research have been presented in the last chapter.

Chapter 8

Conclusions and Future Work

8.1 Summary

In this research, a structure for determining *optimal space-time transmit codes* for a high altitude multi-aperture SAR has been presented. The codes are optimized with respect to the various *illumination optimization* criteria, and their performance has been evaluated for a number of different scenarios. Special attributes of these codes which make them different and more effectual than conventional radar solutions, along with some of their unique abilities have also been highlighted.

Toward this goal of developing optimal space-time codes, a space-time radar model was developed that accurately represent a multi-aperture radar system. The propagation from the radar to the targets is modeled fairly accurately, and provisions are also made to incorporate any complex target geometry - consisting of a combination of stationary, moving, airborne, point or distributed targets. A transmit signal model is then introduced which enables writing an arbitrary space-time transmit signal as a combination of wide timewidth, wide bandwidth orthonormal basis functions, that span the full spatial extent of the transmit array. Since the weights of these basis functions completely specify the transmit signal, the problem of determining the optimal signal is now simply reduced to finding the optimal set of weights for these basis functions – i.e. a vector. The two models are also represented

in terms of vector-matrix notations, and hence the complete arrangement allows for the use of linear algebraic techniques to solve the problem.

As the perfect radar transmit signal cannot exist (for most problems), a set of optimization criteria are defined with respect to "*illumination optimization*" principle, and solutions are found which satisfy these criteria to the greatest possible extent. However it's found that the criteria which are most easy to satisfy – like maximizing the overall illumination energy on the targets, minimizing the overall illumination energy on clutter, or even maximizing the ratio of the two (signal to clutter or SCR), do not make for very good radar solutions. In trying to optimize their overall respective criterion, these solutions neglect some of the individual targets completely. Since all targets are equally important for a radar, the total loss of some targets in return of increased accuracy for the others does not present an acceptable proposition. These solutions are inadequate for most radar scenarios, and therefore there's a need to come up with more appropriate optimization criteria.

The alternate mini-max or maxi-min algorithm is thus developed, which aims at maximizing the minimum or the worst SCR – (SCR_{min}) for any of the targets. However solutions to these more advanced criteria are not as straightforward, and there's no way by which the solution resulting in the best possible SCR_{min} can be directly determined. Contrarily, since finding the worst solutions are easy, an iterative procedure is developed which increases the lower bound on the SCR_{min} by throwing out the worst solutions from a finite dimensional transmit signal search space. With each projection this lower bound is raised, and results are presented which show that

we converge to pretty decent solutions at the end. The heart of all our algorithms is eigen analysis, which can be directly be used in conjunction with our vector-matrix models defined earlier. Based on the way we form our matrices and define our vector spaces, four versions of the maxi-min algorithm are developed. Although all four are intended for the same purpose, we find that each performs differently and one particular algorithm of the four is most often the best of the lot.

Therefore, based on the many test cases tried we converge to our champion code or champion algorithm, which we call the "*Heuristic SCR convergence*" owing to it's inherent design. The algorithm is seen to give significantly better solutions compared to the basic or standard criteria mentioned earlier; several results to support the claim have been included. Some extra analysis is also performed to understand the true behavior and/or the functioning of the maxi-mins, which once again confirms the supremacy and optimality of our champion algorithm out of the four possible methods. However the one limitation of our algorithm is the amount of processing time it takes. Several remedial measures are tried for this problem, and have also been included in the later chapters.

Towards the end, the form of the transmit signal and also the signals incident on the targets is investigated. This is probably the most interesting discovery in the whole study as we find that for producing the desirable max-min illumination solutions, the transmit signal has to take a non-separable form at the transmitter – i.e. dissimilar and uncorrelated temporal signals on each of the individual transmit elements. This attribute is completely different for the standard code solutions which

resemble the conventional phased array systems, i.e. the same temporal signal propagates on each antenna with an additional complex weighting on top – the idea of spatial beamforming or separable space-time transmit signals. Such space-time signals also result in dissimilar time-frequency spectrums on the different targets, which can have significant implications of its own - in terms of the target response correlation and the main lobe width of the radar ambiguity function. Since the incident responses at different targets are not related by a simple translation in phase shift anymore, the targets give the impression of receiving energy from independent time-frequency transmitters, and hence the potential for decorrelating these targets is improved considerably.

Finally few techniques like *operations in subspaces orthogonal to clutter* and the *fast codes* are described, which aid/can aid the regular algorithms under special circumstances. A small introduction to some of the really big ideas - like the use of true space-time codes for augmenting MTI performance, and reducing the cross-correlation between target responses for improving detection/estimation abilities has also been provided.

8.2 Future Work

The first and foremost point that needs to be accorded top priority, is improving the computational efficiency of our algorithms. Although interesting results have been observed, and the workability of our algorithms has been established beyond doubt, 31×31 grid sizes (or ≈ 1000 targets) do not make for very

impressive real life scenarios. To appreciate the actual might of these algorithms (for practical situations), we need to run bigger simulations with larger grid sizes – 63×63, 127×127 or even 255×255. Also, since it has been observed that the effectiveness of the maxi-mins greatly improves with more space-time dimensions, we would like to run some cases for even larger number of basis functions - assess the resulting effects on the algorithm performance, and thus extend the plots of Figures 4.16-4.19 beyond 25 and 49 basis functions. For this purpose we again need to improve the algorithmic efficiency, which calls for some restructuring and even modification of the software.

One application which naturally follows from whatever work has been done up till now, is extending the process to the adaptive case. In this idea of *adaptive space-time illumination optimization*, the radar continuously adapts to the target scenario below - i.e. it keeps modifying the transmit signal to best suit the requirements based on the information collected. The idea is more akin to optimal code selection (out of a finite set of codes) rather than optimal code generation in real time, but the increased numbers of available transmit signal options, still paint a better picture then transmitting the same radar signal over and over again. The work on this idea of *information theoretic selection criteria* has already been started by my colleague, Mr. Ambika Nanda under the direction of Dr. James Stiles, and it would be interesting to see how productive the idea actually turns out to be.

Multi-mode operation is one other possibility of multi-aperture radar systems which can be more fruitfully realized using true space-time codes. The multi-aperture

sensor collects independent information across time, frequency and space (due to the spatial extent of array), and is thus better suited for a range of radar applications like wide area SAR (needs large time-width and band-width for fine resolution) or GMTI and AMTI (require wide array extent for high angular resolution). Thus a state can be visualized in which parts of the time and bandwidth is allocated to regions where we wish to detect moving targets (MTI/ AMTI), and most of the remaining resources are allocated to other areas for which we are doing a fine resolution SAR (generating SAR maps) *–in other words, a hybrid or true multi-mode operation with different radar modes across different spatial locations*. Along with suitable definitions for targets and clutter, the application of our algorithms to such applications can result in some potentially exciting work

As already pointed out, applications like GMTI with stationary objects as clutter and moving ones as targets can also be endeavored. It's known that moving targets can be separated from ground clutter in terms of correlation (owing to the doppler associated with such targets); whether the same can be done in energy using space-time codes, would be something interesting to find out. Moreover since our model includes provisions for specifying targets in all the three dimensions of space, besides one of radial velocity, the algorithms can even be extended to the AMTI. The definitions obviously have to be suitably modified – now regard airborne moving objects as targets, and surface objects as clutter.

The potential of space-time codes with regard to reducing the correlation between target responses has also been touched upon in this research. Although it has

not been entirely validated, results are shown that indicate the existence of a possibility. A real challenge however remains to combine this aspect of space-time codes (ambiguity optimization), with the initiative undertaken in this thesis (illumination optimization) and come up with the most ideal radar transmit signals.

Finally the algorithm performance can be also be evaluated for other kinds of basis functions (which may have the potential for further improving the results), and also different spatial array arrangements. Almost all our simulations were conducted for a single 14 element sparse array, and it would be interesting to note the algorithm performance dependence on the actual spatial array design.

8.3 Conclusions

It is found that for exploiting the true potential of a multi-aperture system, a dissimilar temporal signal needs to propagate on the different spatial elements - else the answers essentially turn out to be spatial beamforming solutions, and the form of the time-frequency signal on each spatial element becomes immaterial. Such true space-time signals were successfully constructed for the illumination optimization criteria using a union of two vector-matrix radar models and linear algebraic techniques, and have been seen to considerably improve the multi-aperture radar system performance. Although the concept of multi-aperture arrays was originally incepted keeping space-borne platforms in mind, their use as such is not limited to only these high-altitude systems.

In addition to the evident advantage of producing more appropriate illumination patterns, space-time signals have shown tremendous promise with respect to the other radar applications as well. Since the incident time-frequency spectrum at each target is now a coherent summation of the dissimilar temporal signals of each individual transmit element, it is found to be different for different target locations, and can therefore open up a whole new array of possibilities for many radar applications. In the future, space-time codes which distribute energy suitably across time and frequency at different target locations can possibly be constructed, so as to satisfy the various criteria regarding the illumination and resolution requirements of radar, and also its multi-mode operation.

REFERENCES

[1] Fawwaz T. Ulaby, Richard K. Moore, Adrian K. Fung, "Microwave Remote Sensing – Active and Passive", Vol. 2, Artech House, Inc., 1986

[2] T. J. Nohara, P. Weber, and A. Premji, "Space-based radar signal processing baselines for air, land and sea applications", *Electronics & Communication Engineering Journal,* vol. 12, no. 5, pp. 229-239, Oct., 2000.'

[3] M. E. Davis, "Technology challenges in affordable space based radar," *Proc. IEEE 2000 Int. Radar Conf.*, Washington DC, pp. 18-23.

[4] Nathan Goodman, "SAR and MTI processing of sparse satellite clusters", Doctoral Dissertation, The University of Kansas, July 2002

[5] Nathan A. Goodman, Sih Chung Lin, Devindran RajaKrishna, J.M. Stiles, "Processing of Multiple-Receiver Spaceborne Arrays for Wide-Area SAR", *IEEE Transactions on Geoscience and Remote Sensing*, Vol.40, No.4, April 2002.

[6] D. Massonnet, "Capabilities and Limitations of the Interferometric Cartwheel", *IEEE Transactions on Geoscience and Remote Sensing*, Vol.39, No.3, March 2001, pp.506-520

[7] Air Force Research Laboratories, "TECHSAT 21 – FACT SHEET" Available: http://www.vs.afrl.af.mil/Factsheets/techsat21.html

[8] Atulya Teja Deekonda, "Optimal Space-Time Transmit Signal Design for Multi-Static Radar", Masters Thesis, The University of Kansas, January 2005

[9] J. Stiles, N.A. Goodman, "Wide Area, Fine Resolution SAR from Multi-Aperture Radar Arrays", *Proc. of the 2003 Advanced SAR Workshop; Montreal, Canada, June 2003.*

[10] E.J. Bond, X. Li, S.C. Hagness, B.D.V. Veen, "Microwave Imaging via Space-Time Beamforming for Early Detection of Breast Cancer", *IEEE Transactions on Antennas and Propagation,* Vol. 51, Issue. 8, August 2003, pp. 1690-1705

[11] S.W. Golomb, H. Taylor, "Constructions and Properties of Costas Arrays", *Proceedings of the IEEE*, Vol. 72, No. 9, September 1984, pp. 1143-1163.

[12] J.P.Costas, "A Study of a Class Detection Waveforms Having nearly Ideal Range-Doppler Ambiguity Properties", *Proceedings of the IEEE*, Vol. 72, 1984, pp. 996-1009.

[13] C.F. Chang, M.R. Bell, "Frequency Coded Waveforms for Enhanced Delay-Doppler Resolution", *IEEE Transactions on Information Theory*, Vol. 49, Issue 11, November 2003, pp. 2960-2971.

[14] Chen Xiao Hua, Oksman J., "A new algorithm to optimize Barker code sidelobe suppression filters", *IEEE Transactions Aerospace and Electronic Systems,* Vol. 26, Issue 4, July 1990 pp. 673 – 677

[15] Chi-Chang Wang, "An extended Frank Code and New technique for implementing P3 and P4 codes", *Proceedings of IEEE Transactions on Aerospace and Electronic Systems,* Vol. 25, No. 4, July 1989.

[16] Rajeswari, K.R.; Gangatharan, N.; Morris, G.E.; Rao, G.S.V.R.; Kumari, M.U.; Swamy, G.N.; "Sidelobe reduction techniques for range-resolution radar", *The 8th International Conference on Communication Systems, 2002*, Vol. 2, 25-28 Nov. 2002, pp. 784 – 789.

[17] Pillai, S.U.; Oh, H.S.; Youla, D.C.; Guerci, J.R.; "Optimal transmit-receiver design in the presence of signal-dependent interference and channel noise", *IEEE Transactions on Information Theory*, Volume 46, Issue 2, March 2000 Page(s):577 - 584

[18] Bergin, J.S.; Techau, P.M.; Don Carlos, J.E.; Guerci, J.R.; "Radar waveform optimization for colored noise mitigation", *IEEE International Radar Conference, 2005*, 9-12 May 2005 Page(s):149 – 154

[19] Garren, D.A.; Osborn, M.K.; Odom, A.C.; Goldstein, J.S.; Pillai, S.U.; Guerci, J.R.; "Enhanced target detection and identification via optimised radar transmission pulse shape ", *IEEE Proceedings - Radar, Sonar and Navigation,* Volume 148, Issue 3, June 2001 Page(s):130 – 138

[20]   Gamal, H.E.; Hammons, A.R., Jr.; "On the design of algebraic space-time codes for MIMO block-fading channels", *IEEE Transactions on Information Theory*, Volume 49, Issue 1, Jan. 2003 Page(s):151 – 163

[21]   Gamal, H.E.; Harnmons, A.R., Jr.; " On the design and performance of algebraic space-time codes for BPSK and QPSK modulation", *IEEE Transactions on Communications*, Volume 50, Issue 6, June 2002 Page(s):907 – 913

[22]   Tarokh, V.; Naguib, A.; Seshadri, N.; Calderbank, A.R.; "Space-time codes for high data rate wireless communication: performance criteria in the presence of channel estimation errors, mobility, and multiple paths", *IEEE Transactions on Communications*, Volume 47, Issue 2, Feb. 1999 Page(s):199 – 207

[23]   El Gamal, H.; "Towards robust space-time coding", *IEEE International Symposium on Information Theory*, 2002. Proceedings. 2002, Page(s):219

[24]   Chen Sun; Karmakar, N.C.; Khoon Seong Lim; Aigang Feng; "Combining beamforming with Alamouti scheme for multiuser MIMO communications", *IEEE 60th Vehicular Technology Conference, 2004*. VTC2004-Fall. 2004, Volume 2, 26-29 Sept. 2004 Page(s):1415 – 1419

[25]   Sethuraman, B.A.; Rajan, B.S.; "An algebraic description of orthogonal designs and the uniqueness of the Alamouti code", *IEEE Global Telecommunications Conference, 2002*. GLOBECOM '02, Volume 2, 17-21 Nov. 2002 Page(s):1088 – 1092

[26]   CDMA development group (CDG), CDMA Technology – Smart Antennas Available: www.cdg.org/technology/cdma_technology/smart_antennas/

[27]   International Engineering Consortium (IEC) – Smart Antenna Systems Tutorial. Available: http://www.iec.org/online/tutorials/smart_ant/

[28]   Metawave, Seminar on - "The evolution of Smart Antennas to 3G", available: http://www.cdg.org/news/events/CDMASeminar/cdg_tech_forum_02/5_metawave_cdg_technology_forum_10-1-02.pdf

[29] S. Barbarossa, G. Levrini, "An Antenna Pattern Synthesis Technique For Spaceborne SAR Performance Optimization", *IEEE Transactions on Geoscience and Remote Sensing*, vol. 29, No. 2, March 1991.

[30] J.M. Stiles, "Space-Time Radar Transmission, Target and Measurement Model", Revision E, Radar Systems and Remote Sensing Laboratory, The University of Kansas; Lawrence, Kansas August 2004

[31] J.M. Stiles, "Transmit Signal Model", Revision 'E', Radar Systems and Remote Sensing Laboratory, The University of Kansas; Lawrence, Kansas August 2004

[32] J.M. Stiles, "Determination of Numeric Model Parameters", Revision 'A', Radar Systems and Remote Sensing Laboratory, The University of Kansas; Lawrence, Kansas August 2004

[33] Jim Stiles, Vishal Sinha, Atulya Deekonda, "Optimal Space-time Transmit Signals for Multi-Mode Radar", Radar Systems and Remote Sensing Laboratory, The University of Kansas; Lawrence, Kansas November 2005

[34] Ashwin Mohan, "Topographic SAR Estimation and Processing for Multi-Aperture Spaceborne Radar", Masters Thesis, The University of Kansas, January 2005

[35] MIT 18.06 Linear Algebra, Spring 2005 Video Lectures Available:http://ocw.mit.edu/OcwWeb/Mathematics/18-06Spring-2005/CourseHome/index.htm